Characteristics of Two-dimensional Flow behind a Normal Plate in Contact with a Boundary on Half Plane

By

Mikio ARIE

(Received June 30, 1956)

TABLE OF CONTENTS

TABLE OF FIGURES

SYMBOLS

A, A_m . . . . . coefficients
B . . . . . height of the stable eddy, height of an imaginary Rankine oval
B_n . . . . . coefficient
b . . . . . width of test plate
c . . . . . absolute velocity, diameter of cylinder
H . . . . . Height of air-tunnel
K . . . . . coefficient or factor
L . . . . . length of a stable eddy behind a plate
i, k . . . . . suffix notations for tensor

M . . . . . strength of doublet
m . . . . . strength of source or sink
P . . . . . point or piezometric pressure
$\bar{P}$ . . . . . mean value of piezometric pressure
p . . . . . intensity of pressure
Q . . . . . total discharge
Q^2 . . . . . $U_k U_k$
q^2 . . . . . $u_k' u_k'$
R . . . . . Reynolds number
r . . . . . radial distance in cylindrical coordinates
U, V . . . . . mean velocity
u, v, w . . . . . components of velocity in x, y and z direction, respectively
u', v', w' . . . . components of fluctuating velocity
x, y, z . . . . . coordinates (z sometimes means a function of x and y)
u_0 . . . . . undisturbed velocity
w . . . . . complex potential

α . . . . . angle, coefficient
β . . . . . coefficient
δ . . . . . thickness of boundary layer
δ^* . . . . . displacement thickness of boundary layer
ζ . . . . . coefficient
ϑ . . . . . coefficient
θ . . . . . angle
λ . . . . . period
μ . . . . . strength of doublet, dynamic viscosity of fluid
ν . . . . . kinematic viscosity of fluid
ρ . . . . . density of fluid
τ . . . . . shear stress
ϕ . . . . . velocity potential
ψ . . . . . stream function

Introduction

The analysis of flow behind an infinitely long flate plat is an old and well known problem. As the geometry is simple in this case, such analysis should clarify the basic features of the mechanism of wakes behind a sufficiently great variety of boundary shapes. The theory of hodograph is important in mathematical analysis, but even though it offers a useful tool for a study of free stream lines, it is not enough to explain even the value of the drag coefficient for the plate. Furthermore, it offers no clue to the behavior of the flow in the wake. It is a well known fact that the actual value of the drag coefficient of a flat plate normal to the flow is about 1.8. However, its evaluation by the aid of the free-streamline theory gives 0.88. Evidently this rather large discrepancy comes from insufficient knowledge of the mechanism of the flow in a wake, particularly in regard to the low pressure in the zone of separation.

The study of the flow behind a body was greatly advanced by Kàrmàn's analysis of the vortex trail. Later, the experimental work by Fage and Johansen [1], [2] presented valuable information, and recently a paper published by Hanin [3] represented a new achievement in this kind of study. The goal of Hanin's theoretical study was to adjust both the position of the generating point of the vortex and the strength of the vortex so that the drag coefficient would agree with the results of experiments. There is also a recent peport of experimental work by Fomichev [4] about the turbulence behind a flat plate in water moving with a free surface, which was reviewed by M. V. Morkovin [5]. Also available is Roshiko's paper [6] on the influence of a tail plate upon the drag and upon the pressure distribution behind bluff bodies.

The present experimental work is an attempt to obtain the characteristics of stable eddy behind a flat plate mounted normally to the general flow in a half plane. Flow past a plate that is fully surrounded by fluid differs in several ways from flow past one that is in contact with a boundary. First of all, the former may be considered to lie in the path of essentially irrotational flow whereas the latter will be immersed in a boundary layer of indefinite thickness. Secondly, the flow in the wake of an isolated plate is free to pendulate about the plane of symmetry, whereas in the vicinity of a longitudinal boundary such pendulation is entirely prevented. The characteristics of the

eddy presented in this paper refer to the pattern of mean flow, to the pressure distribution, and to the distribution of turbulence.

Two kinds of Pitot cylinders were used for the measurements of velocities, and the characteristics of a cylinder in parallel shear flow were studied analytically. Pressure distributions were obtained with a sharp-edged plate which was mounted parallel to the side walls of the air tunnel. The reasonability of the velocity and pressure measurements was shown by the validity of the Bernoulli equation outside the wake, and by the relation of continuity. The values of $\sqrt{\overline{u'^2}}$, $\sqrt{\overline{v'^2}}$, $\sqrt{\overline{w'^2}}$, $\overline{u'v'}$, and $\sqrt{\overline{\left(\frac{\partial u'}{\partial t}\right)^2}}$ were measured with a single hot wire for the characteristics of turbulence, of which the first four terms are presented in this paper.

At first, in order to find the interference of the test section on the size of the stable eddy, three kinds of ratios between the width of the test plate and the height of the wind tunnel were investigated. In this case, instead of changing the height of the tunnel, the number of test plates was changed to yield a geometry equivalent to a change in tunnel height. Finally, in order to approximate an infinite spacing, the profile of the stable eddy was replaced with an imaginary Rankine oval to indicate the stream-line form of the ceiling and the floor of the tunnel. The actual results of the velocity measurements were compared with the velocity distributions obtainded analytically for the flow around the imaginary Rankine oval. Since it was noticed that the magnitudes of the velocities in these two cases differ appreciably when the point of observation moves downstream, two kinds of analytical correction for the distributions of velocity and pressure were attempted.

In the last parts of this study, the forms of the momentum equation and the energy equation of the mean flow, which are applicable for the present investigation, are derived. The corrected results of velocity and the pressure fields and the results of the turbulence measurement were substituted into the momentum equation, to obtain the drag of the test plate. This result was compared with the drag obtained directly by the integration of the pressure distribution over the surface of the test plate. At the same time, the distributions of the significant terms in the momentum equation and the energy equation of mean flow are presented. The balance of momentum and the balance of energy are also considered for the purpose of assuring the reasonability of the experimental results as a whole.

Experimental Equipment

1. Air tunnel.

All the experiments were carried out in one of the three air tunnels of the Iowa Institute of Hydraulic Research, State University of Iowa in the U. S. A. This tunnel is of the recirculating type, the flow being produced by a multi-vane type of radial-flow fan driven by a 7.5-H. P. electric motor. Two sets of lattices are arranged at the exit part of the fan to make uniform the flow in the tunnel. Guide vanes are also arranged at three bends of the tunnel. The cross section of the test section of the tunnel is 3 feet $\times$ 3 feet, and there are glass side walls over its whole length of about 12 feet. A variable resistor on the motor and three pivoted plates at the entrance of the fan furnish the adjustment of the velocity in the tunnel.

The velocity of the undisturbed flow in the test section was determined by calibration in terms of the pressure difference between two piezometer holes, one of them located about one foot downstream from the end of the converging part of the entrance to the test section and the other located farther upstream where the cross section is large.

2. Test plates.

The test plate was made of brass plate 1/4 inch in thickness, 3 inches in width, and 3 feet in length so that the span coincided with the width of the tunnel. The plate was fixed with screws to the side walls at both ends. The edges of the plate were given a 30 degree bevel on the downstream side. Piezometric holes 0.03 inch in diameter were also arranged on the upper half of the test plate for the purpose of measuring the pressure distribution, seven of them on the upstream suface and one on the downstream.

As will be seen in Fig. 1, the tail plate which corresponds to the border of the half plane was made of an aluminum plate 1/16 inch in thickness. It was screwed to the test plate at one end and secured with four thin steel guy wires to the ceiling and the bottom of the tunnel in order to eliminate undesirable vibration. Piezometer holes 0.04 inch in diameter were also arranged on the testing side to obtain the pressure distribution on the surface. The length of the tail plate was determined by trial. It might be worth mentioning that the length of the stable eddy behind the plate is controlled by the length of the tail plate to some degree, becoming equal to that of the tail plate when the tail plate is short but not shorter than a certain length which

Fig. 1

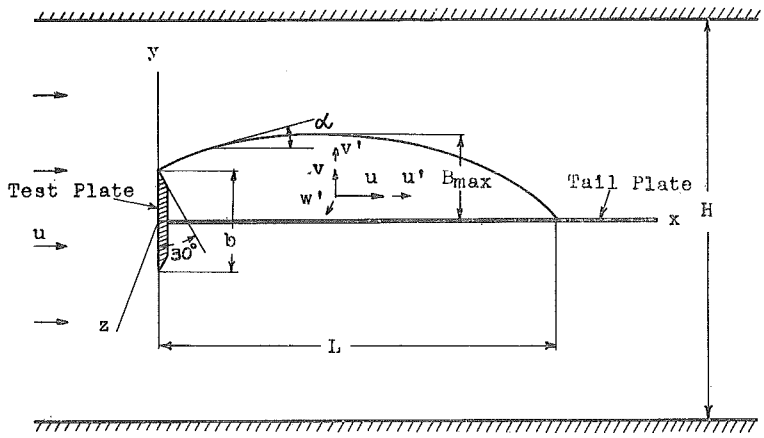

was not determined in this study. The length of the tail plate used was 30 1/4 inches, or 20 times the height of the test plate above the tail plate. This was enough greater than the eddy length to ensure the latter's independence of it. The span of the tail plate was 3 feet. The experiment was carried out on only the upper side of the tail plate.

3. Cylinders for the measurement of velocity.

a. 30.6° cylinder.

(1) Selection of the angle between two holes.

The Pitot-cylinder is used sometime for the measuremants of both the magnitude and the direction of velocity. When two holes are made on the surface of a cylinder at a properly selected angle, the angular position of the cylinder when the pressures at these holes balance provides a means of determining the direction of flow. At the same time, once the cylinder has been calibrated, it is possible to measure the magnitude of the velocity too. So far as the phenomenon of separation of flow around a cylinder is recognized, the angle between the holes must be selected so that they will not be located in the region of separation, in order to maintain the directional sensitivity. In order to decrease the error in estimating the magnitude of velocity, it is also preferable to have a cylinder of small dimension with a small angle between the holes. On the other hand, the angle should not be so small that the directional sensitivity cannot be maintained.

As the first step, angles of 55.8° and 30.6° were selected arbitrarily to find the sensitivity for the direction of flow. The diameter of the

cylinder was 1/8 inch. The diameter of the holes on the cylinder was 0.015 inch. The results of the experiment which was carried out in a uniform flow in the air tunnel are plotted in Fig. 2.

Fig. 2

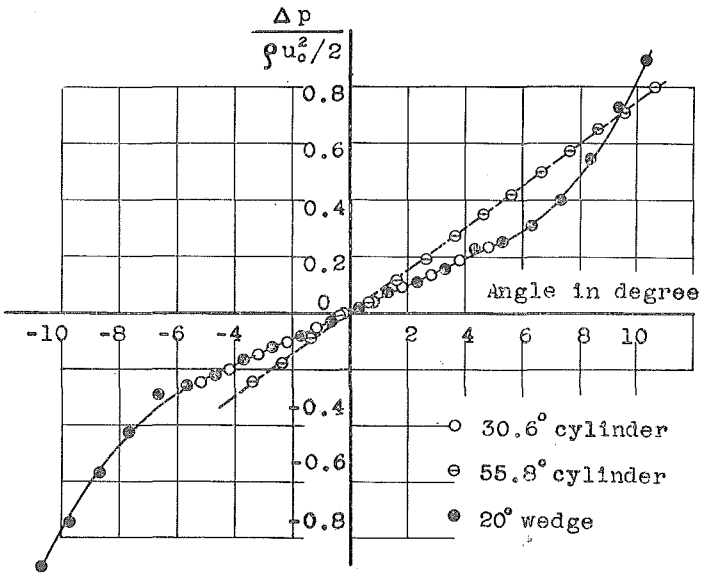

As a wedge is usually understood to be sensitive to the direction of flow, the result of an experiment with 20° wedge is plotted in that figure for comparison. The vertical axis $\Delta p/\frac{1}{2}\rho u_0^2$ is the pressure difference between the two holes in dimensionless form. The horizontal axis gives the angle of rotation of the cylinder and of the wedge against the uniform flow. The dimension of the wedge which was used for reference is shown in Fig. 3.

Fig. 3

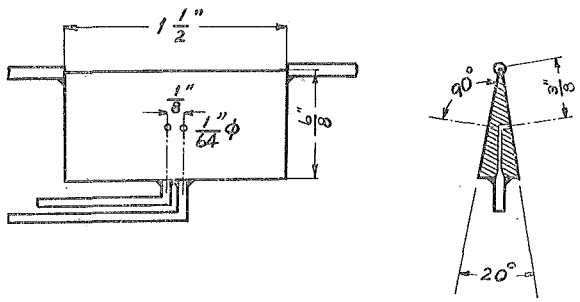

The 30.6° cylinder was the one finally employed. As will be seen in Fig. 3, the 30.6° cylinder has almost the same sensitivity to the direction of flow as the wedge, and the accuracy of 0.2 degree was experienced during the course of the present experiment.

(2) Calibration.

The calibration for the measurement of the velocity magnitude was also carried out in a uniform flow in the air tunnel. A 6-inch orifice in the tunnel was used to increase the velocity of the calibration. The standard gage was a Prandtl-type Pitot tube which was known to have a velocity coefficient of unity after a calibration with a flow of water through a circular submerged orifice. At first, one hole of the cylinder was set precisely in the upstream direction of the flow with a protractor so that the stagnation pressure could be taken from this hole. The pressure difference between the two holes was read with a Wahlen type of gage which gives the accuracy of 0.001 inch in an alcohol column. After that, the cylinder was rotated 30.6° so that the other hole would be upstream. This procedure established the proper angular location of the cylinder. The comparison between this cylinder and a Prandtl-tube is shown in Fig. 4. Since the results of the experiment fall on a straight line, the cylinder has a constant value of the velocity coefficient.

Fig. 4

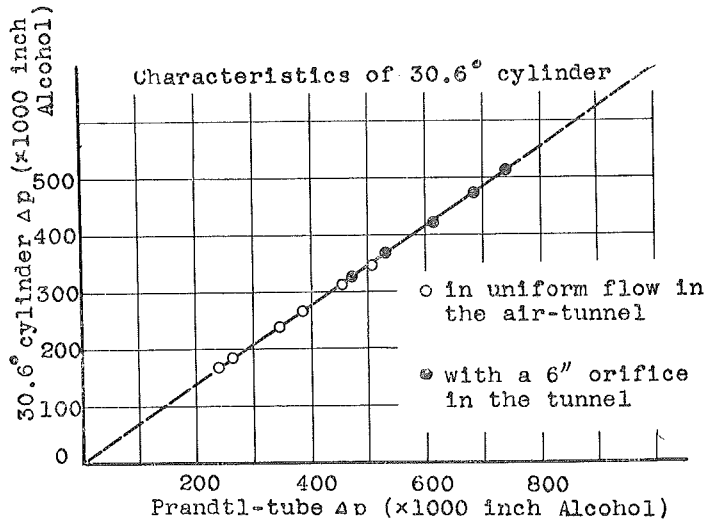

b. 180° cylinder.

(1) Estimation of the velocity magnitude.

When the velocity gradient is steep, the measurement of the direction of flow with the 30.6° cylinder becomes difficult, as will be discussed later, and therefore in measuring the velocity in such a region and in the wake, a 180° cylinder was used. When the direction of flow is not of primary interest, the pressure difference between these holes gives a fair indication of the magnitude of velocity even if the angle between them is large. When the cylinder is mounted in the tunnel so that one hole is precisely in the upstream direction, the other hole will of course be directed downstream. Four different magnitudes of velocity were used to find the effect of the Reynolds number, because the velocity in the wake of the test plate was known to change from zero to a value higher than the uniform velocity far upstream. The cylinder was rotated through various angles to the uniform flow, and the pressure differences between the two holes were obtained as in the case of the 30.6° cylinder. The results of the experiments are plotted in Fig. 5, which shows that the effect of the Reynolds number may be considered to be negligible within the range of the present tests. If there were some device to find the direction of flow, the magnitude of the velocity would also be obtainable with the aid of this curve through the step method of correction if necessary. In the preformance of the experiment, the cylinder was always supported in the flow so that the line which passed the two holes on the cylinder was parallel to the x axis-i. e., the axis of the tunnel test section. When the flow is horizontal, the value of $\Delta p/(\rho u_0^2/2)$ should be 1.74, as will be found in Fig. 5. Accordingly, if the flow has a certain angle α against the x axis, the correction factor for the horizontal component of the velocity must be $\cos\alpha\sqrt{1.74/\zeta}$.

A series of values of ζ and $\cos\alpha\sqrt{1.74/\zeta}$ against various values of α as obtained from this curve is tabulated in Table 1. Actually, the angle α is small in the wake at almost every point except in the region where the direction of flow changes from plus to minus or from minus to plus. In this region, the accuracy of measurement becomes poor. As the line of $\cos\alpha\sqrt{1.74/\zeta}$ values in Table 1 shows, when α is less than 30 degrees, the correction is not important as far as the horizontal component which is necessary to construct the flow pattern is concerned.

Fig. 5

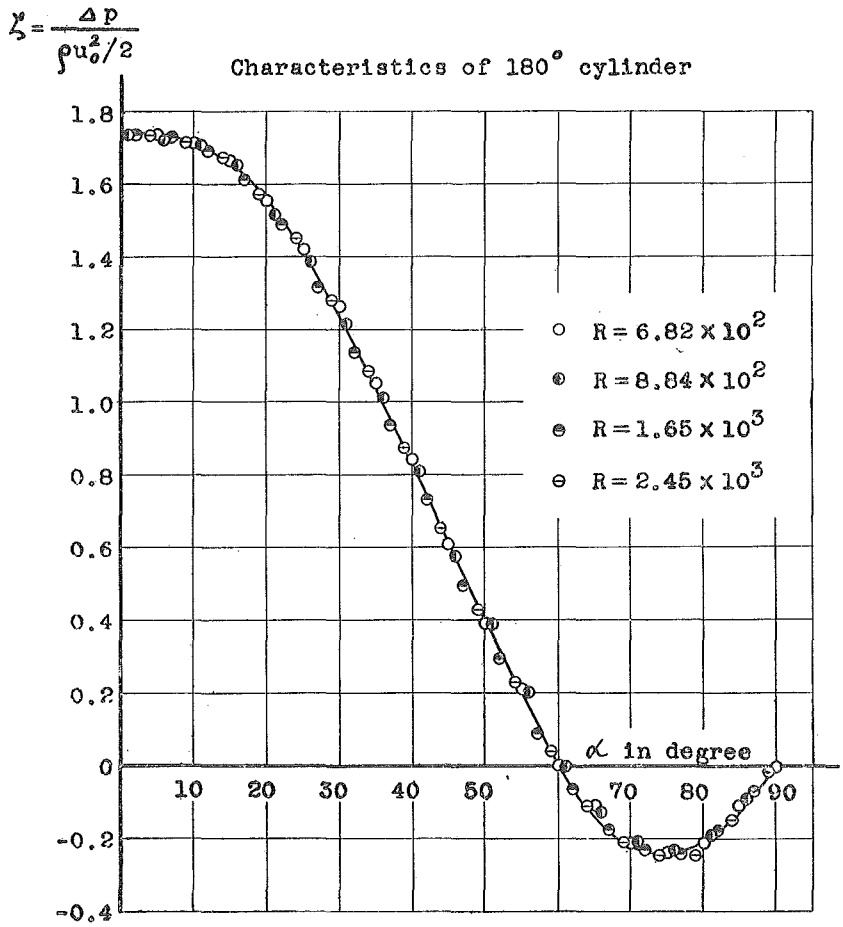

TABLE 1

α	0°	5°	10°	15°	20°	25°	30°	35°	40°
ζ	1.740	1.733	1.709	1.658	1.548	1.416	1.220	1.018	0.817
$\cos\alpha\sqrt{1.74/\zeta}$	1.000	0.998	0.993	0.991	0.9965	1.005	1.033	1.070	1.118

(2) Estimation of the direction of flow.

As described in the previous section, one hole in the cylinder was directed upstream, the other hole then naturally being directed downstream, and the pressure difference between these holes was obtained.

If the flow is assumed to be horizontal, the velocity coefficient of 1.74 will be available to find the magnitude of velocity, for the first step. Since the stream function ψ is obtainable through the integral $\int udy$, the integration of the velocity which will be obtained in this manner makes it possible to estimate the approximate flow pattern corresponding to the constant increments of discharge which determine lines of constant stream function. The tangents of these stream lines at any point give the first approximation of the direction of flow, with which the correction of the magnitude of velocity will be performed. Again the integration of this corrected velocity gives the corrected pattern, and the tangents of the stream lines will then give the second approximation of the direction of flow.

4. Plate for the measurement of the pressure distribution.

Pressures were measured with a plate having a cross section similar to that of the test plate but placed with its plane normal to those of the test plate and tail plate. The width of this brass plate was 5'/16 inches and the thickness 1/8 inch. Piezometric holes having a diameter of 0.03 inch were drilled on one surface midway between the leading and trailing edges. One end of the plate was fixed on the surface of the tail plate and the other end was screwed to the ceiling of the tunnel.

5. Turbulence measurements.

The values of $\sqrt{\overline{u'^2}}$, $\sqrt{\overline{v'^2}}$, $\sqrt{\overline{w'^2}}$ and $\overline{u'v'}$ were measured with a constant-temperature type of hot-wire anemometer [7] using a single-hot-wire technique. Tungsten wire of 0.00014-inch diameter was copper plated with $CuSO_4$ before soldered onto a probe. When the copper was removed by etching with HNO_3 to produce 5 ohms of electric resistance as indicated in the instruction booklet [8], the, length of the acting part of the wire was about 0.025 inch and the total length of the wire was approximately 1/8 inch. The calibration of this hot wire was made in a uniform flow in

Fig. 6
Example of the hot-wire calibration

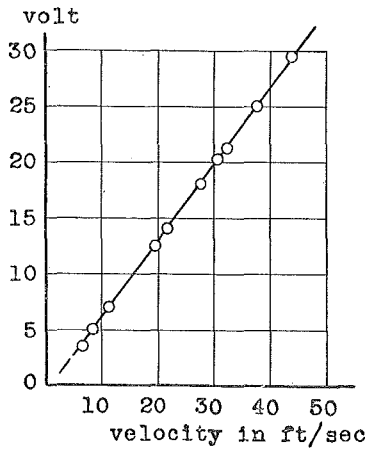

the tunnel by comparing with a standard Prandtl-type Pitot-tube and the chang of voltage necessary to keep the temperature of the wire constant for various speeds of air was obtained. Through calibration the characteristics of this hot-wire were found to be linear as intended. As will be judged from the diameter of the tungsten wire, the hot wires are very slender and so a number of wires were used after calibrating each of them. One example of the results of their calibration is shown in Fig. 6.

Experimental Procedure and Results

1. Primary measurement of velocity.

In order to find the effect of the tunnel (i. e., the constriction effect of the test section) on the size of the stable eddy behind the plate, three series of primary measurements were carried out. The geometry when one plate is mounted in the wind tunnel is shown schematically in Fig. 7 (a). In this case, the ratio betwween H and b is

$$H/b = 36/3 = 12$$

The situation when two plates are mounted is shown in Fi. 7 (b).

Fig. 7 (a)

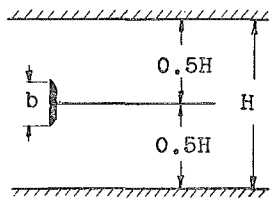

Fig. 7 (b)

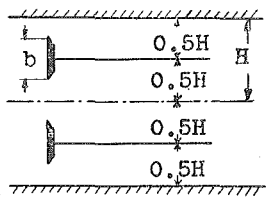

Since the center line between two plates indicated by the broken line in Fig. 7 (b) corresponds to an imaginary tunnel wall, the ratio between H and b is decreased by half in this case—namely, $H/b=6$. The same concept is applicable when four plates are mounted in the tunnel; in this case, the value of H/b is 3.

Before starting the measurement, the proper length of the tail plate had to be determined. It was rather easy to detect the end of the eddy with the 180° cylinder. When the cylinder was moved downstream, keeping its position near to the tail plate, the indication of the pressure difference between the two holes on the gage reveals the position of the end of the eddy clearly. Of course, the two holes of the cylinder had to be kept in a horizontal plane, and the point

where the pressure at the upstream and downstream holes balanced was then the end of the eddy. A diagonal arrangement of pieces of a light string on the tail plate also made it easy to detect the approximate end of the eddy by the eyes. As described before, the proper length of the tail plate was decided by trial to be 30 inches or ten times of b. When this length of the tail plate was employed, the eddy behind the test plate was about 8.12 times b, which was taken to indicate that the tail plate was sufficiently long.

a. The case of one test plate ($H/b=12$).

(1) Measurement of velocity.

As described above, the 30.6° Pitot cylinder was used primarily for the measurement outside the wake. The cylinder was set at the point of observation parallel to the test plate and rotated until the pressure difference between the two holes became equal to zero. When it was zero, the intersecting direction between the two holes corresponded to the direction of flow, which was read on a protractor. The next step was to rotate the cylinder $30.6°/2=15.3°$ in either direction so that one hole would be exactly at the stagnation point on the cylinder; the pressure difference between the two holes was then read. For the purpose of assuring the proper measurement, the cylinder was finally rotated 30.6° in the other direction so that the other hole would be at the stagnation point. When the cylinder was located outside the wake, these two angular positions of the cylinder gave almost the identical pressure difference, but the difference became larger when the cylinder went into the wake. When the difference was small, these two pressure differences were averaged and the magnitude of the velocity was estimated from the characteristics of the cylinder shown in Fig. 4.

When the point of observation was in the wake, the 180° cylinder was used and the device described before was employed to estimate the velocity at that point.

(2) Construction of the flow pattern.

The results of the velocity measurements were arranged to find u/u_0 at a series of several vertical sections. After plotting u/u_0 against y/b, the integration $\phi=\int(u/u_0)dy$ was performed by Simpson's method to obtain a group of curves on ϕ : y/b plane for the different values of x/b. This plot yields the coordinates x/b and y/b for different values of the discharge integral—that is the coordinates of the stream-line.

FIG. 8

FLOW PATTERN BEHIND A PLATE $\left(\frac{H}{b}=12\right)$

$R = 5{\cdot}52 \times 10^4$

○ WITH 30·6° CYLINDR

• WITH 180° CYLINDER

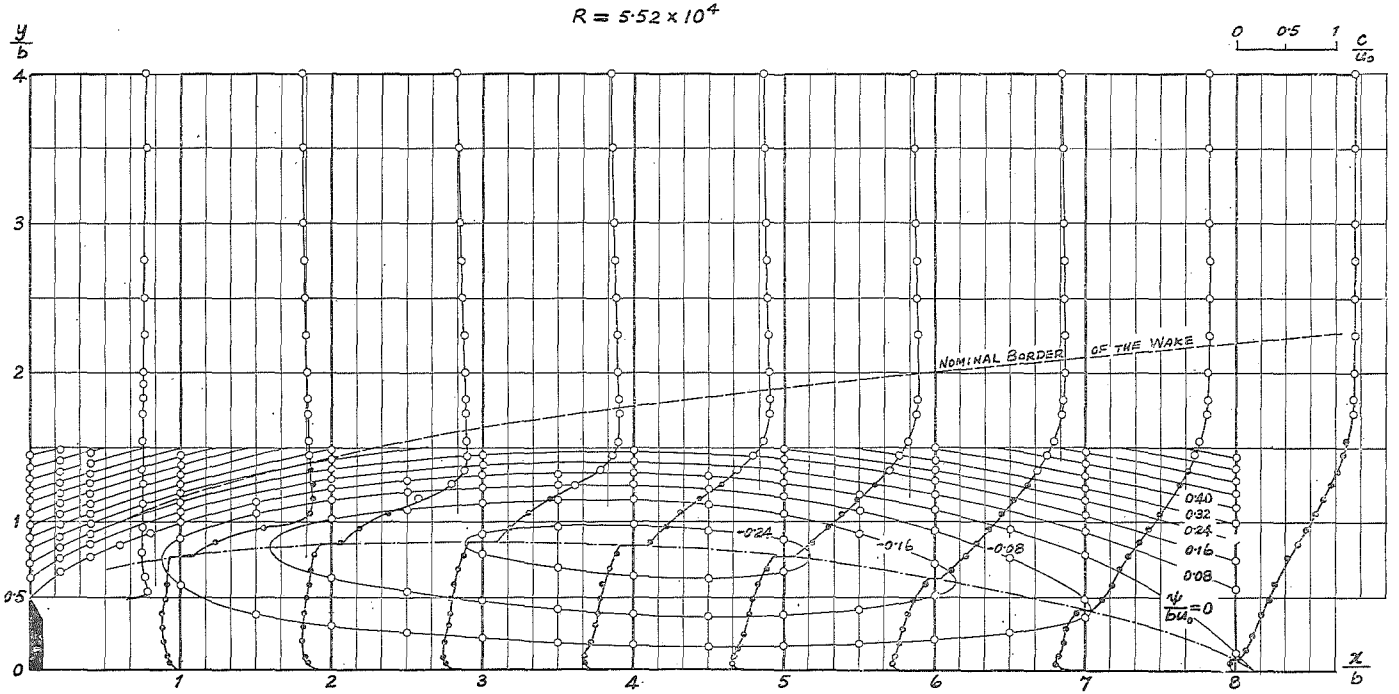

With the aid of these stream lines, the direction of the mean flow inside the wake was obtained by drawing a tangent at the point desired. The correction of the velocity was performed in the manner explained above, wherever necessary. Integration of these corrected distributions of u/u_0 then gave the corrected flow pattern. Actually, this procedure of correction did not change the flow pattern very much.

The final form of the flow pattern obtained is shown in Fig. 8.

Distributions of c/u_0 are also presented in this figure for reference. The points of maximum velocity are rather clear when x/b is small, but they become quite vague as the point of observation is moved downstream. The estimated points of the maximum velocity are also indicated at each section, and they are connected with a smooth curve which might be called the border of the wake. The results of velocity measurements made with 30.6° cylinder and the 180° cylinder are indicated separatedly by means of different symbols.

b. The cases of two plates ($H/b=6$) and four plates ($H/b=3$).

The same procedures as described in the preceding section were repeated for the case in which two test plates were mounted in the air tunnel. The final results are shown in Fig. 9. It will be clearly seen that the length and the height of the profile of the stable eddy are smaller in this case than before. This fact shows that the interferance of the tunnel ceiling should not be overlooked. Close comparison of Figs. 8 and 9 will also reveal a change in the distribution of velocity, which was accompanied by a rather appreciable change in the pressure distribution in the field.

In this case, as it was possible to measure the velocity distribution up to the imaginary tunnel wall already shown in Fig. 7, the continuity relation can be examined. The schematic sketch of the situation is shown in Fig. 10. The discharge can then be computed at the upstream section, where there is no disturbance, as 12 dimensionless units for the tunnel as a whole, or 3 units for the field of each half plate. On the other hand, the integration of the velocities actually measured gives the discharge as shown in Table 2 at several vertical sections.

In this table, the estimated errors in discharge are also indicated. The error will be seen to be about (-4~0.7%) in gross. Actually, as the thickness of the boundary layer at the floor of the air tunnel should decrease at the section of the test plate, the error in discharge will be lower than the figures in this table. This table shows that the

FIG. 9

FLOW PATTERN BEHIND A PLATE $\left(\frac{H}{b}=6\right)$

$R = 5{\cdot}52 \times 10^4$

○ WITH 30·6° CYLINDER

• WITH 180° CYLINDER

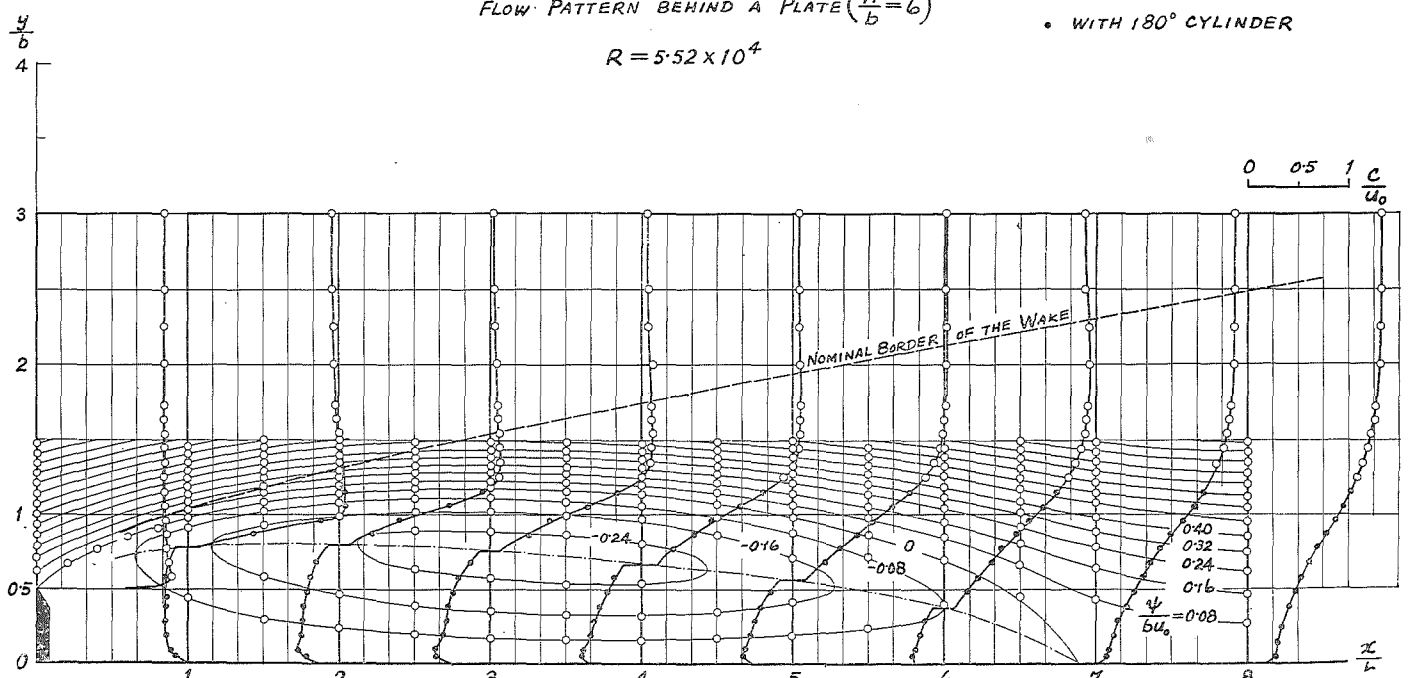

Fig. 10

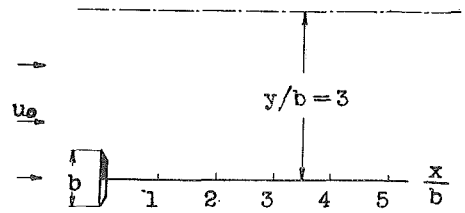

TABLE 2.

x/b	0	1	2	3	4	5	6	7	8
Q	2.951	2.934	2.876	2.868	2.871	2.906	2.942	3.020	3.022
Error in %	− 1.6	− 2.0	− 4.1	− 4.4	− 4.3	− 3.1	− 1.9	0.7	0.7

measurement of velocity was performed within reasonable limits of error on the whole.

When four plates were mounted in the tunnel, the flow among the plates was found to be asymmetrical with respect to the mid-section between any two plates. Furthermore, the flow seemed to be unstable, as any slight disturbance in the field changed the direction of flow. This fact was detected by arranging pieces of light string diagonally on the surface of the tail plates that correspond to the boundary of the half plane. The inclination of the swinging strings gave the approximate direction of flow. Since the flow was asymmetric, the idea of the imaginary wall between two plates would not be applicable in this case and the detailed measurement was not carried out.

2. An approximation to infinite spacing (formation of the ceiling and the floor of the air tunnel).

When a body is located in an infinite space, a noticeable distortion of the stream lines extends rather far away from the body in comparison with the size of the body. It is also a widely known fact that the interaction of the wind-tunnel walls is sometimes appreciable. Going back to the present study, it was of primary interest to investigate the characteristics of the flow downstream from a vertical plate in a half plane. The preliminary experiments already described revealed that the height of the tunnel made an appreciable change in the field, yet it was not determined whether the ratio $H/b=12$ was

comparable to the infinite spacing. In order to realize the next step of this approximation, a means of effecting a curvature corresponding to a probable stream line at the boundaries of the air tunnel was considered. As the present study is a two-dimensional one, consideration of the ceiling and the floor of the tunnel would be sufficient. The profile of the stable eddy for $H/b=12$ which was already shown in Fig. 8 offered the shape of an equivalent imaginary body for this purpose. This profile of the stable eddy was replaced with an imaginary Rankine oval to compute conventionally the shape of the stream lines at the ceiling and the floor of the air tunnel. The reason that a Rankine oval was employed was simply that it was easy to handle the solution of the velocity field. If the profile of the eddy is considered to be the zero discharge line of the eddy pattern, one can easily estimate the distortion of the stream line at any point in the field. In this case, it was deemed proper to consider the displacement thickness of the boundary layer in the tunnel, too.

a. Estimation of an imaginary Rankine oval to replace the profile of the stable eddy.

A Rankine oval in two dimensions is realized by combining a uniform flow with a paired source and sink of equal strength located at $(-1,0)$ and $(1,0)$ respectively. The uniform flow is understood to be from left to right, and the situation is shown schematically in Fig. 11.

Fig. 11

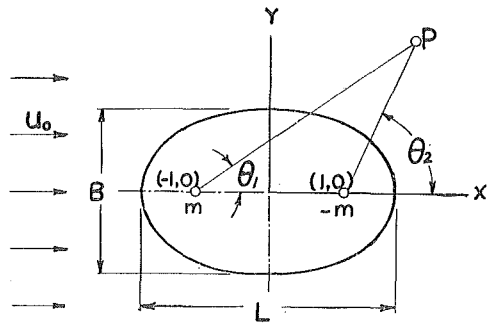

The complex potential of a source located at $(-1,0)$ is

$$w_1 = -m \log z = -m(\log r_1 + i\theta_1) \qquad (1)$$

In the same way, the complex potential of a sink located at (1,0) is

$$w_2 = m \log z = m\ (\log r_2 + i\theta_2) \qquad (2)$$

The complex potential of a uniform flow in the direction of positive x is

$$w_3 = -u_0 z = -u_0 (x+iy) \tag{3}$$

Accordingly, the stream function which passes an arbitrary point P located outside the Rankine oval must be the sum of the imaginary parts of Eqs. (1), (2), and (3):

$$\psi = -u_0 y - m\theta_1 + m\theta_2$$

or

$$\frac{\psi}{u_0} = -y - \frac{m}{u_0}\tan^{-1}\frac{y}{x+1} + \frac{m}{u_0}\tan^{-1}\frac{y}{x-1} \tag{4}$$

The stream function ψ must be zero on the surface of the Rankine oval. Consequently, Eq. (4) gives

$$\frac{u_0}{m}y = -\tan^{-1}\frac{y}{x+1} + \tan^{-1}\frac{y}{x-1}$$

or

$$\tan\left(\frac{u_0}{m}y\right) = \frac{2y}{x^2+y^2-1} \tag{5}$$

The length of the Rankine oval can be obtained by letting y be very small in Eq. (5). Then, neglecting square and high powers of y, one obtains

$$L = 2\sqrt{1+\frac{2m}{u_0}} \tag{6}$$

In the same way, the condition $x=0$ gives the expression of the width of the oval B:

$$\frac{B}{\frac{B^2}{4}-1} = \tan\frac{B}{\frac{L^2}{4}-1}$$

or

$$L = 2\sqrt{1+\frac{B}{\tan^{-1}\frac{4B}{B^2-4}}} \tag{7}$$

This is the relation between B and L of a Rankine oval. The next step was to find the combination of B and L which will make the shape of the Rankine oval practically identical with the profile of the stable

eddy shown in Fig. 8. It is impossible to give the exact shape of the eddy to the oval of course, and for convenience the Rankine oval which passed the edge of the test plate and the point of the maximum height of the stable eddy was used.

Now, taking B as a unit of length, the coordinate of the upper edge of the test plate was found to be $(-1.404B, 0.187B)$ from the eddy profile. Substitution of these coordinates into Eq. (5) gave

$$\frac{u_0}{m} = \frac{1}{0.187} \tan^{-1}\left(\frac{0.374\,B}{2.007B^2-1}\right) \tag{8}$$

Substitution of Eq. (8) into Eq. (6) gave the relation between B and L which was suitable for the approximation considered:

$$L = 2\sqrt{1+\frac{0.374\,B}{\tan^{-1}\dfrac{0.374B}{2.007B^2-1}}} \tag{9}$$

Accordingly, the combination of B and L which satisfied both Eqs. (7) and (9) simultaneously had to be the values of B and L one is seeking for. As it is difficult to solve these equations simultaneously, Eqs. (7) and (9) were computed separatedly for a certain series of B to obtain the corresponding series of L. The results of this computation are

Fig. 12

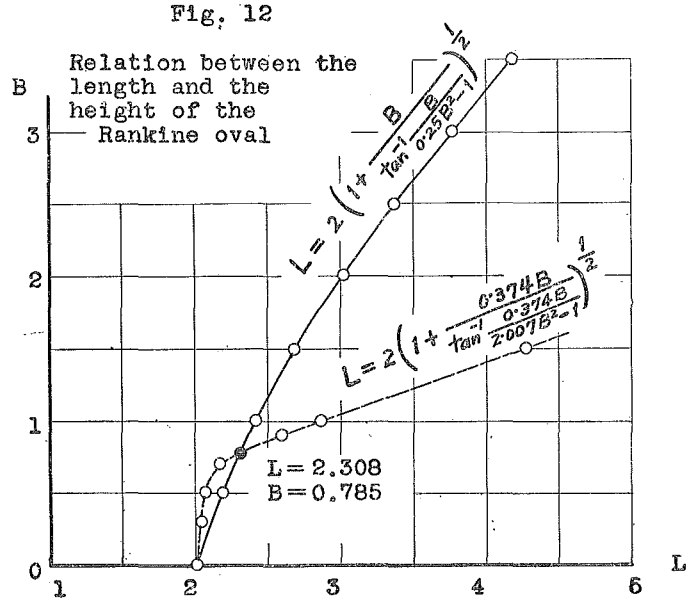

plotted in Fig. 12, and the point of intersection of these two equations was read as

$$L = 2.308\,, \qquad B = 0.785$$

as indicated in this same figure.

It must be remembered that these values of L and B were expressed by taking the unit length as the x coordinate of the source or sink. Knowing that the width of the test plate is 3 inches, the chief dimensions of the Rankine oval could at once be obtained. The results are shown schematically in Fig. 13.

Fig. 13

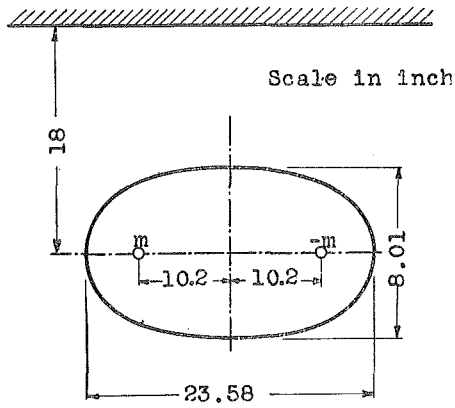

Substitution of $B = 0.785$, obtained from Fig. 13, into Eq. (8) gave the expression of the strength of the source and sink—namely, $u_0/m = 6.08$. Accordingly, the equation of the suitable Rankine oval was obtained from Eq. (5) as

$$\frac{2y}{x^2+y^2-1} = \tan(6.08\,y) \qquad (10)'$$

or

$$x = \pm\left\{\frac{2y}{\tan(6.08\,y)} - y^2 + 1\right\}^{\frac{1}{2}} \qquad (10)$$

TABLE 3

y	x	y	x	y	x
0.034	3.921	0.238	3.885	0.851	3.332
0.068	3.92	0.272	3.872	1.020	2.952
0.102	3.915	0.306	3.86	1.19	2.255
0.136	3.915	0.340	3.84	1.335	0.204
0.170	3.90	0.51	3.742		
0.204	3.895	0.68	3.58		

As stated before, the x coordinate of source and sink is the unit length in this equation. In other words, 1=10.2 inches. The results of computations of Eq. (10) are tabulated in Table 3 after converting the unit

FIG. 14

VARIATION OF THE DISPLACEMENT THICKNESS OF BOUNDARY LAYER ALONG THE WIND-TUNNEL AND THE ESTIMATED FORM OF THE CEILING AND THE BOTTOM

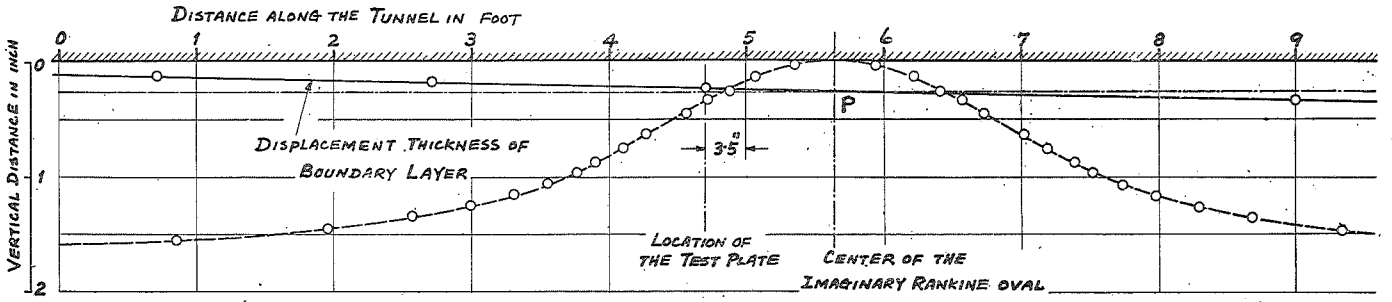

FIG. 15

COMPARISON BETWEEN THE EDDY PROFILE AND THE IMAGINARY RANKINE OVAL

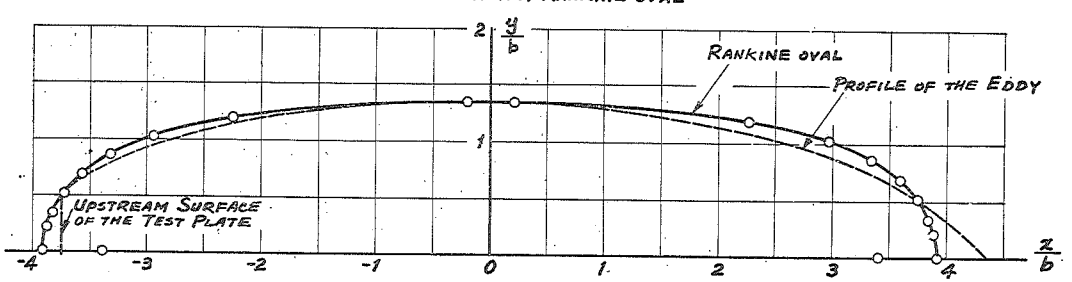

length to the width of the test plate, and the comparison between the imaginary Rankine oval and the eddy profile obtained in Fig. 8 is shown in Fig. 15. It will be seen that the two shapes are very similar.

It is convenient to convert the chief dimensions into the x coordinate of source or sink as unity in order to derive the equation of the stream line at the ceiling of the air tunnel. The chief dimensions are shown schematically in Fig. 16.

Fig. 16

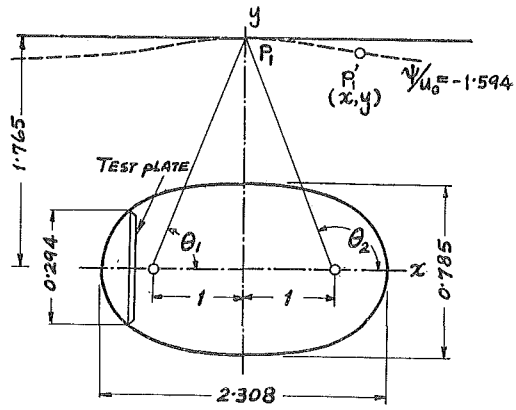

From this figure, it is clear that $\tan\theta_1 = 1.765$. Consequently, $\theta_1 = 1.052$ radians and $\theta_2 = (\pi - 1.052)$ radians for the stream line at the ceiling of the tunnel. Substitution of $u_0/m = 6.08$, $\theta_1 = 1.052$ radians, and the coordinates of $P_1(0, 1.765)$ into Eq. (4) gave the value of the stream function at the ceiling of the tunnel as $\phi/u_0 = -1.594$. The locus of $P_1'(x, y)$ then gave the form of the stream line at the ceiling of the tunnel. Substitution of $\phi/u_0 = -1.594$ into Eq. (4) yielded the locus of $P_1'(x, y)$. Accordingly, the equation of the form of the ceiling of the air tunnel had to be

$$1.594 = y + \frac{1}{6.08}\left(\tan^{-1}\frac{y}{x+1} - \tan^{-1}\frac{y}{x-1}\right)$$

or

$$x^2 = 1 - y^2 - \frac{2y}{\tan\{6.08(1.594-y)\}} \qquad (11)$$

$$1.765 \geqq y \geqq 1.594$$

The results of the computation of this squation are plotted in Fig. 14.

b. Estimation of the boundary-layer development at the ceiling of the air tunnel.

At first, in order to estimate the boundary-layer thickness defined by 99% of the general velocity, the velocity distributions at four vertical sections in the tunnel were measured with a Prandtl-Pitot

Fig. 17
VELOCITY DISTRIBUTIONS IN THE BOUNDARY LAYER AT THE CEILING OF THE WIND TUNNEL

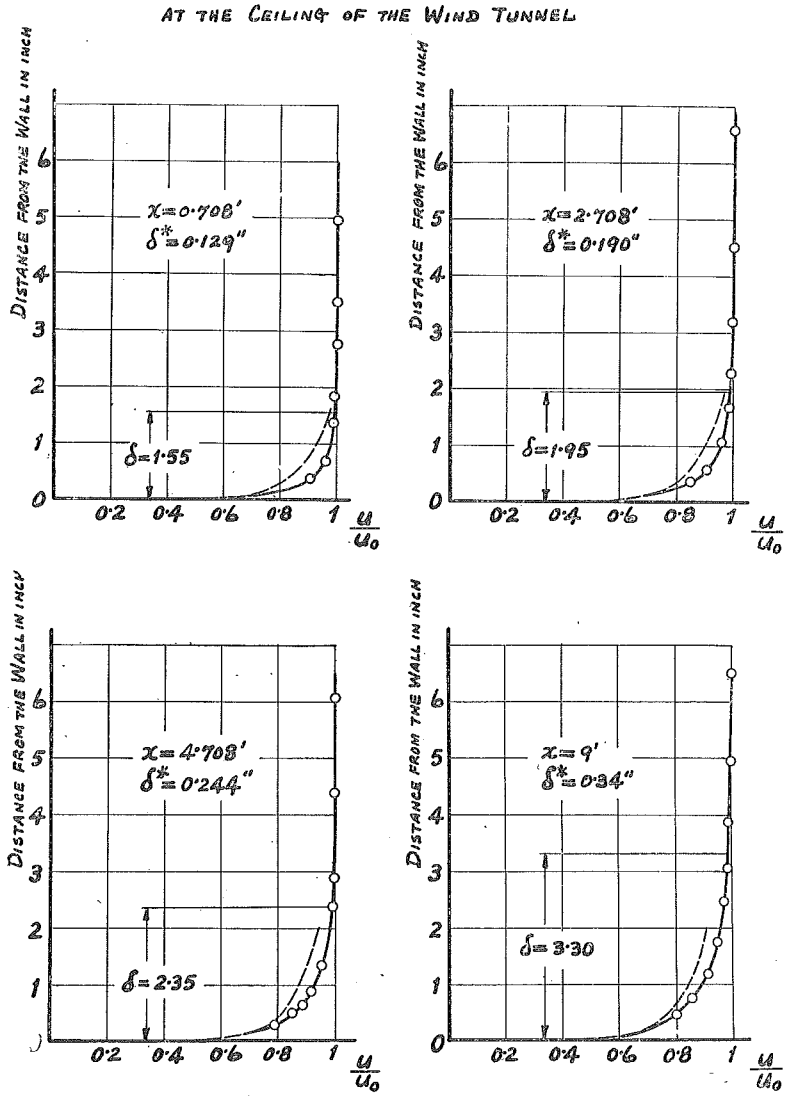

tube up to 0.4 inch from the ceiling. The results of the measurements are shown in Fig. 17. The values of x to show the positions of observations were measured from a fixed point about 1 foot downstream from the end of the bell inlet to the test section. The estimated values of the boundary-layer thickness δ are also indicated in this figure. In order to estimate the constricting effect of the development of the boundary layer, the displacement thickness of the boundary layer δ^* defined by $\int_0^\delta (1-u/u_0)\,dy$ must be obtained. When one desires to do so, it is necessary to find the velocity distribution near the surface of the ceiling of the tunnel. As a matter of practice, it is difficult to measure the velocity near the wall, therefore an approximate extrapolating device was employed. The sketch of the end of the inlet bell of the tunnel is shown in Fig. 18.

Fig. 18

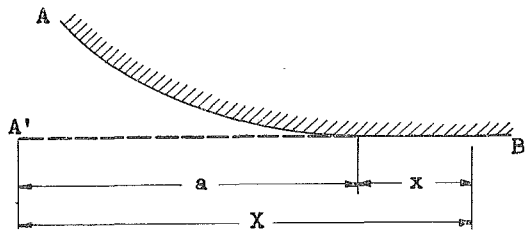

Even though the actual form of this part is AB as shown in Fig. 18, a flat plate A'B was imagined to replace the ceiling of the tunnel, because many experimental measurements of the boundary-layer thickness for a flat plate are available:

$$\frac{\delta}{X}=\frac{\delta}{x+a}=\frac{0.377}{R^{\frac{1}{5}}} \tag{12}$$

X is the distance from the leading edge of the imaginary palte, and x is the distance from a fixed reference point in the tunnel. The results of the estimation of the boundary-layer thickness δ defined by 99% of the general flow velocity are plotted in Fig. 19 against distance along the test section. By trial-and-error calculation, it was found that $a=5.27$ feet, so that the actual longitudinal variation of δ fits fairly well with values of δ computed from Eq. (12). Equation (12) is

$$\frac{0.377}{(x+a)^{\frac{1}{5}}}\left(\frac{\nu}{u_0}\right)^{\frac{1}{5}}=\frac{\delta}{x+a}$$

and the conditions of the experiment gave $\nu = 1.70 \times 10^{-4} ft^2/\text{sec}$ and $u_0 = 45.9\, ft/\text{sec}$. Accordingly, this equation resulted in

$$\delta = 0.0508(x+a)^{\frac{4}{5}} \tag{13}$$

The results of computations of this equation with the value of $a = 5.27$ feet are tabulated in Table 4 and indicated by a curve in Fig. 19. It will be seen that the value of "a" or the length of the extending length of the imaginary plate gives a fairly close approach for the development of boundary layer in the tunnel, except at $x = 10$ feet. This position is far downstream, and hence it was not considered dangerous to use the variation of δ shown in Table 4.

TABLE 4.

$x\, ft$	$(x+a)''$	δ'' from Eq. (13)
0	63.28	1.407
1.667	83.28	1.753
3.332	103.28	2.07
5.000	123.28	2.385
6.664	143.28	2.68
8.333	163.28	2.99
10.000	183.28	3.295

The Prandtl-Kármán equation for the velocity distribution in the boundary-layer of a flat plate is

$$\frac{u}{\sqrt{\frac{\tau_0}{\rho}}} = 5.5 + 5.75 \log_{10} \frac{\sqrt{\frac{\tau_0}{\rho}}\, y}{\nu} \tag{14}$$

in which

$$\tau_0 = \frac{0.059}{R^{\frac{1}{5}}} \frac{\rho u_0^2}{2}$$

Accordingly,

$$\frac{u}{u_0} = \frac{0.1717}{R^{\frac{1}{10}}} \left(5.5 + 5.75 \log_{10} \frac{0.1717\, u_0 y}{\nu R^{\frac{1}{10}}} \right) \tag{15}$$

Equation (15) was adapted for each section indicated in Fig. 17 and the results are tabulated in Table 5. The equation of u/u_0 in Table 5 were computed and the results are shown in Fig. 17 as broken lines. These

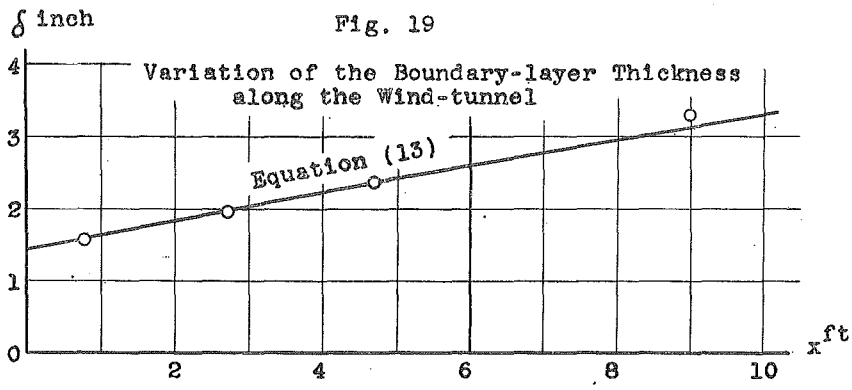

lines were used for the extrapolation of the velocity distribution near the ceiling of the air tunnel. As the velocity distributions in the boundary-layer along the ceiling combined the experimental results and the conventional empirical formulas, the displacement thickness of the boundary-layer δ^* could be obtained for each section. The results of the estimation of δ^* are indicated in Fig. 17 and the variation along the tunnel test section is shown in Fig. 14.

TABLE 5 Velocity distribution in the boundary-layer

Position	1	2	3	4
x ft	0.708	2.705	4.700	9.000
R	1.615×10^6	2.155×10^6	2.69×10^6	3.85×10^6
u/u_0	$0.226+0.2363\log 925y$	$0.220+0.230\log 900y$	$0.215+0.2248\log 881y$	$0.207+0.2164\log 848y$

c. Formation of the ceiling and the floor of the air tunnel.

As already seen from the scatter of points in Fig. 14, a certain amount of error in computation of the stream line at the ceiling of the tunnel was unavoidable. As shown in Fig. 14, the results of the computation were connected with a smooth curve. The scale in Fig. 14 is distorted in the horizontal and vertical directions for convenience. Now, the ceiling must be constructed by superposition of the shape of the stream line and the variation of the displacement thickness of the boundary-layer. This superposition was performed graphically with the aid of Fig. 14. The vertical line which passes through the center of the imaginary Rankine oval intersects the variation curve of the

displacement thickness of the boundary-layer at point P as shown in Fig. 14. A horizontal line which passes P is indicated as dot-dash line. The stream line was displaced graphically, at each point along the tunnel, by the magnitude of the vertical difference between this horizontal line and the variation curve of the displacement thickness of the boundary-layer.

As the test plate was mounted exactly at the midheight of the tunnel, the floor of the tunnel was made exactly symmetrical with the ceiling. The distances from the flat ceiling to the imaginary stream line were read from Fig. 14, and transferred to wood templates which posses the curve of the stream line. These templates supported a flexible hardboard sheet of the same width as that of the tunnel, so that the desired stream-line shape was obtained in the longitudinal direction.

The ends of the hardboard at the entrance and at the end of the test section of the air tunnel were smoothly connected with the flat ceiling and floor with proper curves. A piezometer hole 0.04 inch in diameter was again arranged near the entrance of the test section in order to obtain, as before, the, velocity of approach after calibration.

3. Measurements of the wake behind the plate in the stream-lined air tunnel.

a. Mean velocity distribution.

The procedures for the measurement of velocity and the construction of the flow pattern were identical with those explained before. The final results are shown in Fig. 20.

Comparison between Fig. 20 and Fig. 8 shows only a slight change in the shape of the eddy profile. Accordingly as far as the size or shape of the profile of the eddy is concerned, the device of replacing the eddy profile with an imaginary Rankine oval may be understood to be proper, for the purpose of realizing an approximation to an infinite spacing.

b. Pressure distribution.

The plate for the measurement of pressure distribution was carefully mounted parallel to the side walls, and the difference between the pressure upstream and the pressure at the piezometer hole on this plate was obtained. The experimental results at several sections are plotted Fig. 21 as broken lines. As will be seen therefrom, the pressure in the region under study is always lower than the pressure in the general flow.

FIG. 20

FLOW PATTERN BEHIND A PLATE IN THE STREAM-LINED TEST SECTION

$R = 5{\cdot}52 \times 10^4$

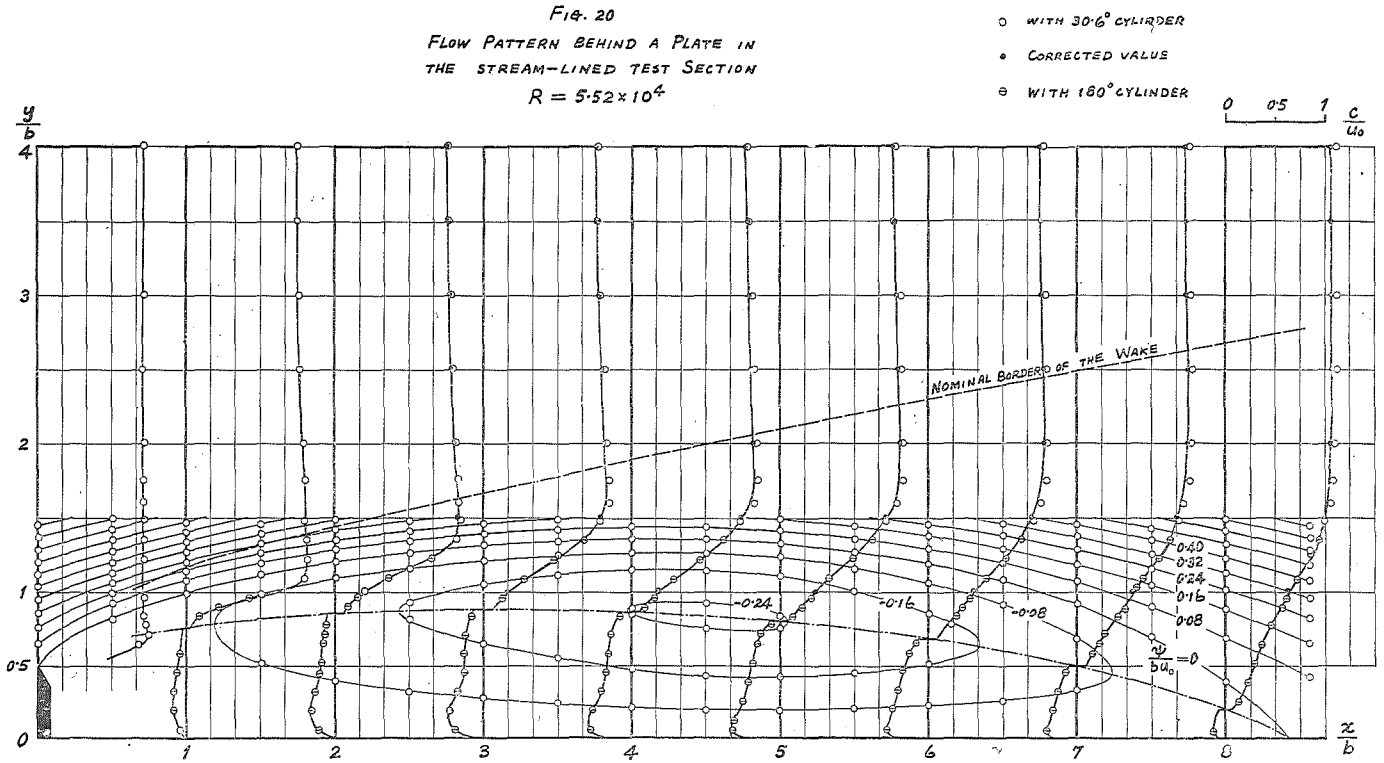

Fig. 21
PRESSURE DISTRIBUTION DOWNSTREAM FROM THE TEST PLATE

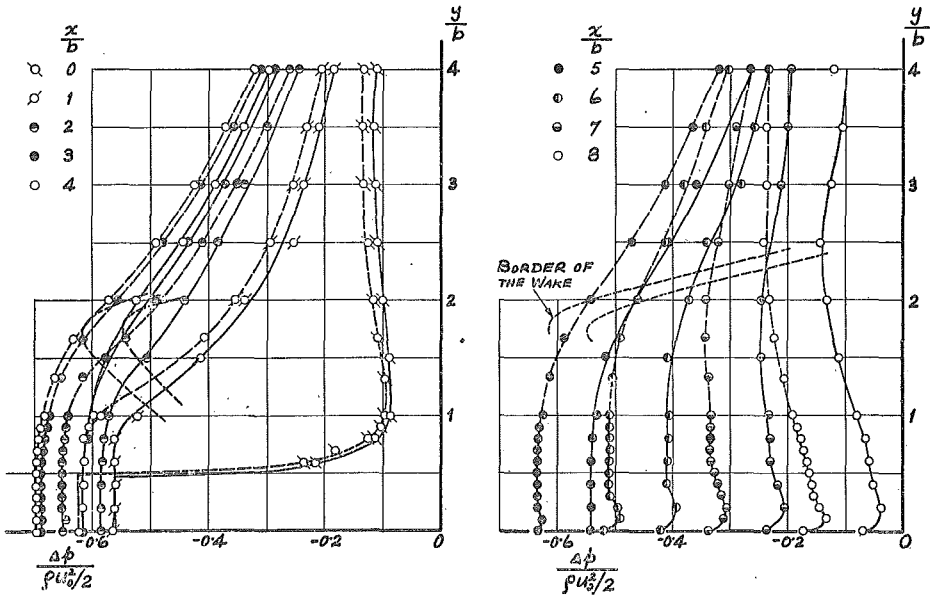

c. Turbulence distribution.

(1) Measurement of $\sqrt{\overline{u'^2}}$.

The single hot wire was supported vertically in xy plane. In this case, the hot wire is sensitive to u' and w', but when u is large, the error for u' which will be caused by w' is negligible. Actually, u is small compared to u' and w' in some regions of the wake, and the accuracy of the measurements of $\sqrt{\overline{u'^2}}$ becomes poor. Since there is no way, at present, to measure the fluctuating components accurately in such a region, the measurement was carried out conventionally. When the hot wire is supported in this manner, the mean horizontal velocity u is also measurable. The measurement of this component of velocity agreed fairly well with the results obtained with cylinders. The quantity $\sqrt{\overline{u'^2}}$ can be computed from

$$\sqrt{\overline{u'^2}} = I_{rms} \times A \times B_n \tag{16}$$

in which I_{rms} is the reading of the root-mean-square value of the fluctuating voltage, A is the slope of the voltage-velocity characteristics of the hot wire, and B_n is the attenuation factor.

(2) Measurements of $\sqrt{\overline{v'^2}}$ and $\overline{u'v'}$.

When the single hot wire is supported at the angle of 60° against the x axist in the xy plane, the reading of the root-mean-square of the fluctuating voltage gives the clue to obtaining $\sqrt{\overline{v'^2}}$ and $\overline{u'v'}$. In this case,

$$(I_{rms}\times A\times B_n)_1=\sqrt{\overline{(u'\cos 60^\circ+v'\sin 30^\circ)^2}}$$

or

$$(I_{rms}\times A\times B_n)_1^2=(0.866\sqrt{\overline{u'^2}})^2+(0.5\sqrt{\overline{v'^2}})^2+0.866\overline{u'v'} \qquad (17)$$

In the same way, when the hot wire is supported at the angle of 120° to the x axis in the xy plane, one obtains

$$(I_{rms}\times A\times B_n)^2=(0.866\sqrt{\overline{u'^2}})^2+(0.5\sqrt{\overline{v'^2}})^2-0.866\overline{u'v'} \qquad (18)$$

The sum of Eqs. (17) and (18) gives

$$(I_{rms}\times A\times B_n)_1^2+(I_{rms}\times A\times B_n)_2^2=1.5(\sqrt{\overline{u'^2}})^2+0.5(\sqrt{\overline{v'^2}})^2$$

or

$$\sqrt{\overline{v'^2}}=\sqrt{2\left[(I_{rms}\times A\times B_n)_1^2+(I_{rms}\times A\times B_n)_2^2-1.5(\sqrt{\overline{u'^2}})^2\right]} \qquad (19)$$

Since $\sqrt{\overline{u'^2}}$ is obtainable with Eq. 16, $\sqrt{\overline{v'^2}}$ can be obtained with Eq. (19).

When Eq. (18) is subtracted from Eq. (17), $\overline{u'v'}$ can be obtained:

$$(I_{rms}\times A\times B_n)_1^2-(I_{rms}\times A\times B_n)_2^2=1.732\overline{u'v'}$$

or

$$\overline{u'v'}=\frac{1}{1.732}\left[(I_{rms}\times A\times B_n)_1^2-(I_{rms}\times A\times B_n)_2^2\right] \qquad (20)$$

(3) Measurement of $\sqrt{\overline{w'^2}}$

The device for the measurement of $\sqrt{\overline{v'^2}}$ can also be used for the measurement of $\sqrt{\overline{w'^2}}$. In this case, the single hot wire must be supported in the xz plane so that the hot wire makes 60° and 120° angles with the x axis. Then the same expression for $\sqrt{\overline{w'^2}}$ as in Eq. (19) can be obtained; since $\sqrt{\overline{u'^2}}$ is already known, $\sqrt{\overline{w'^2}}$ can be evaluated.

The results of measurements are plotted on Figs. 22, 23, 24, and 25 for several vertical sections.

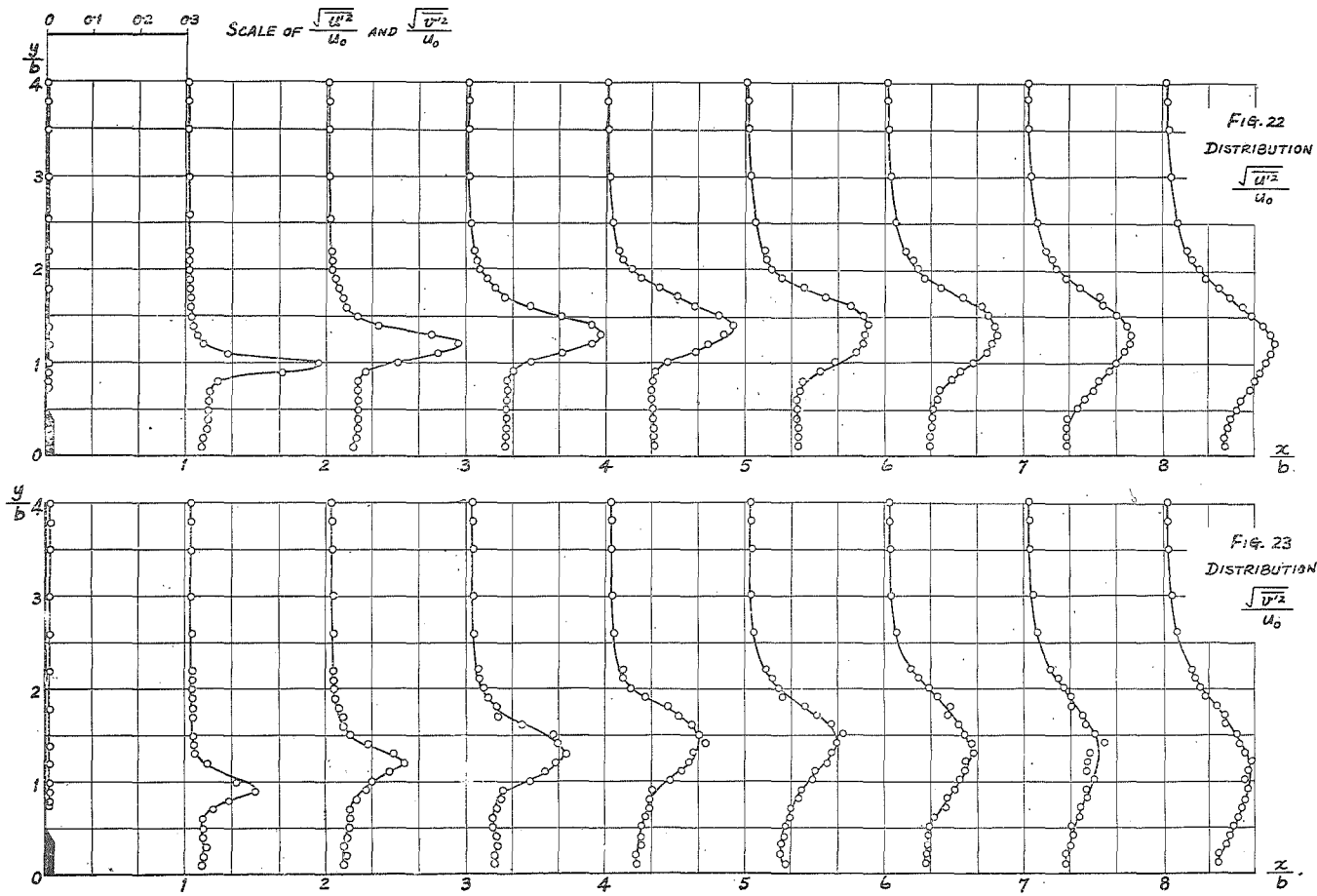

FIG. 22
DISTRIBUTION OF
$\frac{\sqrt{\overline{u'^2}}}{u_0}$

FIG. 23
DISTRIBUTION OF
$\frac{\sqrt{\overline{v'^2}}}{u_0}$

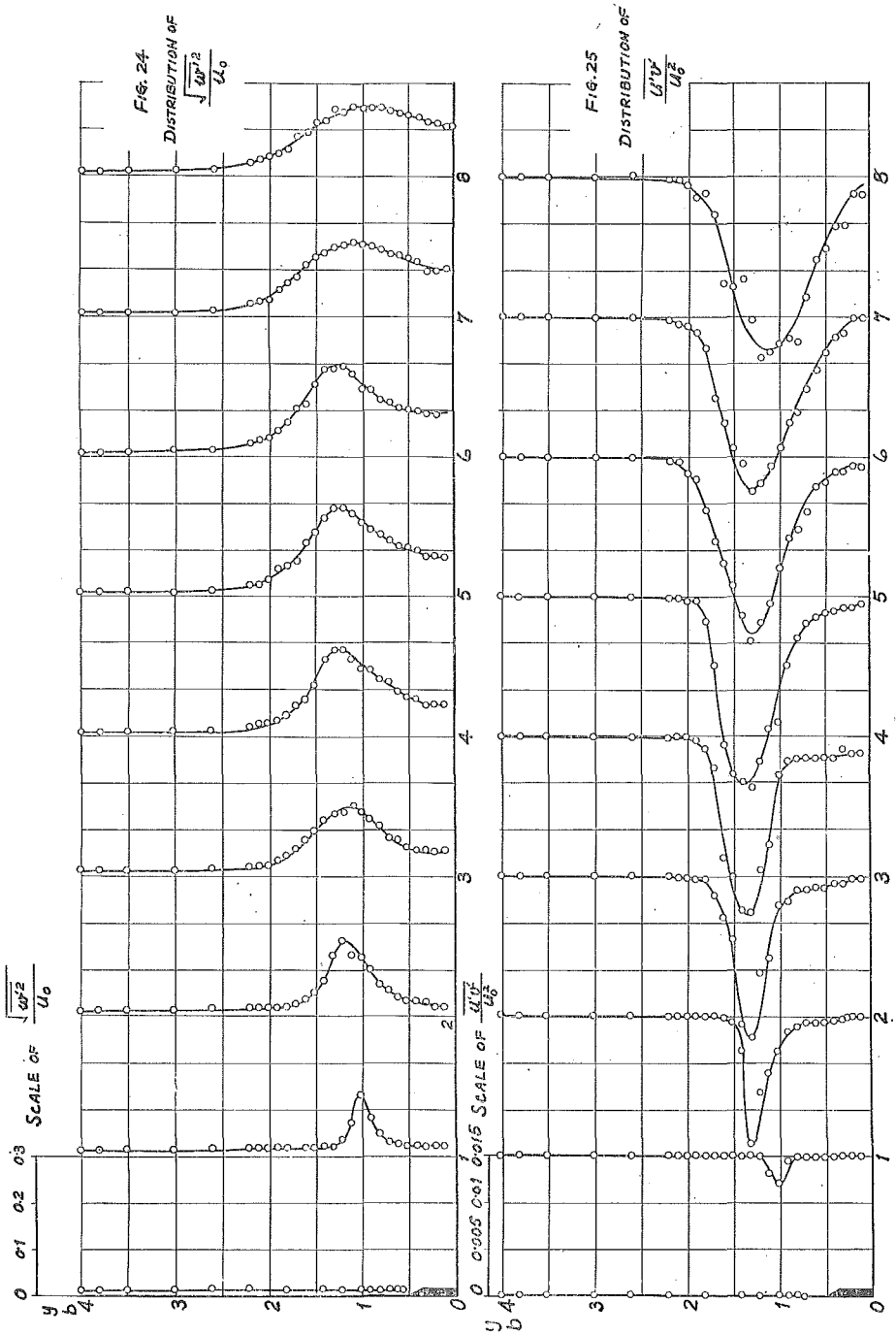
FIG. 24.
DISTRIBUTION OF
$\frac{\sqrt{\overline{u'^2}}}{U_0}$
FIG. 25
DISTRIBUTION OF
$\frac{\overline{u'v'}}{U_0^2}$
SCALE OF $\frac{\sqrt{\overline{u'^2}}}{U_0}$
0 0·1 0·2 0·3
SCALE OF $\frac{\overline{u'v'}}{U_0^2}$
0 0·005 0·01 0·015
$\frac{y}{b}$
0 1 2 3 4
1 2 3 4 5 6 7 8

Discussion of Results

1. Mean flow.

It may be worth-while to compare the experimental results to find the influence of the tunnel boundaries upon the eddy. The points of the maximum velocity at several vertical sections which were obtained in Figs. 8, 9, and 20 are plotted on Fig. 26. The results of Fig. 20 are marked with $H/b=\infty$. As will be seen Fig. 26, when the height of the air tunnel is small, the vertical distance from the tail plate to the point of maximum velocity moves. If the border of a wake is understood to be the line which connects the points of maximum velocity at each vertical section behind the test plate, the fact described above means that the height of the tunnel has an influence on the shape of the wake. The comparison of y/b for $H/b=\infty$ and for $H/b=12$ at $x/b=8$ will show that the effect of H/b becomes quite appreciable with distance downstream. The expansion of the border of the wake also be seen in these plots as well as in Figs. 8, 9, and 20.

The magnitudes of the maximum velocity at these points are also plotted in Fig. 26. It can be clearly seen that the constriction effect causes an increase in velocity in the field behind the test plate. It will also be seen that the maximum velocity in this region always appears at the section $x/b\approx 2.5$ instead of at the edge of the test plate. Moreover, it will be noted that the magnitude of the maximum velocity changes along the border of the wake. This fact means that the pressure in the wake should not be understood to be constant as is assumed in the free-streamline theory. The estimation of the location of the points of the maximum velocity becomes difficult when x/b is large, because the border of the wake becomes vague in accordance with the increase of x/b.

Fig. 27 is presented in order to clarify the effect of the limited height of the tunnel upon the size of the eddy. The estimated length L and the maximum height B_{max} of the stable eddy obtained in Figs. 8, 9, and 20 are plotted in this figure. The values $B_{max}/b=1.36$ and $L/b=8.43$ correspond to the size of eddy in the stream-lined tunnel shown in Fig. 20. As described before, the variation of B_{max} and L between the stable eddies shown in Figs. 8 and 20 is small, and judging from the plotting of Fig. 27 it may be understood that $B_{max}/b=1.36$ and $L/b=8.43$ give a fair indication of the size of a stable eddy behind a vertical plate in a half plane in contact with a boundary. The

FIG. 26

MAGNITUDE AND POSITION OF THE MAXIMUM VELOCITY

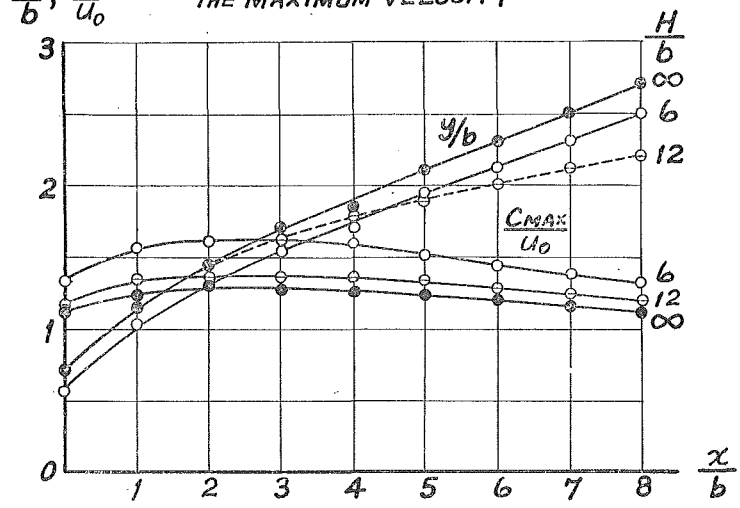

FIG. 27

COMPARISON OF THE SIZES OF THE EDDIES

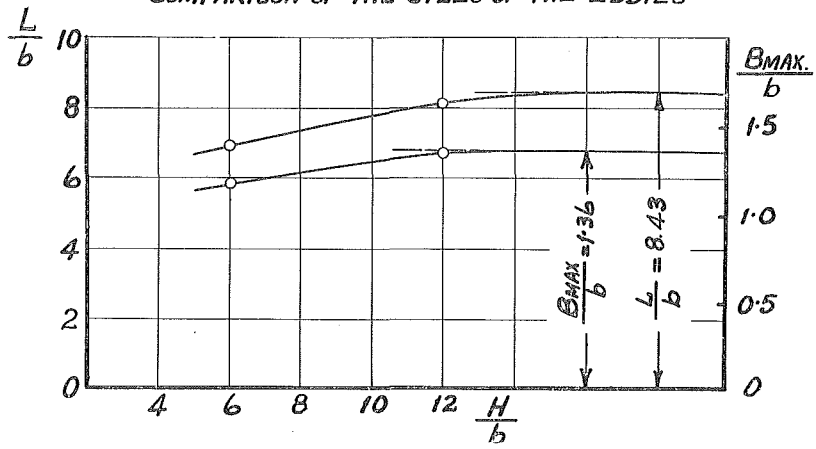

effect of H/b on the size of the stable eddy will also be clearly seen in Fig. 27.

The combination of the velocity measurement and the pressure measurement gives the variation of the total head in the field behind the plate. The results for several vertical sections are shown in Fig. 28.

As will be seen in this figure, the total head begins to decrease at the border of the wake, and the smaller the value of x/b, the larger

Fig. 28

VARIATION OF THE TOTAL HEAD

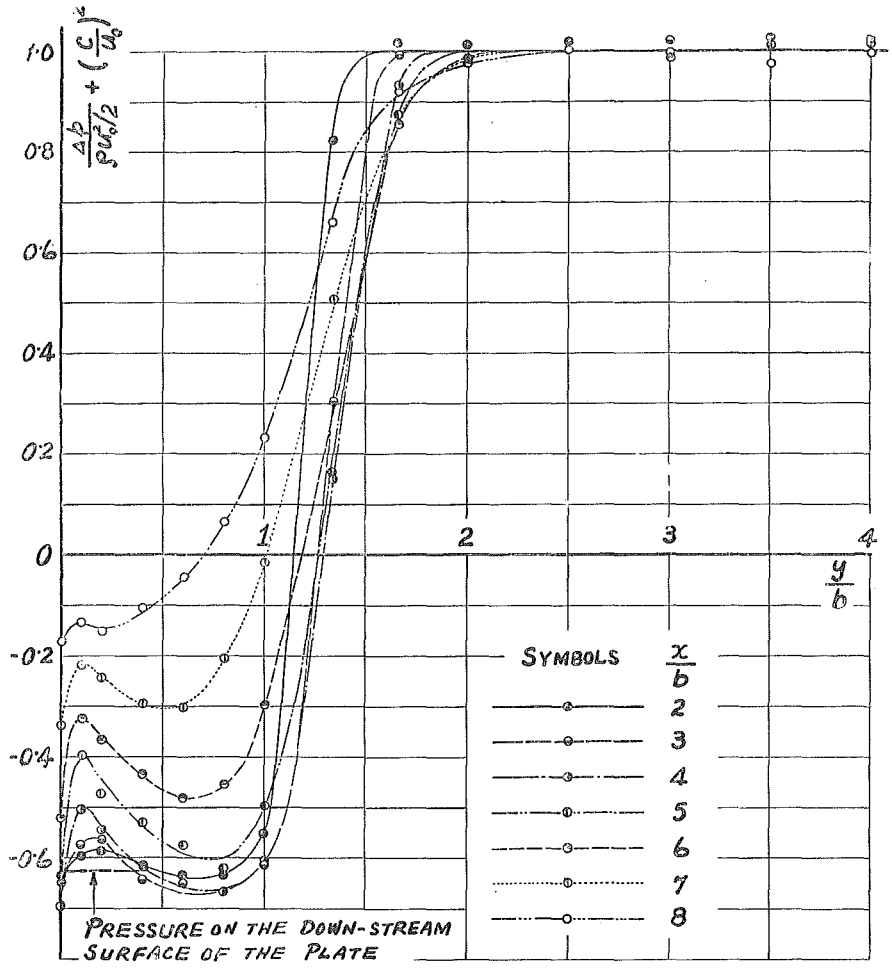

the gradient of the total head. When x/b is small, the total head attains practically a constant value, as do also the pressure variations already shown in Fig. 21. As will further be seen in Fig. 28, the total head is practically unity outside the wake in a dimensionless expression. Since the reasonability of the velocity measurement has already been shown, this fact means that the pressure measurement was also properly performed.

It is also seen that the total head and the pressure both increase with x/b. This fact may be caused by the decrease of the velocity at the border of the wake and by the mixing process of the flow behind the plate. The total head, as shown in Fig. 28, decreases rapidly in the wake although it begins to increase at a position near the tail plate. This phenomenon may be caused by a backward flow within the eddy. The same behavior is seen in the pressure distribution in Fig. 21.

The distributions of the horizontal component and the vertical component of velocity were also estimated and they are shown in Figs. 29 and 30.

As already explained, the estimation of the direction of flow was performed in two ways—one directly with the 30.6° cylinder and the other with the 180° cylinder by successive approximation. The direction of flow near the border of the wake had previously been determined by Fage and Johansen [2] for a flat plate without tail plate, using the device of the shielding effect of a cylinder against a hot wire. As a cylinder was used in the present experimental work, the author attempted to compare the workability of the 30.6° cylinder with the results they obtained. The experiment was performed in the parallel test section before inserting the stream-line ceiling and floor, without tail plate, and it was found that the evaluation with 30.6° cylinder agreed fairly well with the Fage and Johansen result. This was one reason why the cylinders were used in the present study. They had to employ an extrapolating method for the estimation of the direction of flow inside the border of the wake, where the 30.6° cylinder did not work. This fact can be seen quite easily. After determining the direction of flow by the pressure balance between the two holes, the velocity head should be obtainable by setting the two holes in turn at the stagnation point on the cylinder. These two readings did not agree when the cylinder was located in the region of steep velocity gradient. Furthermore, the duplicate measurement with the 180° cylinder showed that use of the 30.6° cylinder gave smaller values of

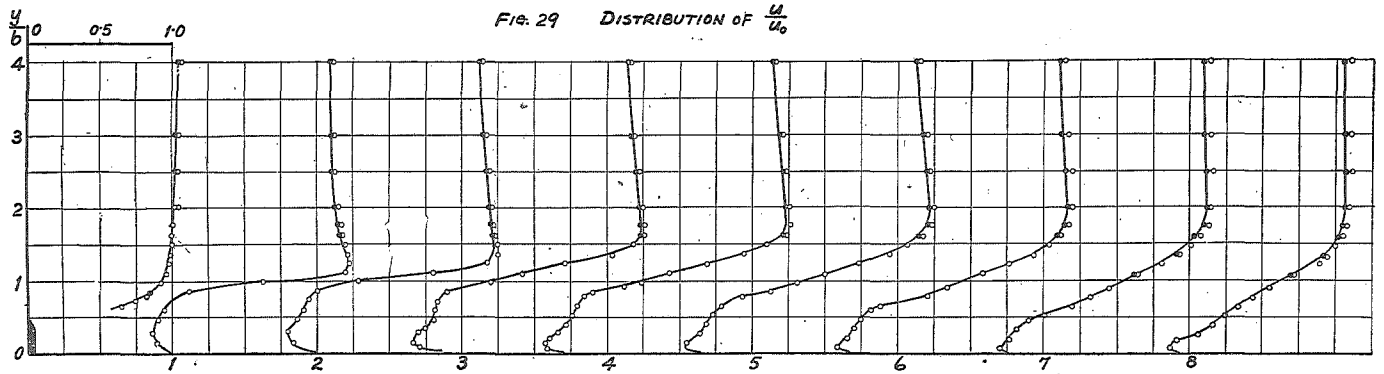

FIG. 29 DISTRIBUTION OF $\frac{u}{u_0}$

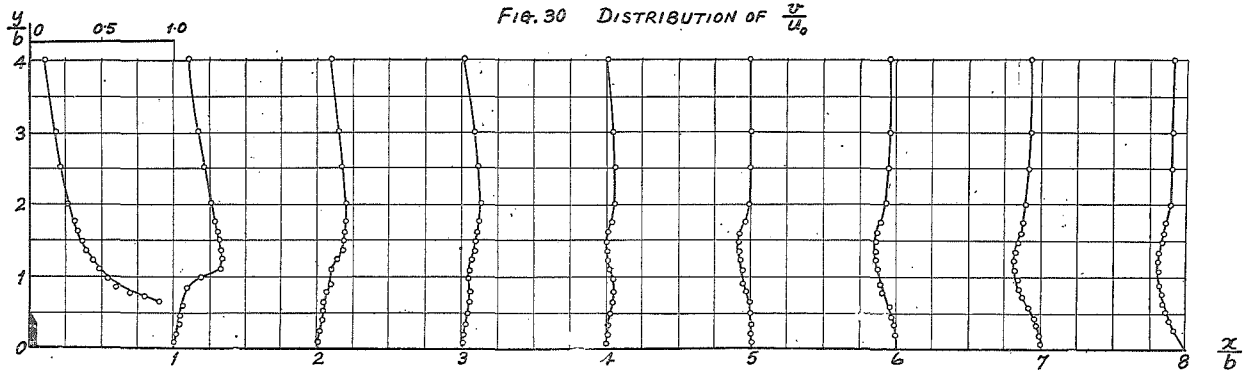

FIG. 30 DISTRIBUTION OF $\frac{v}{u_0}$

α than that indicated by the 180° cylinder in the region of shear flow. A possible cause of the error in this kind of instrumentation when used in shear flow will be discussed analytically in the Appendix.

2. Correction of the velocity distribution and of the pressure distribution.

As the ceiling and the floor of the test section were formed according to the shape of a streamline caused by flow around a Rankine oval, if the shape of the boundaries was correct, the actual results of the velocity measurements must be identical with those which one can obtain analytically for the flow around the imaginary Rankine oval. The latter resulted from a combination of an imaginary source, sink, and uniform flow. The complex potentials of the source, sink, and uniform flow are $w_1=-m\log z_1$, $w_2=m\log z_2$, and $w_3=-u_0 z$, respectively. Accordingly, the velocity components which will be derived from these complex potentials must be

$$u=\frac{mx_1}{x_1^2+y_1^2}-\frac{mx_2}{x_2^2+y_2^2}+u_0$$

$$v=\frac{my_1}{x_1^2+y_1^2}-\frac{my_2}{x_2^2+y_2^2}$$

Herein x_1 and y_1 are the distance from the source to an arbitrary point, and x_2, y_2 are the corresponding distance from the sink. Since the strengths of the imaginary source and sink were selected to be $m/u_0=6.08$, the dimensionless forms of these equations are

$$\frac{u}{u_0}=\frac{1}{6.08}\frac{x_1}{x_1^2+y_1^2}-\frac{1}{6.08}\frac{x_2}{x_2^2+y_2^2}+1 \tag{21}$$

$$\frac{v}{u_0}=\frac{1}{6.08}\frac{y_1}{x_1^2+y_1^2}-\frac{1}{6.08}\frac{y_2}{x_2^2+y_2^2} \tag{22}$$

$$\frac{c}{u_0}=\sqrt{\left(\frac{u}{u_0}\right)^2+\left(\frac{u}{v_0}\right)^2} \tag{23}$$

It is quite obvious that these equations would not be applicable exactly for the flow inside the wake, but for convenience the computations were carried out in the range $2\leqq y\leqq 4$. The results of the computations and the results of the actual measurements are listed in Table 6 for the purpose of comparison.

A close inspection of this table will show that the differences among the analytical values and the experimental values are very small when the position of observation is near the test plate and that they

TAELB 6.

(Figures in parentheses are interpolated)

	$x/b=0$		$x/b=1.0$		$x/b=2.0$		$x/b=3.0$		$x/b=4.0$	
y/b	Eq.(23)	Experiment	Eq.(23)	Exper.	Eq.(23)	Exper.	Eq.(23)	Exper.	Eq.(23)	Exper.
4.0	1.052	1.07	1.089	1.108	1.119	1.139	1.135	1.161	1.137	1.17
3.5	1.054	(1.07)	1.102	(1.12)	1.138	(1.16)	1.154	(1.17)	1.158	(1.19)
3.0	1.055	1.063	1.120	1.033	1.162	1.180	1.181	1.198	1.184	1.217
2.5	1.056	1.052	1.144	1.14	1.197	1.196	1.212	1.226	1.213	1.232
2.0	1.053	1.063	1.185	1.178	1.238	1.225	1.244	1.249	1.243	1.265
	$x/b=5.0$		$x/b=6.0$		$x/b=7.0$		$x/b=8.0$			
y/b	Eq.(23)	Exper.	Eq.(23)	Exper.	Eq.(23)	Exper.	Eq.(23)	Exper.		
4.0	1.128	1.158	1.072	1.151	1.072	1.14	1.030	1.110		
3.5	1.148	(1.17)	1.080	(1.16)	1.081	(1.14)	1.034	(1.10)		
3.0	1.171	1.204	1.090	1.17	1.091	1.142	1.025	1.108		
2.5	1.207	1.22	1.105	1.197	1 105	1.155	1.015	1.113		
2.0	1.248	1.242	1.128	1.2	1.128	1.152	0.991	1.10		

become larger and larger as it moves downstream. In all cases, the experimental values are higher than the analytical values. These facts show that there must be some throttling effect on the air. In order to estimate the displacement thickness of the wake, measurements of velocity distributions at two vertical sections far downstream from the test plate were added. The variation of the displacement thickness of the wake in the longitudinal direction is shown in the upper half of Fig. 31. The shaded part of the imaginary Rankine oval was taken into consideration in the estimation of the tunnel shape. The displacement thickness of the wake was computed for the following equation:

$$\frac{\delta^*}{b}=\int_0^{\frac{\delta}{b}}\left(1-\frac{u}{u_0}\right)d\left(\frac{y}{b}\right) \tag{24}$$

Herein δ represents the value of y where the maximum velocity was first observed. The remaining part of the displacement thickness of the wake after deducting the area occupied by the Rankine oval must also be taken care of, which can be done by replacing it with a proper distribution of doublets.

In order to clarify the situation, a schematic representation is given in Fig. 33. The head forms shown correspond to a body in a flow.

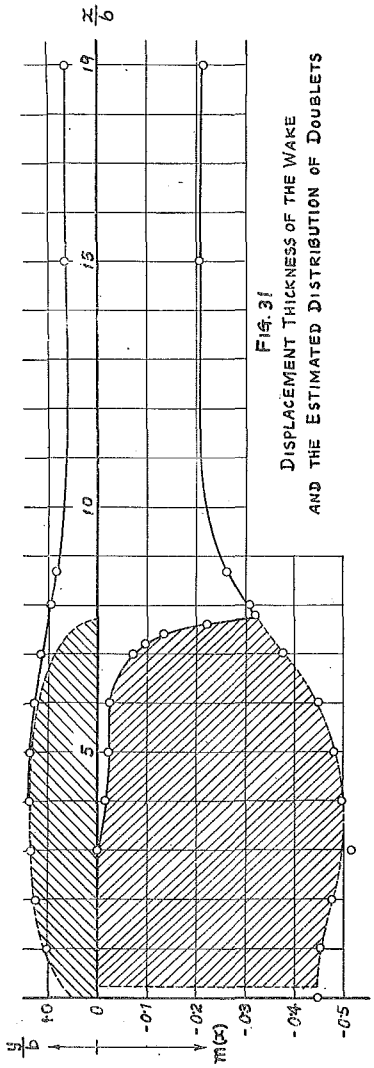

FIG. 31
DISPLACEMENT THICKNESS OF THE WAKE AND THE ESTIMATED DISTRIBUTION OF DOUBLETS

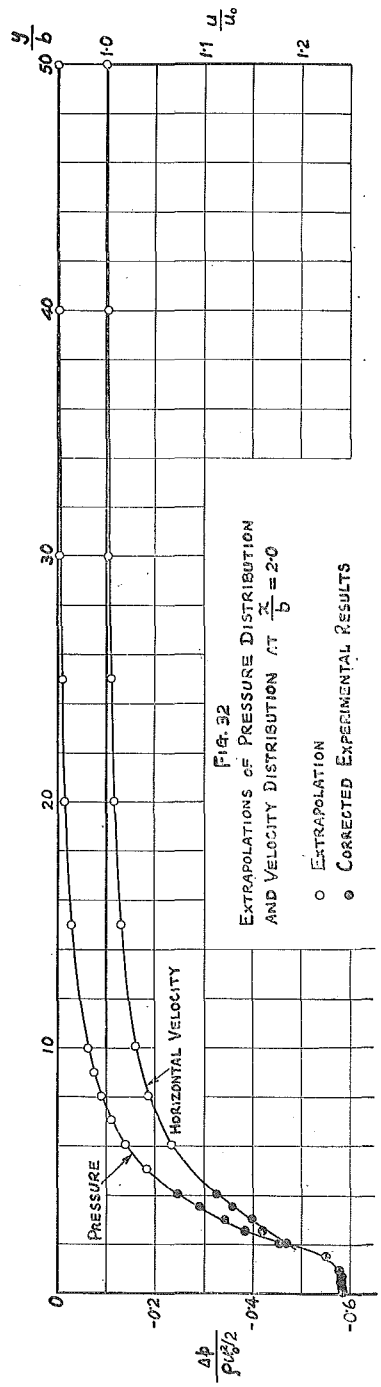

FIG. 32
EXTRAPOLATIONS OF PRESSURE DISTRIBUTION AND VELOCITY DISTRIBUTION AT $\frac{x}{b} = 2{\cdot}0$

Figure 33 (A) shows the case for which the spacing is infinite. On the other hand, the interference of the wind tunnel wall will be investigated by means of an infinite series of images of the body as shown in Fig. 33 (B).

The purpose of the present study is to investigate the case shown in Fig. 33 (A), but actually it was the field shown in Fig. 33 (B) that was measured, because only the upstream portion—i. e., the stable eddy—was used in designing the form of the ceiling and the floor of the tunnel. In other words, the head forms shown in Fig. 33 correspond to the remaining part of the displacement thickness of the wake to be considered. At first, the field shown in Fig. 33 (B) will be considered.

Fig. 33

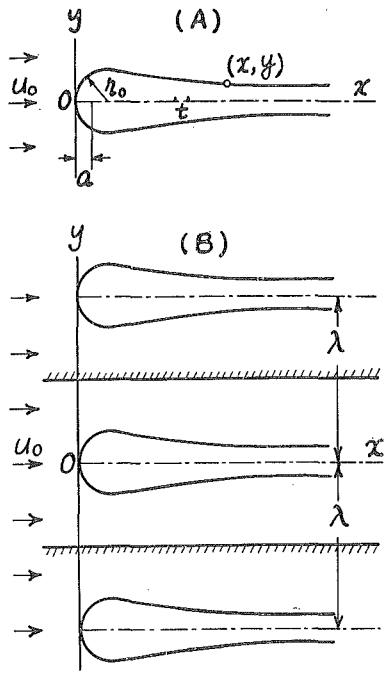

Generally, the complex potential of source located on the y axis at equal distance λ is

$$w_1 = c\left[\log z + \log(z-i\lambda) + \log(z+i\lambda) + \log(z-2i\lambda) + \log(z+2i\lambda) + \cdots\right]$$

An addition of a constant or constants to this equation does not change the flow pattern in this field. Consequently,

$$\begin{aligned} w_1 &= c\left[\log_e z + \log_e(z-i\lambda) + \log_e(z+i\lambda) + \log_e(z-2i\lambda) + \log_e(z+2i\lambda) + \cdots\right] \\ &\quad + c\left[\log_e \frac{\pi}{\lambda} - \log_e \lambda^2 - \log_e 4\lambda^2 - \cdots\right] \\ &= c\log_e\left[\frac{\pi z}{\lambda}\left(1+\frac{z^2}{\lambda^2}\right)\left(1+\frac{z^2}{4\lambda^2}\right)\cdots\right] \\ &= c\log_e\left[\frac{\pi z}{\lambda}\prod_{n=1}^{\infty}\left(1+\frac{z^2}{n^2\lambda^2}\right)\right] \\ &= c\log_e \sinh\frac{\pi z}{\lambda} \end{aligned} \tag{25}$$

When these sources located on the y axis are replaced with doublets,

the complex potential of these doublets can be obtained by differentiating Eq. (25) with respect to z:

$$w_3 = \frac{d}{dz}\left(c \log_e \sinh \frac{\pi z}{\lambda}\right) = \frac{\pi c}{\lambda} \coth \frac{\pi z}{\lambda}$$

Accordingly, when the doublets are distributed on the x axis and on straight lines which are parallel to the x-axis with a spacing of λ, so that the strength at $z=t$, $t\pm i$, $t\pm 2i$ and so on is $M(t)$, the complex potential of this distribution of doublets must be

$$w_3 = \frac{\pi}{\lambda}\int_a^b M(t) \coth \frac{\pi[(x-t)+iy]}{\lambda}\, dt \tag{26}$$

Here (x, y) are the coordinates of a doublet element, and a and b are limits of the location of the distribution of doublets. The separation of the imaginary and real parts of Eq. (26) gives

$$\phi_3 = \frac{\pi}{\lambda}\int_a^b M(t) \frac{\sinh \frac{2\pi(x-t)}{\lambda}}{\cosh \frac{2\pi(x-t)}{\lambda} - \cos \frac{2\pi y}{\lambda}}\, dt$$

$$\psi_3 = -\frac{\pi}{\lambda}\int_a^b M(t) \frac{\sin \frac{2\pi}{\lambda} y}{\cosh \frac{2\pi(x-t)}{\lambda} - \cos \frac{2\pi y}{\lambda}}\, dt$$

When a parallel uniform flow $w_4 = -u_0 z$ is added to above equation, one obtains

$$\phi = -u_0 x + \frac{u_0 \pi}{\lambda}\int_a^b m(t) \frac{\sinh \frac{2\pi(x-t)}{\lambda}}{\cosh \frac{2\pi(x-t)}{\lambda} - \cos \frac{2\pi}{\lambda} y}\, dt$$

$$\psi = -u_0 y + \frac{u_0 \pi}{\lambda}\int_a^b m(t) \frac{\sin \frac{2\pi}{\lambda} y}{\cosh \frac{2\pi(x-t)}{\lambda} - \cos \frac{2\pi}{\lambda} y}\, dt$$

in which $M(t) = u_0 m(t)$. Consequently, the velocity in this field must be, in dimensionless form,

$$\frac{u_a}{u_0} = 1 - \frac{2\pi^2}{\lambda^2}\int_a^b m(t) \frac{1 - \cosh \frac{2\pi(x-t)}{\lambda} \cos \frac{2\pi}{\lambda} y}{\left[\cosh \frac{2\pi(x-t)}{\lambda} - \cos \frac{2\pi}{\lambda} y\right]^2} dt \tag{27}$$

$$\frac{v_a}{u_0}=\frac{2\pi^2}{\lambda}\int_a^b m(t)\frac{\sinh\frac{2\pi(x-t)}{\lambda}\sin\frac{2\pi}{\lambda}y}{\left[\cosh\frac{2\pi(x-t)}{\lambda}-\cos\frac{2\pi}{\lambda}y\right]^2}dt \tag{28}$$

$$\frac{c_a}{u_0}=\sqrt{\left(\frac{u_a}{u_0}\right)^2+\left(\frac{v_a}{u_0}\right)^2} \tag{29}$$

Next, the field of the distribution of doublets in one row on the real axis shown in Fig. 33 (A) will be considered. The complex potential for a point doublet is $w_5=\frac{\mu}{z}=\phi_5+i\psi_5$. Accordingly,

$$\phi_5+i\psi_5=\frac{\mu(x-iy)}{x^2+y^2}$$

and

$$\psi_5=-\frac{\mu y}{x^2+y^2}$$

When the doublets are distributed from $x=a$ to $x=b$ with the strength of $\mu=u_0m(t)$ at $x=t$,

$$\psi_6=-\int_a^b\frac{u_0m(t)y}{(x-t)^2+y^2}dt$$

When a uniform flow is superposed upon this field,

$$\psi=-u_0\left[y+\int_a^b\frac{m(t)y}{(x-t)^2+y^2}dt\right] \tag{30}$$

Hence, the velocity which will be induced by this stream function is

$$\frac{u_\beta}{u_0}=1+\int_a^b m(t)\frac{(x-t)^2-y^2}{[(x-t)^2+y^2]^2}dt \tag{31}$$

$$\frac{v_\beta}{u_0}=2\int_a^b m(t)\frac{y(x-t)}{[(x-t)^2+y^2]^2}dt \tag{32}$$

$$\frac{c_\beta}{u_0}=\sqrt{\left(\frac{u_\beta}{u_0}\right)^2+\left(\frac{v_\beta}{u_0}\right)^2} \tag{33}$$

If $\Delta c_1/u_0$ represents the error which will be caused by the part of the imaginary Rankine oval, and if $\Delta c_2/u_0$ represedts the error caused by the other part of the displacement thickness of the wake, the total error which may be introduced by the whole is approximately $(\Delta c_1+\Delta c_2)/u_0$. As the tunnel was formed so that $\Delta c_1/u_0=0$, the possible error included in the results of experiment is $\Delta c_2/u_0$. If c/u_0 represents the

local velocity which one is interested to measure, the actual measurement was $(c+\Delta c_2)/u_0$ instead of c/u_0. As obtained above, $(c+\Delta c_2)/u_0$ corresponds to c_α/u_0 in Eq. (29), and c/u_0 corresponds to c_β/u_0 in Eq. (33). Consequently,

$$\frac{c+\Delta c_2}{u_0} = \frac{c_\alpha}{u_0}$$

$$\frac{c}{u_0} = \frac{c_\beta}{u_0}$$

From these equations, one obtains

$$\frac{c}{c+\Delta c_2} = \frac{c_\beta}{c_\alpha} = K \tag{34}$$

or

$$\frac{c}{u_0} = K\frac{c+\Delta c_2}{u_0} \tag{35}$$

Since $(c+\Delta c_2)/u_0$ was the quantily actually measured, including the error of the tunnel interference, Eq. (35) means that K is the correction factor for velocity. In order to obtain K defined by Eq. (34), $m(t)$ must first be found.

The stream function ψ given in Eq. (30) gives an imaginary stream line which will be caused by an imaginary body corresponding to the displacement thickness of the wake remaining after deducting the part of the Rankine oval described before. If $y(x)$ represents the difference of the ordinates between the imaginary Rankine oval and the displacement of the wake, $y(x)$ must be the ordinate of the imaginary body to determine the value of $m(t)$ signifying the strength of the distributed doublets. Since the stream function is zero on the imaginary body, Eq. (30) gives

$$\int_a^b \frac{m(t)\,y(x)}{(x-t)^2+y^2(x)}\,dt = -y(x)$$

This is an integral equation of the Fredholm type of the first kind. As a first approximation, assume that $m(t)=m(x)$. Then,

$$m(x)\int_a^b \frac{y(x)}{(x-t)^2+y^2(x)}\,dt = -y(x)$$

or

$$m(x)\left[\tan^{-1}\frac{t-x}{y(x)}\right]_a^b = -y(x)$$

When $(b-x)$ is large compared to $y(x)$, the above equation gives

$$m(x)=\frac{-y(x)}{\frac{\pi}{2}+\tan^{-1}\frac{x-a}{y(x)}}=\frac{y(x)}{\tan^{-1}\frac{y(x)}{x-a}} \tag{36}$$

By inspection of Fig. 31, the quantity "a" was selected to be $x/b=3$, and the value of $y(x)$ and the values of $m(x)$ computed with Eq. (36) are shown in Table 7 for a series of values of x/b.

TABLE 7.

x/b	3	4	5	6	7	7.2	7.4
y/b	0	0.0564	0.0726	0.0837	0.2267	0.303	0.418
$m(x)$	0	− 0.0183	− 0.0234	− 0.0269	− 0.0735	− 0.0988	− 0.1371
x/b	7.6	7.8	8	8.6	15	19	
y/b	0.663	0.975	0.9395	0.807	0.6412	0.6738	
$m(x)$	− 0.2212	− 0.325	− 0.311	− 0.264	− 0.2065	− 0.2168	

$x/b=19$ is large enough for the computation of Eqs. (29) and (33). The variation of $y(x)$ will be seen in the upper half of Fig. 31 and the variation of $m(x)$ in tihe lower half.

Since it was found that it would be better to employ the whole region of the displacement thickness of the wake in determining the form of the ceiling and the floor of the air tunnel, the distribution of $m(x)$ in this case is also shown in Fig. 31, for the purpose of future reference. The shaded part corresponds to the portion of the imaginary Rankine oval which was used in this study. The accuracy with regard to the beginning point of the distribution of doublets is discussed in the paper of L. Landweber [9]. As shown in Fig. 33 (A), the beginning point is recommended to be half of the radius of curvature ($a=r_0/2$) of the head form. If the head part of the Rankine oval is considered for this purpose, the mathematical expression for the radius of curvature for the imaginary Rankine oval which was used in this study is

$$\rho=\frac{\left[\left(\frac{\cos\alpha}{\sin\alpha}-\frac{1}{\sin\alpha}-\frac{\sin\alpha}{6.08}\right)^2+x^2\right]^{\frac{3}{2}}}{\left[\left(\frac{\cos\alpha}{\sin\alpha}-\frac{1}{\sin\alpha}-\frac{\sin\alpha}{6.08}\right)^2+12.16x^2\cos\alpha\left(\frac{\cos\alpha}{\sin^2\alpha}-\frac{1}{\sin^2\alpha}-\frac{1}{6.08}\right)+x^2(13.16+2\cos\alpha)\right]}$$

in which $\alpha=6.08y$. This equation can be obtained from Eq. (10)'. The evaluation of this equation for $y=0$ gives $\rho/b=0.555$. Referring to Fig. 14, this value seems to be too small for practical purposes, and so a proper radius of curvature was estimated to be $\rho/b=0.79$. If $\rho/b=0.79$ is employed, the distribution of doublets begins at $x/b=0.242$ as shown in Fig. 31. This distribution of doublets may be helpful for the extrapolation of velocity distribution at the section where x/b is large.

As only part of the displacement thickness of the wake, excluding the region of the imaginary Rankine oval, was used in the present study, the radius of curvature at $x/b=3.0$ was understood to be zero, and the distribution of the doublets was started from that point. After computing Eqs. (29) and (33), the correction factor K was computed by Eq. (34), the results of which are plotted in Fig. 34.

FIG. 34

CORRECTION FACTOR FOR VELOCITY

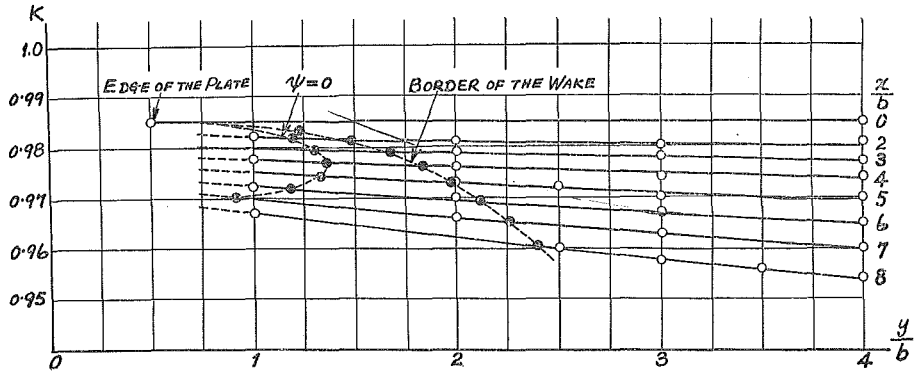

Both the border of the wake where the maximum velocity appears and the profile of the eddy are indicated in this figure, in order to show the probable percentage at these positions. When the actual results of measurement of velocity are multiplied by K as read in Fig. 34, the approximate corrections can be performed according to Eq. (35). Actually, this device of correction is applicable only for the magnitude of velocity, because the value of u is usually much larger than v, as will be seen in Figs. 29 and 30. Since the contribution of v to the magnitude of the velocity is very small, the correction of the direction of flow was not performed in this study.

As this device of correction is applicable outside the wake where

the Bernoulli equation is valid, the pressure distribution can be corrected simultaneously by the following relation:

$$\frac{\Delta p}{\frac{1}{2}\rho u_0^2} = 1 - \left(\frac{c}{u_0}\right)^2 \tag{37}$$

The results of the velocity corrections are shown in Table 8 for convenience in comparing with Table 6. The results of velocity calculations obtained from the flow around the imaginary Rankine oval are repeated in this table.

TABLE 8.

	$x/b = 0$		$x/b = 1.0$		$x/b = 2.0$	
y/b	Eq. (23)	Corrected c/u_0	Eq. (23)	Corrected c/u_0	Eq. (23)	Corrected c/u
4.0	1.052	1.053	1.089	1.089	1.119	1.116
3.5	1.054	1.053	1.102	1.100	1.138	1.137
3.0	1.055	1.047	1.120	1.113	1.162	1.158
2.5	1.056	1.036	1.144	1.120	1.197	1.177
2.0	1.053	1.049	1.185	1.158	1.238	1.207
	$x/b = 3.0$		$x/b = 4.0$		$x/b = 5.0$	
y/b	Eq. (23)	Corrected c/u_0	Eq. (23)	Corrected c/u_0	Eq. (23)	Corrected c/u_0
4.0	1.135	1.134	1.137	1.131	1.128	1.125
3.5	1.154	1.144	1.158	1.159	1.148	1.135
3.0	1.181	1.171	1.184	1.186	1.171	1.170
2.5	1.212	1.200	1.213	1.210	1.207	1.186
2.0	1.244	1.221	1.243	1.225	1.248	1.210
	$x/b = 6.0$		$x/b = 7.0$		$x/b = 8.0$	
y/b	Eq. (23)	Corrected c/u_0	Eq. (23)	Corrected c/u_0	Eq. (23)	Corrected c/u_0
4.0	1.072	1.111	1.072	1.094	1.030	1.060
3.5	1.082	1.121	1.081	1.095	1.034	1.051
3.0	1.090	1.131	1.091	1.100	1.025	1.061
2.5	1.105	1.159	1.105	1.114	1.015	1.070
2.0	1.128	1.161	1.128	1.113	0.991	1.058

A close inspection of Table 8 will show that the corrected velocities and the results estimated from Eq. (23) agree fairly well outside the wake. When x/b is large, the difference between these two estimations seems to increase. This means that Eq. (23) must be replaced by Eq. (33) when the point of observation is in the downstream region. Still, the difference is only a few percent. It should be understood that the computations of velocity were very carefully performed. The results shown in Table 8 are plotted in Fig. 20, and they are connected with velocity-distribution curves. The same device of correction was performed for u/u_0 and the results are shown in Fig. 29. As the magnitude v/u_0 was usually small, correction of the latter does not make much difference.

The correction of the pressure distribution was performed at the same time in the region outside and a short distance inside the wake where the velocity correction was significant. The corrections of velocity and pressure well inside the wake, however, were quite different, since the assumption of irrotational flow could no longer be made. The Navier-Stokes equation in tensor notation is

$$\frac{\partial u_i}{\partial t}+u_k\frac{\partial u_i}{\partial x_k}=-\frac{1}{\rho}\frac{\partial P}{\partial x_i}+\nu\frac{\partial}{\partial x_k}\left(\frac{\partial u_i}{\partial x_k}+\frac{\partial u_k}{\partial x_i}\right) \tag{38}$$

Since the continuity relation gives $\partial u_k/\partial x_k=0$, the second term on the right-hand side of this equation becomes

$$\nu\frac{\partial}{\partial x_k}\left(\frac{\partial u_i}{\partial x_k}+\frac{\partial u_k}{\partial x_i}\right)=\nu\frac{\partial^2 u_i}{\partial x_k\partial x_k}$$

Accordingly,

$$\frac{\partial u_i}{\partial t}+u_k\frac{\partial u_i}{\partial x_k}=-\frac{1}{\rho}\frac{\partial P}{\partial x_i}+\nu\frac{\partial^2 u_i}{\partial x_k\partial x_k} \tag{39}$$

When the relations $u_i=U_i+u_i'$ and $P=\bar{P}+p'$ are substituted, this equation becomes

$$\frac{\partial}{\partial t}(U_i+u_i')+(U_k+u_k')\frac{\partial}{\partial x_k}(U_i+u_i')=-\frac{1}{\rho}\frac{\partial(\bar{P}+p')}{\partial x_i}+\nu\frac{\partial^2(U_i+u_i')}{\partial x_k\partial x_k} \tag{40}$$

U and $\bar{P}$ represent, of course, the mean velocity and the mean piezometric pressure, respectively; u' and p' are the fluctuating components of U and $\bar{P}$, respectively. Since $\overline{u_i'}=0$, $\partial U_k/\partial x_k=0$, $\dfrac{\overline{\partial u_k'}}{\partial x_k}=0$, and $\overline{p'}=0$,

when a time average of Eq. (40) is considered, one obtains

$$\frac{\partial U_i}{\partial t}+U_k\frac{\partial U_i}{\partial x_k}+\overline{u_k'\frac{\partial u_i'}{\partial x_k}}=-\frac{1}{\rho}\frac{\partial \bar{P}}{\partial x_i}+\nu\frac{\partial^2 U_i}{\partial x_k\partial x_k} \tag{41}$$

This is the Reynolds equation. In the case of a two dimensional flow, Eq. (41) leads to the following equations:

$$\begin{aligned}&\frac{\partial u}{\partial t}+u\frac{\partial u}{\partial x}+v\frac{\partial u}{\partial y}+\overline{u'\frac{\partial u'}{\partial x}}+\overline{v'\frac{\partial u'}{\partial y}}=-\frac{1}{\rho}\frac{\partial \bar{P}}{\partial x}+\nu\left(\frac{\partial^2 u}{\partial x^2}+\frac{\partial^2 u}{\partial y^2}\right)\\&\frac{\partial v}{\partial t}+u\frac{\partial v}{\partial x}+v\frac{\partial v}{\partial y}+\overline{u'\frac{\partial v'}{\partial x}}+\overline{v'\frac{\partial v'}{\partial y}}=-\frac{1}{\rho}\frac{\partial P}{\partial y}+\nu\left(\frac{\partial^2 v}{\partial x^2}+\frac{\partial^2 v}{\partial y^2}\right)\end{aligned} \tag{42}$$

When the flow is steady, the terms $\partial u/\partial t$ and $\partial v/\partial t$ vanish. As the pressure distribution was measured along a vertical section in the present experimental work, consideration of the second of Eqs. (42) is sufficient. Since $\partial u'/\partial x+\partial v'/\partial y=0$,

$$\begin{aligned}\overline{u'\frac{\partial v'}{\partial x}}+\overline{v'\frac{\partial v'}{\partial y}}&=\overline{\frac{\partial}{\partial x}u'v'}+\overline{\frac{\partial v'^2}{\partial y}}-\overline{v'\frac{\partial u'}{\partial x}}-\overline{v'\frac{\partial v'}{\partial y}}\\&=\overline{\frac{\partial}{\partial x}u'v'}+\overline{\frac{\partial v'^2}{\partial y}}\end{aligned}$$

Accordingly, the second of Eqs. (42) becomes

$$\frac{1}{\rho}\frac{\partial \bar{P}}{\partial y}+v\frac{\partial v}{\partial y}+\overline{\frac{\partial v'^2}{\partial y}}=-u\frac{\partial v}{\partial x}+\nu\left(\frac{\partial^2 v}{\partial x^2}+\frac{\partial^2 v}{\partial y^2}\right)-\overline{\frac{\partial u'v'}{\partial x}} \tag{43}$$

With δ as the vertical distance from the tail plate to the border of the wake where the maximum velocity appears, integration of Eq. (43) across the wake from y to δ gives

$$\frac{\bar{P}}{\rho}+\frac{v^2}{2}+\overline{v'^2}=\frac{\bar{P}_1}{\rho}+\frac{v_1^2}{2}+\overline{v_1'^2}+\int_y^\delta\left[u\frac{\partial v}{\partial x}-\nu\left(\frac{\partial^2 v}{\partial x^2}+\frac{\partial^2 v}{\partial y^2}\right)+\overline{\frac{\partial u'v'}{\partial x}}\right]dy \tag{44}$$

The symbols without suffix correspond to the values at an arbitrary point y in the wake, and the suffix 1 means the values at the border of the wake $y=\delta$. The quantity $\overline{v_1'^2}$ is practically zero. Differentiation of Eq. (44) yields

$$\begin{aligned}\frac{\Delta\bar{P}}{\rho}+v\Delta v+\overline{\Delta v'^2}&=\frac{\overline{\Delta P_1}}{\rho}+v_1\Delta v_1\\&+\int_y^\delta\left[u\frac{\partial(\Delta v)}{\partial x}+\Delta u\frac{\partial v}{\partial x}-\nu\left(\frac{\partial^2\Delta v}{\partial x^2}+\frac{\partial^2\Delta v}{\partial y^2}\right)+\overline{\frac{\partial\Delta u'v'}{\partial x}}\right]dy\end{aligned}$$

Since

$$\frac{\partial(\Delta v)}{\partial y} = -\frac{\partial(\Delta u)}{\partial x}, \quad \left[-\frac{\partial(\Delta u)}{\partial x}\right]_y^\delta = \frac{\partial(\Delta u)}{\partial x} - \frac{\partial(\Delta u_1)}{\partial x}$$

the foregoing equation becomes

$$\frac{\overline{\Delta P}}{\rho} + v\Delta v + \overline{\Delta v'^2} = \frac{\overline{\Delta P}_1}{\rho} + v_1\Delta v_1 - \nu\left(\frac{\partial \Delta u}{\partial x} - \frac{\partial \Delta u_1}{\partial x}\right) + \int_y^\delta \left[u\frac{\partial \Delta v}{\partial x} + \Delta u\frac{\partial v}{\partial x} - \nu\frac{\partial^2 \Delta v}{\partial x^2} + \frac{\partial \overline{\Delta u'v'}}{\partial x}\right] dy$$

When dynamical similarity is assumed, one has

$$\begin{aligned} K' &= 1-K \\ \Delta u &= K'u \\ \overline{\Delta v'^2} &= 2K'\overline{v'^2} \\ \Delta v_1 &= K'v_1 \\ \overline{\Delta u'v'} &= 2K'\overline{u'v'} \end{aligned}$$

Accordingly, since $\frac{\overline{\Delta P}_1}{\rho} = -(u_1\Delta u_1 + v_1\Delta v_1)$,

$$\frac{\overline{\Delta P}}{\rho} = -K'\left\{u_1^2 + v_1^2 + v^2 + \overline{2v'^2} - v_1^2 + \nu\left(\frac{\partial u}{\partial x} - \frac{\partial u_1}{\partial x}\right) - \int_y^\delta \left[2u\frac{\partial v}{\partial x} - \nu\frac{\partial^2 v}{\partial x^2} + 2\frac{\partial \overline{u'v'}}{\partial x}\right] dy\right\}$$

When this equation is transformed into a dimensionless form,

$$\frac{\overline{\Delta P}}{\frac{1}{2}\rho u_0^2} = -2K'\left[\frac{u_1^2}{u_0} + \frac{v^2}{u_0^2} + \frac{\overline{2v'^2}}{u_0^2} + \frac{1}{R}\frac{\partial\left(\frac{u}{u_0}\right)}{\partial\left(\frac{x}{b}\right)} - \frac{1}{R}\frac{\partial\left(\frac{u_1}{u_0}\right)}{\partial\left(\frac{x}{b}\right)} - 2\int_{\frac{y}{b}}^{\frac{\delta}{b}} \frac{u}{u_0}\frac{\partial\left(\frac{v}{u_0}\right)}{\partial\left(\frac{x}{b}\right)} d\left(\frac{y}{b}\right) + \frac{1}{R}\int_{\frac{y}{b}}^{\frac{\delta}{b}} \frac{\partial^2\left(\frac{v}{u_0}\right)}{\partial\left(\frac{x}{b}\right)^2} d\left(\frac{y}{b}\right) - 2\int_{\frac{y}{b}}^{\frac{\delta}{b}} \frac{\partial\left(\frac{\overline{u'v'}}{u_0^2}\right)}{\partial\left(\frac{x}{b}\right)} d\left(\frac{y}{b}\right)\right] \tag{44}$$

In this equation, $R=bu_0/\nu$. This is the relation which gives the magnitude of the pressure correction in the wake, K being the correction factor already shown in Fig. 34. As will be seen in Eq. (44), the most important term to govern the magnitude of correction of the pressure

is the relative velocity at the border of the wake, which is larger than unity. Consequently, in order to evaluate Eq. (44) the terms which are small compared to unity can be neglected. As the Reynolds number $u_0 b/\nu$ was 5.52×10^4 for the condition of the experiment (as may be seen from the preceding plottings of the experimental results), the terms which are divided by R are very small compared to u_1^2/u_0^2. Fig. 35 is shown for the computation of

$$\int_{\frac{y}{b}}^{\frac{\delta}{b}} \frac{u}{u_0}\frac{\partial\left(\frac{v}{u_0}\right)}{\partial\left(\frac{x}{b}\right)}d\left(\frac{y}{b}\right)$$

FIG. 35

$u\frac{\partial v}{\partial x}-\frac{y}{b}$ RELATION

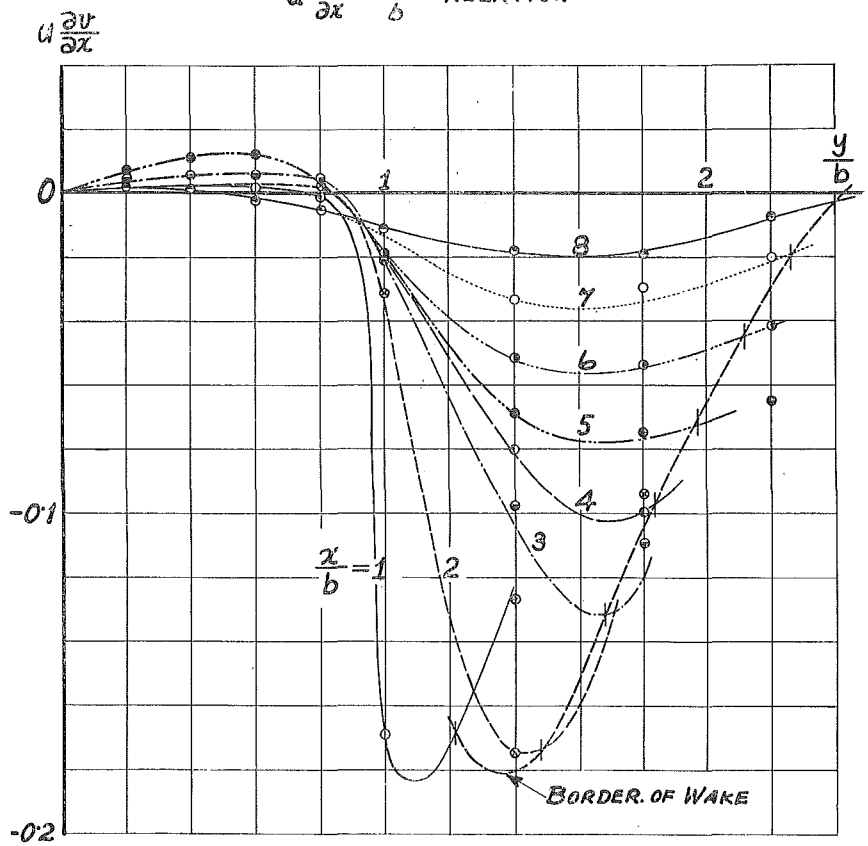

In the vertical axis $u\partial v/\partial x$ indicates the value of $(u/u_0)\partial(v/u_0)/\partial(x/b)$. The border of the wake is shown for convenience of integration in Fig. 35.

The results of the correction of the pressure distribution with the aid of Eq. (44) are all plotted in Fig. 21 as full lines. Evidently, the magnitude of the correction increases with distance downstream, the interference of the air-tunnel boundaries eventually becoming very significant.

3. Estimation of the Drag Coefficient of the Test Plate.

The drag acting on the test plate can be obtained by the integration of the pressure distribution on the surface of the plate. The results of the measurement of the pressure distribution and the corrected results are plotted in Fig. 36. The pressure distribution on the surface of the tail plate is also shown in this figure for reference. On the other hand, one can also estimate the drag of the plate by considering the change in momentum flux between two vertical sections located upstream and downstream from the plate.

a. Integration of the pressure distribution on the surfaces of the test plate.

The integration of the pressure distribution on the surfaces of the test plate shown in Fig. 36 gives

$$\left[\int_0^{0.5} \frac{\Delta p}{\frac{1}{2}\rho u_0^2}\, d\left(\frac{y}{b}\right)\right]_{\text{upstream}} = 0.409$$

and

$$\left[\int_0^{0.5} \frac{\Delta p}{\frac{1}{2}\rho u_0^2}\, d\left(\frac{y}{b}\right)\right]_{\text{downstream}} = -0.281$$

Consequently, the drag coefficient for half width of the test plate is

$$\frac{D/A}{\frac{1}{2}\rho u_0^2} = 0.409 + 0.281 = 0.690 \tag{45}$$

in which D/A is the force per unit area exerted by the flow upon the plate. The pressure on the downstream surface of the test plate was measured at only one piezometer hole; however, as will be seen in Fig. 21, the pressure distribution immediately behind the plate is practically constant, and so the estimation of the force on the down-

FIG. 36
PRESSURE DISTRIBUTION ON THE SURFACE OF THE TEST PLATE

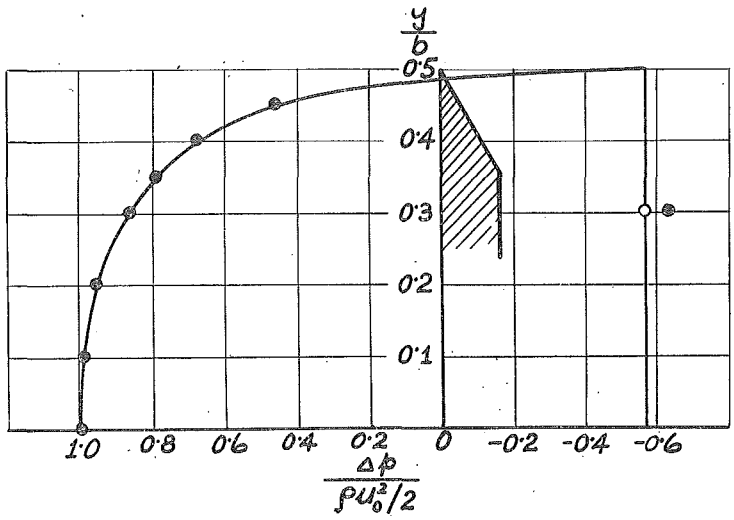

● EXPERIMENT
○ CORRECTED

FIG. 37
PRESSURE DISTRIBUTION ON THE TAIL PLATE

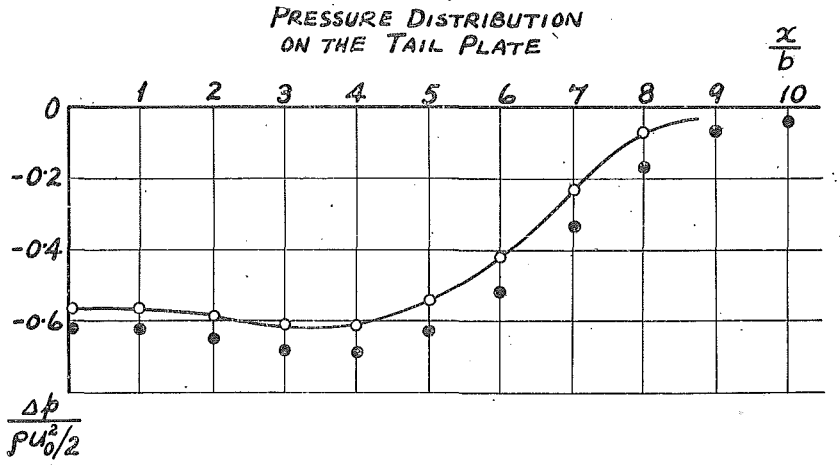

stream surface of the test plate may be considered reasonable. In the case of a flat plate without a tail plate, which was investigated by Fage and Johansen [1].

$$\left[\frac{D/A}{\frac{1}{2}\rho u_0^2}\right]_{\text{upstream}} = 0.75$$

$$\left[\frac{D/A}{\frac{1}{2}\rho u_0^2}\right]_{\text{downstream}} = -1.38$$

Compared with the results observed in the present study, it can be said that the tail plate caused a slight increase in the force acting on the upstream surface of the test plate and a rather remarkable alleviation of the low pressure immediately behind the test plate. The latter effect of a tail plate coincides with the results presented by Hanin [3] for bluff bodies.

b. Estimation of the drag on the test plate by the momentum principle.

It was shown in Table 8 that the corrected velocity distribution outside the wake coincided practically with the velocity distribution around the imaginary Rankine oval which was used for the formation of the test section profile. Since the validity of the Bernoulli equation outside the wake had already been checked, it was considered reasonable to exptrapolate the velocity and pressure distribution, in the region where y/b was larger than 4.0, in accordance with the analytical values for the flow around the imaginary Rankine oval.

A volume integration of the Reynolds equation obtained in Eq. (41) gives

$$\rho\int\frac{\partial U_i}{\partial t}d\varpi+\rho\int U_k\frac{\partial U_i}{\partial x_k}d\varpi+\rho\int\overline{u_k'\frac{\partial u_i'}{\partial x_k}}d\varpi=-\int\frac{\partial P}{\partial x_i}d\varpi+\mu\int\frac{\partial^2 U_i}{\partial x_k\partial x_k}d\varpi \tag{46}$$

Generally, Green's theorem states that

$$\int\frac{\partial G}{\partial x_i}d\varpi=\int n_i G dS$$

in which n_i are the direction cosines of a unit normal vector at surface element dS and the positive direction of the normal is understood to be outward from the surface; G is a function of x, y, and z. Ac-

cordingly, Eq. (46) takes the form

$$\rho\int\frac{\partial U_i}{\partial t}d\varpi+\rho\int n_k U_k U_i dS+\rho\int n_k\overline{u_k' u_i'}dS=-\int n_i P dS+\mu\int n_k\frac{\partial U_i}{\partial x_k}dS \tag{46}'$$

Since $\int(\partial U_i/\partial t)d\varpi=0$ for a steady flow, this equation becomes

$$\rho\int n_k U_k U_i dS+\rho\int n_k\overline{u_k' u_i'}dS=-\int n_i P dS+\mu\int n_k\frac{\partial U_i}{\partial x_k}dS \tag{47}$$

This is the general equation of momentum for steady flow. When a vertical section far upstream from the test plate is considered, $n_k=(-1,0,0)$, and at the section right at the upstream of the test plate $n_k=(1,0,0)$. Consequently, when these two sections are considered for the first step, one obtains

$$-\rho\int_0^\infty u_0^2 dy+\rho\int_{\frac{b}{2}}^\infty u_{\mathrm{up}}^2 dy=\int_0^\infty P_0 dy-\int_0^{\frac{b}{2}}P_{\mathrm{up}}dy-\int_{\frac{b}{2}}^\infty P_{\mathrm{up}}dy+\mu\int_{\frac{b}{2}}^\infty\frac{\partial u_{\mathrm{up}}}{\partial x}dy \tag{48}$$

in which the fact that the turbulence is practically zero is applied. Herein P_0 is the pressure far upstream and P_{up} and u_{up} are the pres sure and horizontal component of velocity just upstream from the test plate. In the same way, the application of Eq. (47) at a section just downstream from the test plate and an arbitrary section behind the plate gives

$$\begin{aligned}&-\rho\int_{\frac{b}{2}}^\infty u_{\mathrm{down}}^2 dy+\rho\int_0^\infty u^2 dy+\rho\int_0^\infty\overline{u'^2}dy\\&=\int_0^{\frac{b}{2}}P_{\mathrm{down}}dy+\int_{\frac{b}{2}}^\infty P_{\mathrm{down}}dy-\int_0^\infty P dy-\mu\int_{\frac{b}{2}}^\infty\frac{\partial u_{\mathrm{down}}}{\partial x}dy+\mu\int_0^\infty\frac{\partial u}{\partial x}dy\end{aligned} \tag{49}$$

in which P_{down} and u_{down} are the terms for the section just downstream from the test plate, and P and u are the terms for the arbitrary section farther downstream. Since the sections just upstream and downstream from the test plate are identical,

$$\rho\int_{\frac{b}{2}}^\infty u_{\mathrm{up}}^2 dy=\rho\int_{\frac{b}{2}}^\infty u_{\mathrm{down}}^2 dy$$

$$\int_{\frac{b}{2}}^\infty P_{\mathrm{up}}dy=\int_{\frac{b}{2}}^\infty P_{\mathrm{down}}dy$$

$$\mu\int_{\frac{b}{2}}^{\infty}\frac{\partial u_{\mathrm{up}}}{\partial x}dy=\mu\int_{\frac{b}{2}}^{\infty}\frac{\partial u_{\mathrm{down}}}{\partial x}dy$$

If it is assumed that

$$D=\int_0^{\frac{b}{2}}P_{\mathrm{up}}\,dy-\int_0^{\frac{b}{2}}P_{\mathrm{down}}dy$$

it will be seen that D is nothing but the force acting on the half of the test plate per unit length. When Eqs. (48) and (49) are added, taking those relations into consideration, one obtains

$$\rho\int_0^{\infty}(u_0^2-u^2)dy+\int_0^{\infty}(P_0-P)\,dy-\rho\int_0^{\infty}\overline{u'^2}dy+\mu\int_0^{\infty}\frac{\partial u}{\partial x}\,dy=D$$

A dimensionless form of this equation is

$$\int_0^{\infty}\left(1-\frac{u^2}{u_0^2}\right)d\left(\frac{y}{b}\right)+\int_0^{\infty}\frac{P_0-P}{\rho u_0^2}d\left(\frac{y}{b}\right)$$

$$-\int_0^{\infty}\frac{\overline{u'^2}}{u_0^2}d\left(\frac{y}{b}\right)+\frac{1}{R}\int_0^{\infty}\frac{\partial\left(\frac{u}{u_0}\right)}{\partial\left(\frac{x}{b}\right)}d\left(\frac{y}{b}\right)=\frac{D}{\rho u_0^2}\qquad(50)$$

in which $R=bu_0/\nu$.

In order to compute this equation, the section $x/b=2.0$ was selected arbitrarily. The extrapolation of u and $P-P_0$ with the aid of the potential flow around the imaginary Rankine oval, is shown in Fig. 32. The integral of $\Delta P/(\rho u_0^2/2)$ in this figure must be multiplied by 1/2 before substituting into Eq. (50). On the other hand, there is no multiplying factor for the integral of $(1-u^2/u_0^2)$. Consequently, the quatity Δp must decay more quickly than $(1-u^2/u_0^2)$. In order to take care of this fact, $\Delta p/(\rho u_0^2/2)$ was integrated from $y/b=0$ to $y/b=30$, and $(1-u^2/u_0^2)$ was integrated from $y/b=0$ to $y/b=50$. These upper limits of integration may be sufficient practically to replace the limit of infinity. It was shown already that the term divided by R is very small. The results of integration are hence as follows:

$$\int_0^{\infty}\left(1-\frac{u^2}{u_0^2}\right)d\left(\frac{y}{b}\right)\fallingdotseq\int_0^{50}\left(1-\frac{u^2}{u_0^2}\right)d\left(\frac{y}{b}\right)=-1.147$$

$$\int_0^{\infty}\frac{P_0-P}{\rho u_0^2}d\left(\frac{y}{b}\right)\fallingdotseq\int_0^{30}\frac{P_0-P}{\rho u_0^2}d\left(\frac{y}{b}\right)=1.522$$

$$\int_0^\infty \frac{\overline{u'^2}}{u_0^2} d\left(\frac{y}{b}\right) \fallingdotseq \int_0^4 \frac{\overline{u'^2}}{u_0} d\left(\frac{y}{b}\right) = 0.027$$

Accordingly,

$$\frac{D/A}{\frac{1}{2}\rho u_0^2} = 2(1.522-1.147-0.027) = 0.696 \qquad (51)$$

It will be seen that the numerical values in Eqs. (45) and (51) agree fairly well.

4. Momentum distribution and momentum balance.

The momentum equation has already been shown in the form of Eq. (46)′ in the previous section. The physical meanings of the terms in Eq. (46)′ are self-evident from their forms:

$\frac{\partial}{\partial t}\int \rho u_i d\bar{w}$; rate of local change of momentum in the region one is concerned,

$\int \rho n_k U_k U_i dS$; rate of outflow of momentum on the surface of the region considered,

$\int \rho n_k \overline{u_k' u_i'} dS$; total Reynolds stresses on the surface of the region considered,

$-\int n_i P dS$; total pressure acting on the surface of the region considered,

$\mu \int n_k \frac{\partial U_i}{\partial x_k} dS = \mu \int \frac{\partial U_i}{\partial n} dS$; total viscous shear stresses on the surface of the region of fluid considered.

Consequently, the meanings of the terms in the left-hand side of Eq. (50) that was derived from Eq. (46)′ can also be clarified as follows:

$\int \left(1-\frac{u^2}{u_0^2}\right) d\left(\frac{y}{b}\right)$; rate of outflow of momentum on the surface of the region considered,

$\int \frac{p-p_0}{\rho u_0^2} d\left(\frac{y}{b}\right)$; total pressure acting on the surface of the region considered,

$-\int \frac{\overline{u'^2}}{u_0^2} d\left(\frac{y}{b}\right)$; total Reynolds stresses acting on the surface of the region considered,

$\frac{1}{R}\int\frac{\partial\left(\frac{u}{u_0}\right)}{\partial\left(\frac{x}{b}\right)}d\left(\frac{y}{b}\right)$; total viscous shear stresses acting on the surface of the region considered.

For the purposes of determining the drag acting on the plate and of demonstrating the reasonability of the measurement performed in the present study, the relation between the drag acting on the test plate and the momentum change was explained in the preceding section. Application of the same process for each section downstream from the test plate as was done at the section of $x/b=2$ yields the distributions of the significant terms in the momentum equation. The results of the computations of these terms are shown in Fig. 38, and are also tabulated in Table 9 for the purpose of verifying once again that the estimation of the drag acting on the test plate was reasonably performed.

Fig. 38

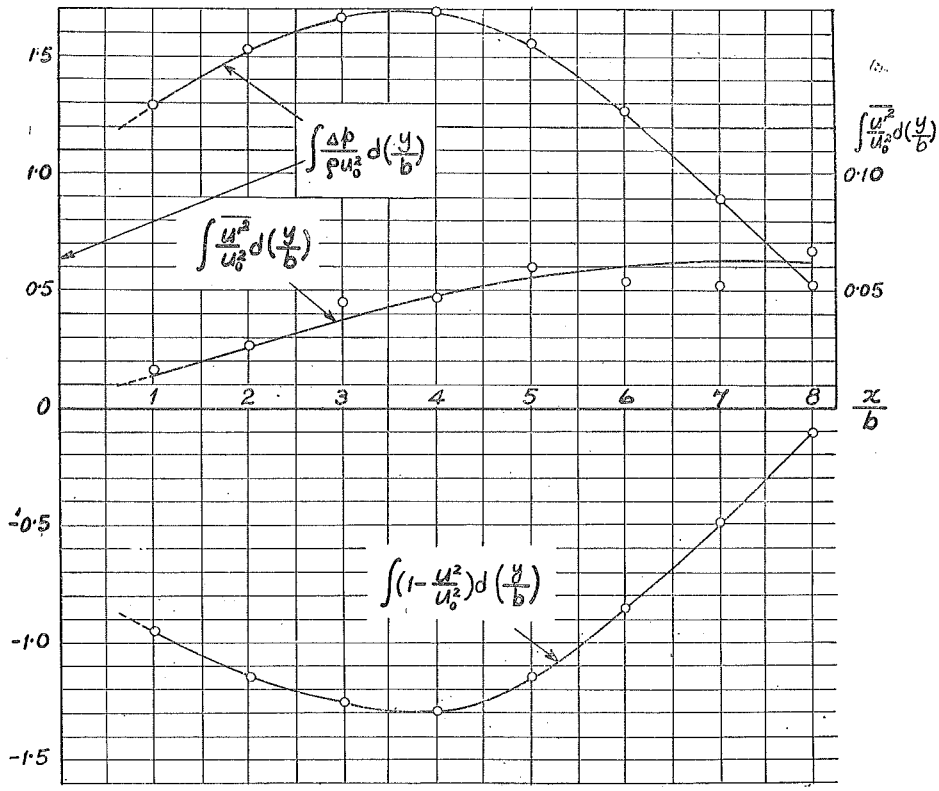

As will be seen in Fig. 38, the most important terms in the momentum equation are the total pressure acting on the surface of the region considered and the rate of outflow of momentum from the surface of the certain volume of the moving fluid. The former increases rapidly at the section where the test plate is located and increases gradually to the maximum value of about 1.7 at around $x/b=4.0$. Then it begins to decrease to the value of the drag of the plate, that is 0.69, at the section far downstream from the plate. It will also be seen that the distance of $x/b=8.0$, which means 16 times the height of the plate on a half plane is still insufficient for the estimation of the drag by the measurements of only the pressure and velocity even for the simple form of the testing body. The latter traces almost the same tendency with the former, and its value continues to be positive quite far away from the body, since the effect of the wake does not decay very easily. The significance of the contribution of the total Reynolds stresses for the accuracy of a few per cent in estimating the drag acting on the test plate, which increases with distance from the body at least to the section of $x/b=8.0$, is also clarified in Fig. 38. Since the decay of the once generated turbulence is very slow, it can be concluded that it is recommendable to perform the measurement of u' for the estimation of the drag of a body in addition to the measurements of the velocity and pressure distributions even if a considerably long distance from the body is taken for the measurements. This object can be easily attained with the hot-wire technique already described above. It can also be said that the measurement of the drag of a body that accompanies the measurement of u' can be done with a comparatively short test section of the tunnel without any danger.

As was already explained before, the order of the viscous shear, that is the order of 10^{-6}, is much smaller than the other terms, and so the values at the each section are not presented in Table 9. The mean value of the drag which was obtained with the data available at each section is shown at the end of Table 9. The value of $\frac{D/A}{(1/2)\rho u_0^2}=0.698$ agrees fairly well with the direct estimation of the drag by the integration of the pressure, that was explained in the previous section, with only the difference of a residual value. As will be seen in the column of the drag, several repetitions of measurement must be recommended at the same section or at different sections for the purpose

of measuring the drag of a body, in order to eliminate the unavoidable experimental errors.

TABLE 9.

x/b	1.0	2.0	3.0	4.0	5.0	6.0	7.0	8.0
$\int\left(1-\frac{u^2}{u_0^2}\right)d\left(\frac{y}{b}\right)$	−0.949	−1.147	−1.255	−1.301	−1.147	−0.855	−0.495	−0.101
$\int\left(\frac{p_0-p}{\rho u_0^2}\right)d\left(\frac{y}{b}\right)$	1.296	1.522	1.665	1.691	1.559	1.267	0.889	0.524
$\int\frac{\overline{u'^2}}{u_0^2}d\left(\frac{y}{b}\right)$	0.016	0.027	0.045	0.047	0.060	0.054	0.052	0.064
$\frac{D/A}{\rho u_0^2/2}$	0.662	0.696	0.730	0.686	0.704	0.716	0.684	0.712

Mean of $\frac{D/A}{\rho u_0^2/2}=\frac{5.590}{8}=0.698$

One can easily obtain the diagram of the momentum balance of the mean flow in x-direction, which is shown in Fig. 39, with the results shown in Table 9. The subtraction of M_1 and the addition of M_2 to the term of the total pressure acting on the surface of the region of the moving fluid give the drag M_3 acting on the test plate. The fact that the points of M_3 were obtained on a horizontal line means that the measurements in this study had been properly performed and that the momentum at each section is balanced. The curves of $\int\frac{\Delta p}{\rho u_0^2}d\left(\frac{y}{b}\right)$ and $\int\frac{\Delta p}{\rho u_0^2}d\left(\frac{y}{b}\right)-M_1$ must be asymptotic to the straight line of M_3 as x/b becomes large. The distribution of shear force which was omitted in Table 9 is shown in Fig. 40. The order of the shear force was 10^{-6} according to the results of the present experimental data, as has already been stated above. The scattering of the points indicates the difficulty of the estimation. An evident fact one can see in this figure is that the sign of the shear force, or the direction of the shear force, changes somewhere around $x/b=5{\cdot}2$. It may be said that a kind of confusion of shear force must be expected around this point. Consequently, smoke pictures across a flat plate that are available in literatures reveal the disappearance of the stream line that passes the edge of the flat plate.

Fig. 39
Momentum balance behind a normal plate
in contact with a boundary

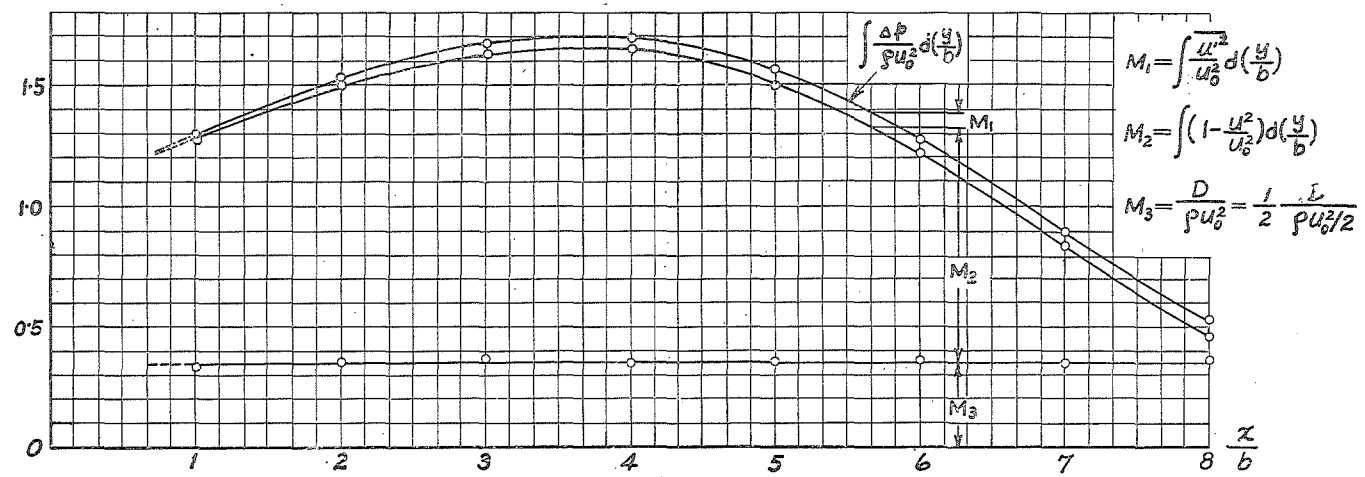

Fig. 40
Distribution of shear force behind a
normal plate in contact with a boundary

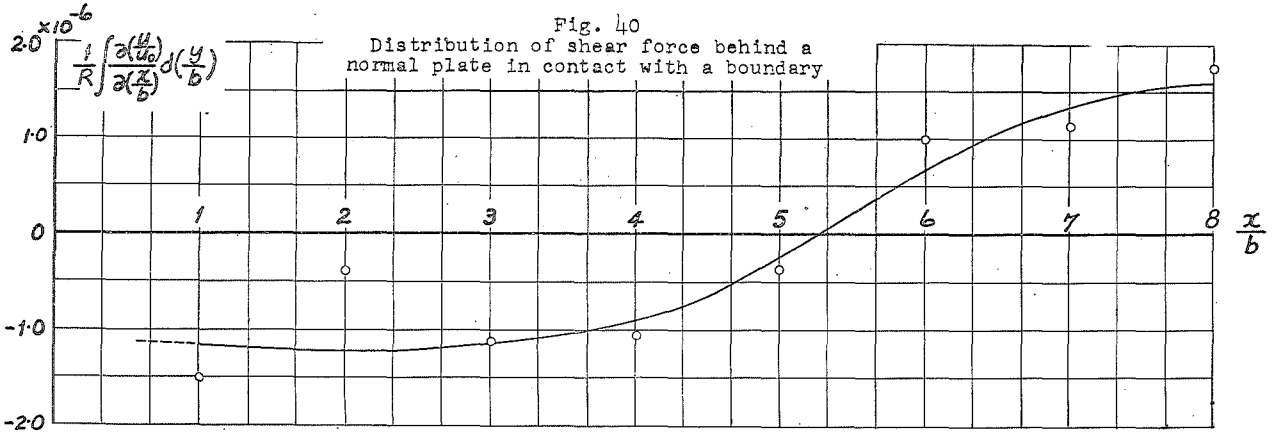

5. Energy distribution and the energy balance of the mean flow behind the test plate.

The kinetic energy of a certain volume of a moving fluid can be expressed by

$$E = \int \frac{\rho}{2} u_i u_i d\varpi$$
$$= \frac{\rho}{2} \int (U_i + u_i')(U_i + u_i') d\varpi \tag{52}$$

Consequently, the mean value of the kinetic energy over a certain period of time is

$$\bar{E} = \int \frac{1}{2} \rho U_i U_i d\varpi + \int \frac{\rho}{2} \overline{u_i' u_i'} d\varpi$$
$$= T + T'$$

in which

$T = \int \frac{\rho}{2} U_i U_i d\varpi$; kinetic energy due to the mean velocity,

$T' = \int \frac{\rho}{2} \overline{u_i' u_i'} d\varpi$; kinetic energy due to the fluctuating velocity.

On the other hand, the rate of the external work done by the external forces acting on the moving fluid must be the sum of the change of the kinetic energy with resqect to time and the internal work done by the internal forces. Consequently,

$$W_e = \frac{dE}{dt} + W_i \tag{53}$$

W_e and W_i in this equation mean the rate of the external work done and the rate of the internal work done, respectively. The external forces acting on the surface of the certain volume of the fluid are pressure and shear forces, and they can be expressed with

$$\sigma_{ik} = -p\delta_{ik} + \tau_{ik} \tag{54}$$

in which

$\tau_{ik} = \mu \left(\frac{\partial u_i}{\partial x_k} + \frac{\partial u_k}{\partial x_i} \right)$; shear forces acting on the surface, (55)

$\delta_{ik} = \begin{cases} 0, & \text{when } i \neq k \\ 1, & \text{when } i = k \end{cases}$; Kronecker delta.

Accordingly, the rate of the work done by the external forces can be obtained as follows:

$$\begin{aligned} W_e &= \int \sigma_{ik} n_k u_i dS \\ &= \int (-p\delta_{ik} + \tau_{ik}) n_k u_i dS \\ &= \int -pn_i u_i dS + \int \mu \left(\frac{\partial u_i}{\partial x_k} + \frac{\partial u_k}{\partial x_i} \right) n_k u_i dS \end{aligned}$$

The relation $\delta_{ik} n_k = n_i$ is taken into consideration in the above process. Dividing the terms u_i, u_k and p in this relation into their average values and fluctuating values, one obtains the following equation when their average over a certain period of time is taken:

$$\begin{aligned} \overline{W}_e &= -\int (P + \overline{p'})(U_i + \overline{u_i'}) n_i dS \\ &\quad + \int \mu \left[\frac{\partial}{\partial x_k} (U_i + \overline{u_i'}) + \frac{\partial}{\partial x_i} (U_k + \overline{u_k'}) \right] n_k (U_i + \overline{u_i'}) dS \\ &= -\int P U_i n_i dS + \mu \int \left(\frac{\partial U_i}{\partial x_k} + \frac{\partial U_k}{\partial x_i} \right) n_k U_i dS \\ &\quad - \int \overline{p' u_i'} n_i dS + \mu \int \overline{\left(\frac{\partial u_i'}{\partial x_k} + \frac{\partial u_k'}{\partial x_i} \right) u_i'} \, n_k dS \end{aligned} \tag{56}$$

In other words, the external work done can be understood to be supplied from two parts of motion. Namely,

$$-\int P U_i n_i dS + \mu \int \left(\frac{\partial U_i}{\partial x_k} + \frac{\partial U_k}{\partial x_i} \right) n_k U_i dS = W \tag{57}$$

is the rate of work done due to the mean forces, and

$$-\int \overline{p' u_i'} n_i dS + \mu \int \overline{\left(\frac{\partial u_i'}{\partial x_k} + \frac{\partial u_k'}{\partial x_i} \right) u_i'} \, n_k dS = W' \tag{58}$$

is the rate of work done due to the fluctuating forces acting on the surface of the volume of the fluid in which one is interested. Consequently,

$$\overline{W}_e = W + W' \tag{59}$$

On the other hand, the rate of the change of the kinetic energy with respect to time is

$$\frac{dE}{dt}=\frac{\partial E}{\partial t}+u_k\frac{\partial E}{\partial x_k}$$
$$=\frac{\partial}{\partial t}\int\frac{\rho}{2}u_iu_i d\varpi+\int\frac{\rho}{2}u_k\frac{\partial}{\partial x_k}(u_iu_i)\,d\varpi$$

Introducing the relations $u_i=U_i+u_i'$ and $u_k=U_k+u_k'$ in the above equation, and taking the average over a certain period of time again, one obtains

$$\frac{d\bar{E}}{dt}=\frac{\partial}{\partial t}\int\frac{\rho}{2}U_iU_i d\varpi+\int\frac{\rho}{2}\left(U_k\frac{\partial}{\partial x_k}U_iU_i+U_k\frac{\partial}{\partial x_k}\overline{u_i'u_i'}\right)d\varpi$$
$$+\frac{\partial}{\partial t}\int\frac{\rho}{2}\overline{u_i'u_i'}d\varpi+\int\frac{\rho}{2}\left(\overline{u_k'\frac{\partial}{\partial x_k}U_iu_i'}+\overline{u_k'\frac{\partial}{\partial x_k}u_i'U_i}+\overline{u_k'\frac{\partial}{\partial x_k}u_i'u_i'}\right)d\varpi$$
$$=\frac{\partial T}{\partial t}+\int\frac{\rho}{2}(n_kU_kU_iU_i+n_kU_k\overline{u_i'u_i'})\,dS$$
$$+\frac{\partial T'}{\partial t}+\int\frac{\rho}{2}n_k(\overline{U_iu_k'u_i'}+\overline{U_iu_k'u_i'}+\overline{u_k'u_i'u_i'})\,dS$$
$$=\frac{\partial T}{\partial t}+\int\frac{\rho}{2}Q^2U_kn_kdS+\int\frac{\rho}{2}\overline{q^2}\,U_kn_kdS$$
$$+\frac{\partial T'}{\partial t}+\int\rho\,\overline{u_i'u_k'}\,U_in_kdS+\int\frac{\rho}{2}\overline{q^2u_k'}n_kdS \qquad (60)$$

Since $E=T+T'$ as was shown in Eq. (52),

$$\frac{dE}{dt}=\frac{dT}{dt}+\frac{dT'}{dt} \qquad (61)$$

The combination of Eqs. (60) and (61) gives

$$\frac{dT}{dt}+\frac{dT'}{dt}=\frac{\partial T}{\partial t}+\int\frac{\rho}{2}Q^2U_kn_kdS+\int\frac{\rho}{2}\overline{q^2}U_kn_kdS$$
$$+\frac{\partial T'}{\partial t}+\int\rho\,\overline{u_i'u_k'}\,U_in_kdS+\int\frac{\rho}{2}\overline{q^2u_k'}n_kdS \qquad (62)$$

The Navier-Stokes equation is

$$\rho\frac{du_i}{dt}=-\frac{\partial p}{\partial x_i}+\mu\frac{\partial^2u_i}{\partial x_k\partial x_k}$$

Multiplication of u_i to both sides of this equation gives

$$\frac{\rho}{2}\frac{d(u_iu_i)}{dt}=-\frac{\partial}{\partial x_i}(pu_i)+\mu u_i\frac{\partial^2u_i}{\partial x_k\partial x_k}$$

Introducing the relations $u_i=U_i+u_i'$ and $p=P+p'$ into this equation, and taking the average over a certain period of time, and operating by a volume integration, one obtains

$$\frac{d}{dt}\int\frac{\rho}{2}(U_iU_i)d\tau+\frac{d}{dt}\int\frac{\rho}{2}\overline{(u_i'u_i')}\,d\tau$$
$$=\frac{dT}{dt}+\frac{dT'}{dt}$$
$$=-\int\frac{\partial}{\partial x_i}(PU_i)\,d\tau-\int\frac{\partial}{\partial x_i}\overline{(p'u_i')}\,d\tau+\mu\int U_i\frac{\partial^2U_i}{\partial x_k\partial x_k}d\tau+\mu\int\overline{u_i'\frac{\partial^2u_i'}{\partial x_k\partial x_k}}\,d\tau$$

Consequently,

$$\frac{dT}{dt}+\frac{dT'}{dt}=-\int n_iPU_i\,dS-\int n_i\overline{p'u_i'}\,dS$$
$$+\mu\int U_i\frac{\partial^2U_i}{\partial x_k\partial x_k}d\tau+\mu\int\overline{u_i'\frac{\partial^2u_i'}{\partial x_k\partial x_k}}\,d\tau \qquad (63)$$

On the other hand, Eq. (56) gives

$$-\int n_iPU_i\,dS-\int n_i\overline{p'u_i'}\,dS=\overline{W}_e$$
$$-\mu\int\left(\frac{\partial U_i}{\partial x_k}+\frac{\partial U_k}{\partial x_i}\right)U_in_k\,dS-\mu\int\overline{\left(\frac{\partial u_i'}{\partial x_k}+\frac{\partial u_k'}{\partial x_i}\right)u_i'}n_k\,dS$$

Substituting the above relation into Eq. (63), one obtains

$$\frac{dT}{dt}+\frac{dT'}{dt}=\overline{W}_e-\mu\int\left(\frac{\partial U_i}{\partial x_k}+\frac{\partial U_k}{\partial x_i}\right)U_in_k\,dS-\mu\int\overline{\left(\frac{\partial u_i'}{\partial x_k}+\frac{\partial u_k'}{\partial x_i}\right)u_i'}n_k\,dS$$
$$+\mu\int U_i\frac{\partial^2U_i}{\partial x_k\partial x_k}d\tau+\mu\int\overline{u_i'\frac{\partial^2u_i'}{\partial x_k\partial x_k}}\,d\tau \qquad (64)$$

When the relations already obtained in Eqs. (53) and (56) are taken into consideration, the average value of the internal work done $\overline{W}_i$ due to the internal forces can be obtained from Eq. (64).
Namely,

$$\overline{W}_i=\mu\int\left(\frac{\partial U_i}{\partial x_k}+\frac{\partial U_k}{\partial x_i}\right)U_in_k\,dS+\mu\int\overline{\left(\frac{\partial u_i'}{\partial x_k}+\frac{\partial u_k'}{\partial x_i}\right)u_i'}n_k\,dS$$
$$-\mu\int U_i\frac{\partial^2U_i}{\partial x_k\partial x_k}d\tau-\mu\int\overline{u_i'\frac{\partial^2u_i'}{\partial x_k\partial x_k}}\,d\tau$$

The combination of the second and the fourth terms in the right-hand side of Eq. (64) can be computed as follows:

$$
\begin{aligned}
&-\mu\int\left(\frac{\partial U_i}{\partial x_k}+\frac{\partial U_k}{\partial x_i}\right)U_i n_k\,dS+\mu\int U_i\frac{\partial^2 U_i}{\partial x_k\partial x_k}\,d\varpi\\
&=-\mu\int\frac{\partial}{\partial x_k}\left(U_i\frac{\partial U_i}{\partial x_k}+U_i\frac{\partial U_k}{\partial x_i}\right)d\varpi+\mu\int U_i\frac{\partial^2 U_i}{\partial x_k\partial x_k}\,d\varpi\\
&=-\mu\int\left(\frac{\partial U_i}{\partial x_k}\frac{\partial U_i}{\partial x_k}+U_i\frac{\partial^2 U_i}{\partial x_k\partial x_k}+\frac{\partial U_i}{\partial x_k}\frac{\partial U_k}{\partial x_i}+U_i\frac{\partial^2 U_k}{\partial x_k\partial x_i}\right)d\varpi+\mu\int U_i\frac{\partial^2 U_i}{\partial x_k\partial x_k}\,d\varpi\\
&=-\mu\int\left(\frac{\partial U_i}{\partial x_k}+\frac{\partial U_k}{\partial x_i}\right)\frac{\partial U_i}{\partial x_k}\,d\varpi
\end{aligned}
\tag{65}
$$

In the same way, the combination of the third and the fifth terms in the right-hand side of Eq. (64) gives

$$
-\mu\int\overline{\left(\frac{\partial u_i'}{\partial x_k}+\frac{\partial u_k'}{\partial x_i}\right)u_i'}\,n_k\,dS+\mu\int\overline{u_i'\frac{\partial^2 u_i'}{\partial x_k\partial x_k}}\,d\varpi=-\mu\int\overline{\left(\frac{\partial u_i'}{\partial x_k}+\frac{\partial u_k'}{\partial x_i}\right)\frac{\partial u_i'}{\partial x_k}}\,d\varpi \tag{66}
$$

and as was already shown in Eq. (59), the external work done was divided into two parts for the convenience of consideration. Substituting Eqs. (65), (66), and (59) into Eq. (64), one obtains

$$
\frac{dT}{dt}+\frac{dT'}{dt}=W+W'-\mu\int\left(\frac{\partial U_i}{\partial x_k}+\frac{\partial U_k}{\partial x_i}\right)\frac{\partial U_i}{\partial x_k}\,d\varpi-\mu\int\overline{\left(\frac{\partial u_i'}{\partial x_k}+\frac{\partial u_k'}{\partial x_i}\right)\frac{\partial u_i'}{\partial x_k}}\,d\varpi \tag{67}
$$

This is the energy equation including the mean motion and the turbulence. In order to obtain this result, u_i which is the combined velocity of the mean velocity and the turbulent velocity, was multiplied to both sides of the Navier-Stokes equation. When U_i is multiplied to the same equation, the energy equation of the mean flow can be obtained easily. Now, multiplying U_i to both sides of Eq. (39), and taking the average over a certain period of time, one obtains

$$
\frac{\rho}{2}\frac{\partial}{\partial t}(U_iU_i)+\rho U_iU_k\frac{\partial U_i}{\partial x_k}+\rho U_i\overline{u_k'\frac{\partial u_i'}{\partial x_k}}=-\frac{\partial}{\partial x_i}(PU_i)+\mu U_i\frac{\partial^2 U_i}{\partial x_k\partial x_k}
$$

Accordingly,

$$
\frac{\rho}{2}\frac{\partial}{\partial t}(U_iU_i)+\frac{\rho}{2}\frac{\partial}{\partial x_k}(U_iU_iU_k)+\rho U_i\overline{u_k'\frac{\partial u_i'}{\partial x_k}}=-\frac{\partial}{\partial x_i}(PU_i)+\mu U_i\frac{\partial^2 U_i}{\partial x_k\partial x_k}
$$

The volume integration of this equation with respect to the volume of the fluid with which one is concerned gives

$$\frac{\partial}{\partial t}\int\frac{\rho}{2}(U_iU_i)\,d\varpi+\int\frac{\rho}{2}\frac{\partial(U_iU_iU_k)}{\partial x_k}\,d\varpi+\int\rho U_i\,\overline{u_k'\frac{\partial u_i'}{\partial x_k}}\,d\varpi$$
$$=-\int\frac{\partial}{\partial x_i}(PU_i)\,d\varpi+\mu\int U_i\frac{\partial^2U_i}{\partial x_k\partial x_k}\,d\varpi \tag{68}$$

The third term in the left-hand side of this equation can be rewritten as follows:

$$\int\rho U_i\,\overline{u_k'\frac{\partial u_i'}{\partial x_k}}\,d\varpi=\int\rho\frac{\partial}{\partial x_k}(U_i\overline{u_i'u_k'})\,d\varpi-\int\rho\,\overline{u_i'u_k'}\frac{\partial U_i}{\partial x_k}\,d\varpi$$
$$=\int\rho U_in_k\overline{u_i'u_k'}\,dS-\int\rho\,\overline{u_i'u_k'}\frac{\partial U_i}{\partial x_k}\,d\varpi$$

Therefore, Eq. (68) results in the following form when the relation given in Eq. (57) is taken into consideration:

$$\frac{\partial T}{\partial t}+\int\frac{\rho}{2}Q^2n_kU_k\,dS+\int\rho U_in_k\,\overline{u_i'u_k'}\,dS-\int\rho\,\overline{u_i'u_k'}\frac{\partial U_i}{\partial x_k}\,d\varpi$$
$$=W-\mu\int\left(\frac{\partial U_i}{\partial x_k}+\frac{\partial U_k}{\partial x_i}\right)n_kU_i\,dS+\mu\int U_i\frac{\partial^2U_i}{\partial x_k\partial x_k}\,d\varpi \tag{69}$$

The combination of the second and the third terms in the right-hand side of Eq. (69) can be computed as follows:

$$-\mu\int\left(\frac{\partial U_i}{\partial x_k}+\frac{\partial U_k}{\partial x_i}\right)U_in_k\,dS+\mu\int U_i\frac{\partial^2U_i}{\partial x_k\partial x_k}\,d\varpi$$
$$=-\mu\int\frac{\partial}{\partial x_k}\left[U_i\left(\frac{\partial U_i}{\partial x_k}+\frac{\partial U_k}{\partial x_i}\right)\right]d\varpi+\mu\int U_i\frac{\partial^2U_i}{\partial x_k\partial x_k}\,d\varpi$$
$$=-\mu\int\frac{\partial U_i}{\partial x_k}\left(\frac{\partial U_i}{\partial x_k}+\frac{\partial U_k}{\partial x_i}\right)d\varpi-\mu\int U_i\left(\frac{\partial^2U_i}{\partial x_k\partial x_k}+\frac{\partial^2U_i}{\partial x_i\partial x_k}\right)d\varpi+\mu\int U_i\frac{\partial^2U_i}{\partial x_k\partial x_k}\,d\varpi$$
$$=-\mu\int\frac{\partial U_i}{\partial x_k}\left(\frac{\partial U_i}{\partial x_k}+\frac{\partial U_k}{\partial x_i}\right)d\varpi \tag{70}$$

Substitution of Eq. (70) into Eq. (69) gives

$$\frac{\partial T}{\partial t}+\int\frac{\rho}{2}Q^2n_kU_k\,dS+\int\rho U_kn_k\overline{u_i'u_k'}\,dS-\int\rho\,\overline{u_i'u_k'}\frac{\partial U_i}{\partial x_k}\,d\varpi$$
$$=W-\mu\int\frac{\partial U_i}{\partial x_k}\left(\frac{\partial U_i}{\partial x_k}+\frac{\partial U_k}{\partial x_i}\right)d\varpi \tag{71}$$

This is the energy equation of the mean flow of a certain volume of the moving fluid. Since the expressions of $\partial T/\partial t$ and W are already obtained, elimination of these terms in the above equation gives the

general form of the energy equation of the mean flow. Namely,

$$-\int PU_i n_i dS+\mu\int U_i n_k\left(\frac{\partial U_i}{\partial x_k}+\frac{\partial U_k}{\partial x_i}\right)dS-\int\rho U_i n_k\overline{u_i' u_k'}\,dS$$
$$=\frac{\partial}{\partial t}\int\frac{\rho}{2}Q^2 d\tilde{\omega}+\int\frac{\rho}{2}Q^2 n_k U_k dS-\int\rho\,\overline{u_i' u_k'}\frac{\partial U_i}{\partial x_k}d\tilde{\omega}+\mu\int\frac{\partial U_i}{\partial x_k}\left(\frac{\partial U_i}{\partial x_k}+\frac{\partial U_k}{\partial x_i}\right)d\tilde{\omega} \tag{72}$$

One can also derive the energy equation of turbulence by subtraction of Eq. (72) from Eq. (67), or by multiplying u_i' to the Navier-Stokes equation.

The physical meanings of each term in Eq. (72) are :

$-\int PU_i n_i dS$; rate of work done by mean pressure acting on the surface of the volume of the fluid one is concerned,

$\mu\int U_i n_k\left(\frac{\partial U_i}{\partial x_k}+\frac{\partial U_k}{\partial x_i}\right)dS$; rate of work done by mean viscous shear stresses on the surface of the volume of the fluid,

$-\int\rho U_i n_k\overline{u_i' u_k'}\,dS$; rate of work done due to Reynolds stresses on the surface of the volume of the flnid,

$\frac{\partial}{\partial t}\int\frac{\rho}{2}Q^2 d\tilde{\omega}$; rate of local change of mean energy in the volume of fluid, and this term must be zero when the flow is understood to be steady,

$\int\frac{\rho}{2}Q^2 n_k U_k dS$; rate of convection of mean energy on the surface of the volume of fluid,

$-\int\rho\,\overline{u_i' u_k'}\frac{\partial U_i}{\partial x_k}d\tilde{\omega}$; rate of work done due to Reynolds stresses in the volume of fluid, or production of the turbulent energy,

$\mu\int\frac{\partial U_i}{\partial x_k}\left(\frac{\partial U_i}{\partial x_k}+\frac{\partial U_k}{\partial x_i}\right)d\tilde{\omega}$; rate of work done by mean viscous stresses in the volume of fluid, or dissipation of energy due to mean motion.

One must note that a two-dimensional flow is under consideration in the present study, and as a result, the surface integration in Eq.

(72) becomes a single integration and the volume integration means a double integration. When the certain volume of the moving fluid, that was considered in the present discussion, is taken as the region between two vertical sections at $x/b=-\infty$ and $x/b=x$ which extends from the boundary of the half plane to $y/b=\infty$, Eq. (72) becomes as follows: (U is replaced by u hereafter for simplicity)

$$\begin{aligned}
&\int_0^\infty \frac{\rho}{2} u_0^2(-1)u_0 dy + \int_0^\infty \frac{\rho}{2} Q^2(+1)u dy + \int_0^\infty \rho\left[u(+1)\overline{u'^2} + v(+1)\overline{u'v'}\right] dy \\
&\quad - \int_{-\infty}^{x}\int_0^\infty \rho\left[\overline{u'^2}\frac{\partial u}{\partial x} + \overline{u'v'}\frac{\partial u}{\partial y} + \overline{u'v'}\frac{\partial v}{\partial x} + \overline{v'^2}\frac{\partial v}{\partial y}\right] dy\, dx \\
&= -\int_0^\infty P_0 u_0(-1)dy + \int_0^\infty -Pu(+1)dy + \mu\int_0^\infty\left[u\left(\frac{\partial u}{\partial x}+\frac{\partial u}{\partial x}\right)(+1)\right. \\
&\quad \left. + v\left(\frac{\partial v}{\partial x}+\frac{\partial v}{\partial y}\right)(+1)\right]dy - \mu\int_{-\infty}^{x}\int_0^\infty\left[\frac{\partial u}{\partial x}\left(\frac{\partial u}{\partial x}+\frac{\partial u}{\partial x}\right)+\frac{\partial v}{\partial x}\left(\frac{\partial v}{\partial x}+\frac{\partial u}{\partial y}\right)\right. \\
&\quad \left. + \frac{\partial u}{\partial y}\left(\frac{\partial u}{\partial y}+\frac{\partial v}{\partial x}\right)+\frac{\partial v}{\partial y}\left(\frac{\partial v}{\partial y}+\frac{\partial v}{\partial y}\right)\right] dy\, dx \qquad (73)
\end{aligned}$$

The equation of continuity in two-dimensional case is

$$\frac{\partial u}{\partial x} + \frac{\partial v}{\partial y} = 0$$

and so,

$$\overline{v'^2}\frac{\partial v}{\partial y} = -\overline{v'^2}\frac{\partial u}{\partial x}$$

Consequently,

$$\overline{u'^2}\frac{\partial u}{\partial x} + \overline{u'v'}\frac{\partial u}{\partial y} + \overline{u'v'}\frac{\partial v}{\partial y} + \overline{v'^2}\frac{\partial v}{\partial y} = (\overline{u'^2}-\overline{v'^2})\frac{\partial u}{\partial x} + \overline{u'v'}\left(\frac{\partial v}{\partial x}+\frac{\partial u}{\partial y}\right)$$

At the same time, the application of the equation of continuity gives

$$\begin{aligned}
&\frac{\partial u}{\partial x}\left(\frac{\partial u}{\partial x}+\frac{\partial u}{\partial x}\right)+\frac{\partial v}{\partial x}\left(\frac{\partial v}{\partial x}+\frac{\partial u}{\partial y}\right)+\frac{\partial u}{\partial y}\left(\frac{\partial u}{\partial y}+\frac{\partial v}{\partial x}\right)+\frac{\partial v}{\partial y}\left(\frac{\partial v}{\partial y}+\frac{\partial v}{\partial y}\right) \\
&= 2\left(\frac{\partial u}{\partial x}\right)^2 + 2\left(\frac{\partial v}{\partial y}\right)^2 + 2\frac{\partial v}{\partial x}\frac{\partial u}{\partial y} + \left(\frac{\partial v}{\partial x}\right)^2 + \left(\frac{\partial u}{\partial y}\right)^2 \\
&= 4\left(\frac{\partial u}{\partial x}\right)^2 + \left(\frac{\partial v}{\partial x}+\frac{\partial u}{\partial y}\right)^2
\end{aligned}$$

Accordingly, Eq. (73) results

$$\int_0^\infty \frac{\rho}{2} u_0^3 dy + \int_0^\infty P_0 u_0 dy = \int_0^\infty P u dy + \int_0^\infty \frac{\rho}{2} Q^2 u dy + \int_0^\infty \rho \left(u\overline{u'^2} + v\overline{u'v'}\right) dy$$
$$- \int_{-\infty}^{x}\int_0^\infty \rho \left[(\overline{u'^2} - \overline{v'^2}) \frac{\partial u}{\partial x} + \overline{u'v'} \left(\frac{\partial v}{\partial x} + \frac{\partial u}{\partial y} \right) \right] dy dx - \mu \int_0^\infty \left[2u \frac{\partial u}{\partial x} + v \left(\frac{\partial v}{\partial x} + \frac{\partial u}{\partial y} \right) \right] dy$$
$$+ \mu \int_{-\infty}^{x}\int_0^\infty \left[4 \left(\frac{\partial u}{\partial x} \right)^2 + \left(\frac{\partial v}{\partial x} + \frac{\partial u}{\partial y} \right)^2 \right] dy dx \qquad (74)$$

In order to change this equation into a dimensionless form, one has to divide both sides of this equation by $\frac{1}{2} \rho u_0^3 b$:

$$\int_0^\infty d\left(\frac{y}{b}\right) + 2\int \frac{P_0}{\rho u_0^2} d\left(\frac{y}{b}\right)$$
$$= 2\int_0^\infty \frac{P}{\rho u_0^2} \left(\frac{u}{u_0}\right) d\left(\frac{y}{b}\right) + \int_0^\infty \frac{Q^2}{u_0^2} \frac{u}{u_0} d\left(\frac{y}{b}\right) - 2\int_0^\infty \left[\left(\frac{u}{u_0}\right) \left(\frac{\overline{u'^2}}{u_0^2}\right) + \left(\frac{v}{u_0}\right) \left(\frac{\overline{u'v'}}{u_0^2}\right) \right] d\left(\frac{y}{b}\right)$$
$$- 2\int_{-\infty}^{\frac{x}{b}}\int_0^\infty \left[\left(\frac{\overline{u'^2} - \overline{v'^2}}{u_0^2} \right) \left(\frac{\partial u/u_0}{\partial x/b} \right) + \left(\frac{\overline{u'v'}}{u_0^2} \right) \left(\frac{\partial v/u_0}{\partial x/b} + \frac{\partial u/u_0}{\partial y/b} \right) \right] \frac{dy dx}{b^2}$$
$$- \frac{2}{R} \int_0^\infty \left[2 \left(\frac{u}{u_0} \right) \left(\frac{\partial u/u_0}{\partial x/b} \right) + \left(\frac{v}{u_0} \right) \left(\frac{\partial v/u_0}{\partial x/b} + \frac{\partial u/u_0}{\partial y/b} \right) \right] d\left(\frac{y}{b}\right)$$
$$+ \frac{2}{R} \int_{-\infty}^{\frac{x}{b}}\int_0^\infty \left[4 \left(\frac{\partial u/u_0}{\partial x/b} \right)^2 + \left(\frac{\partial v/u_0}{\partial x/b} + \frac{\partial u/u_0}{\partial y/b} \right)^2 \right] \frac{dy dx}{b^2} \qquad (75)$$

Dividing the terms in this equation into two parts upstream and downstream of the test plate, one obtains the folowing relation:

$$\int_0^\infty d\left(\frac{y}{b}\right) + 2\int_0^\infty \frac{P_0}{\rho u_0^2} d\left(\frac{y}{b}\right) + 2\int_{-\infty}^0\int_0^\infty \left[\frac{\overline{u'^2} - \overline{v'^2}}{u_0^2} \left(\frac{\partial u/u_0}{\partial x/b} \right) + \frac{\overline{u'v'}}{u_0^2} \left(\frac{\partial v/u_0}{\partial x/b} + \frac{\partial u/u_0}{\partial y/b} \right) \right] \frac{dy dx}{b^2}$$
$$- \frac{2}{R} \int_{-\infty}^0 \int_0^\infty \left[4 \left(\frac{\partial u/u_0}{\partial x/b} \right)^2 + \left(\frac{\partial v/u_0}{\partial x/b} + \frac{\partial u/u_0}{\partial y/b} \right)^2 \right] \frac{dy dx}{b^2}$$
$$= 2\int_0^\infty \frac{P}{\rho u_0^2} \left(\frac{u}{u_0}\right) d\left(\frac{y}{b}\right) + \int_0^\infty \left(\frac{Q^2}{u_0^2}\right) \left(\frac{u}{u_0}\right) d\left(\frac{y}{b}\right) - 2\int_0^\infty \left(\frac{u}{u_0} \frac{\overline{u'^2}}{u_0^2} + \frac{v}{u_0} \frac{\overline{u'v'}}{u_0^2} \right) d\left(\frac{y}{b}\right)$$
$$- 2\int_0^{\frac{x}{b}}\int_0^\infty \left[\frac{\overline{u'^2} - \overline{v'^2}}{u_0^2} \frac{\partial u/u_0}{\partial x/b} + \frac{\overline{u'v'}}{u_0^2} \left(\frac{\partial v/u_0}{\partial x/b} + \frac{\partial u/u_0}{\partial y/b} \right) \right] \frac{dy dx}{b^2}$$
$$- \frac{2}{R} \int_0^\infty \left[2 \frac{u}{u_0} \frac{\partial u/u_0}{\partial x/b} + \frac{v}{u_0} \left(\frac{\partial v/u_0}{\partial x/b} + \frac{\partial u/u_0}{\partial y/b} \right) \right] d\left(\frac{y}{b}\right)$$
$$+ \frac{2}{R} \int_0^{\frac{x}{b}}\int_0^\infty \left[4 \left(\frac{\partial u/u_0}{\partial x/b} \right)^2 + \left(\frac{\partial v/u_0}{\partial x/b} + \frac{\partial u/u_0}{\partial y/b} \right)^2 \right] \frac{dy dx}{b^2} \qquad (76)$$

The physical meanings of the terms in this equation can be understood by reference to the meanings of the terms in Eq. (72). The left-hand side of Eq. (76) represents the terms which appear in the region upstream and the right-hand side represents those which appear in the region downstream from the normal plate in contact with the boundary. When the terms in this equation are computed with the data obtained in the experiment, the distribution of the significant terms that appear in the energy equation of the mean flow across the plate can be obtained. Looking at the integration in the vertical section, one may see that the upper limit of the integration extends to an infinity, and that the performance of the computation is meaningless, since the energy integration up to $y=$infinity becomes infinity. Consequently, the terms were integrated to the upper limit of $y/b=50$ which was already employed for the computation of the drag acting on the plate and that was found to be large enough to avoid the influence of the existence of the test plate. When the pressure is measured with reference to the pressure at a point far upstream from the plate in the manner employed in the present experiment, the term of pressure in the left-hand side of Eq. (76) vanishes and the pressure in the right-hand side becomes the pressure difference between the pressure at the point interested in and that of the point far upstream. Since the flow was uniform in x-direction and there was no turbulence at the point far upstream, the only term that remains at that point is $\int_0^0 dy$, and the integration of this term must be 50. Consequently, the result of integration of the right-hand side must also be 50 so far as the measurements are reasonably performed. In other words, this is a good point at which one can check the accuracy of measurements as a whole as well as the comparison between the two ways of estimating the drag already described above. It may be worth-while to note here that all the measurements were carried out up to $y/b=4.0$ because of the dimension of the wind tunnel, and that the terms of pressure and velocity were extrapolated in an analytical way that was already employed in the section on estimation of the drag. Still, as will be seen in Figs. 22, 23, 24, and 25, it can be judged that the measurement of turbulence and the estimations of the velocity gradients were obtained to the extent of sufficient vertical distance, since the value of turbulence is sufficiently small when $y/b>4.0$ and since the reasonability of extrapolating the velocity

by the aid of the flow around the imaginary Rankine oval and the imaginary potential flow caused by the distribution of doublets were already established by the validity of Bernoulli equation in the region where $y/b>4.0$. The results of computation of each term in Eq. (76) are plotted in Fig. 41 to show their distributions behind the test plate to the distance $x/b=8$ where the standing eddy almost ends. Fig. 41(B) shows the distribution of the rate of convection of mean energy that is the most important term in the energy equation. Since the flow is accelerated at first behind the plate, this term increases rather rapidly and it reaches the maximum value of about 52.85 somewhere at around $x/b=3$. After that the flow is decelerated and this term begins to decrease to the value of the general flow. The rate of work done due to the mean pressure is shown in Fig. 41(A). Since the existence of a plate causes pressure drop in the region behind the plate, the value of this term is always negative. This term reaches the minimum value of -3 at around $x/b=3$ again, since the flow is accelerated at first. This term must be always negative even at the point sufficiently far downstream from the plate, since the drag acting on the plate causes a pressure drop. The rate of work done by Reynolds stresses, that is shown in Fig. 41(C), reaches to about -0.10 and it must be destined to decrease with the distance from the plate. Fig. 41(D) shows the work done by the Reynolds stresses in the volume of the moving fluid which means the production of the turbulent energy. It can be seen that the maximum production of the turbulent energy occurs at around $x/b=5$. Since the decay of the once generated turbulence is slow, the production of this energy continues at a considerable distance. Fig. 41(E) shows the distribution of the rate of work done by mean viscous stresses in the volume of the moving fluid, that is the dissipation of energy. Its value is maximum at the section where the test plate is located. Still, its order is 10^{-4}. This term has the tendency to increase further with the distance from the plate. The rate of work done due to the mean viscous stresses on the surface of the fluid volume is shown in Fig. 41(F). The sign of this term changes because the direction of acceleration changes. The order of this term was 10^{-5}.

All the terms computed in the energy equation are tabulated in Table 10 to explain the results shown in Fig. 41 and to show the energy balance that is shown in Fig. 42. The most important terms are indicated in Fig. 42, and the energy balance among them is shown

FIG. 41
DISTRIBUTION OF ENERGIES OF THE MEAN FLOW BEHIND THE TEST PLATE

FIG. 41(A)
RATE OF WORK DONE BY MEAN PRESSURE

$$E_2=\int\frac{P}{\rho U_0^2/2}\frac{u}{u_0}d\left(\frac{y}{b}\right)$$

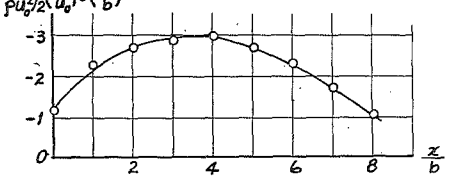

FIG. 41(B)
RATE OF CONVECTION OF MEAN ENERGY

$$\int\frac{q^2}{u_0^2}\frac{u}{u_0}d\left(\frac{y}{b}\right)$$

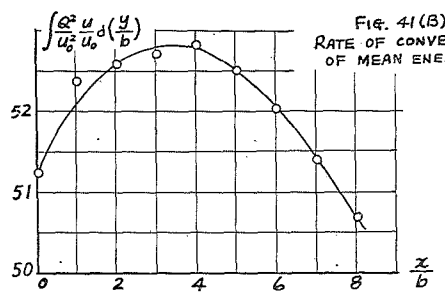

FIG. 41(C)
RATE OF WORK DONE BY REYNOLDS STRESSES

$$E_3=-2\int\left[\frac{u}{u_0}\frac{\overline{u'^2}}{u_0^2}+\frac{v}{u_0}\frac{\overline{u'v'}}{u_0^2}\right]d\left(\frac{y}{b}\right)$$

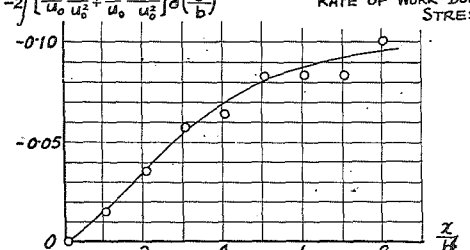

FIG. 41(D)
PRODUCTION OF TURBULENT ENERGY

$$-2\int\left[\frac{\overline{u'^2}-\overline{v'^2}}{u_0^2}\frac{\partial u/u_0}{\partial x/b}+\frac{\overline{u'v'}}{u_0^2}\left(\frac{\partial v/u_0}{\partial x/b}+\frac{\partial u/u_0}{\partial y/b}\right)\right]d\left(\frac{y}{b}\right)$$

$$E_1=-2\iint\left[\frac{\overline{u'^2}-\overline{v'^2}}{u_0^2}\frac{\partial u/u_0}{\partial x/b}+\frac{\overline{u'v'}}{u_0^2}\left(\frac{\partial v/u_0}{\partial x/b}+\frac{\partial u/u_0}{\partial y/b}\right)\right]\frac{dydx}{b^2}$$

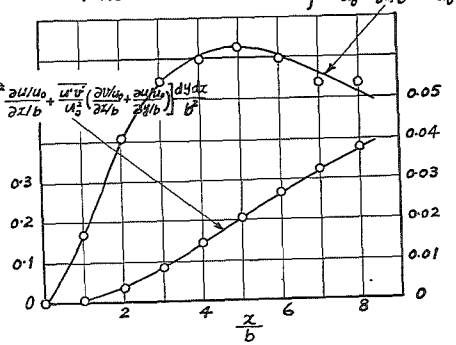

FIG. 41(E)
DISSIPATION DUE TO MEAN MOTION

$$\frac{2}{R}\int\left[4\left(\frac{\partial u/u_0}{\partial x/b}\right)^2+\left(\frac{\partial v/u_0}{\partial x/b}+\frac{\partial u/u_0}{\partial y/b}\right)^2\right]d\left(\frac{y}{b}\right)$$

$$E_5=\frac{2}{R}\iint\left[4\left(\frac{\partial u/u_0}{\partial x/b}\right)^2+\left(\frac{\partial v/u_0}{\partial x/b}+\frac{\partial u/u_0}{\partial y/b}\right)^2\right]\frac{dydx}{b^2}$$

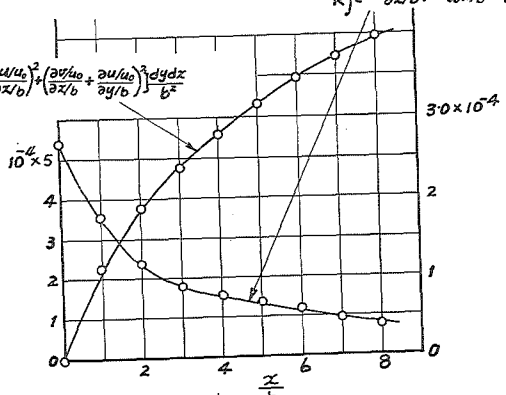

FIG. 41(F)

RATE OF WORK DONE BY MEAN VISCOUS STRESSES

$$E_6=-\frac{2}{R}\int\left[\left(2\frac{U}{U_0}\frac{\partial u/u_0}{\partial x/b}+\frac{v}{u_0}\left(\frac{\partial v/u_0}{\partial x/b}+\frac{\partial u/u_0}{\partial y/b}\right)\right]\frac{dy}{b}\right.$$

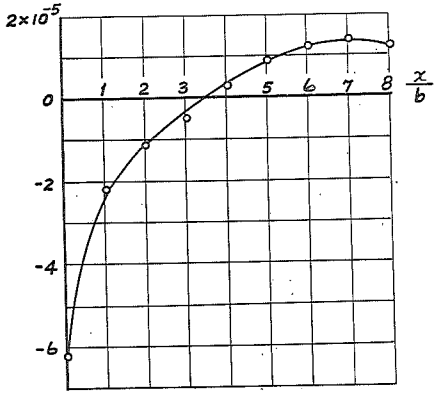

FIG. 42

ENERGY BALANCE OF THE MEAN FLOW

$$E_1=-2\iint\left[\frac{\overline{u^2}-\overline{v^2}}{u_0^2}\frac{\partial u/u_0}{\partial x/b}+\frac{\overline{u'v'}}{u_0^2}\left(\frac{\partial v/u_0}{\partial x/b}+\frac{\partial u/u_0}{\partial y/b}\right)\right]\frac{dy\,dx}{b^2}$$

$$E_2=2\int\frac{\Delta P}{\rho u_0^2}\left(\frac{u}{u_0}\right)d\left(\frac{y}{b}\right)$$

$$E_3=-2\int\left[\frac{u}{u_0}\frac{\overline{u^2}}{u_0^2}+\frac{v}{u_0}\frac{\overline{u'v'}}{u_0^2}\right]d\left(\frac{y}{b}\right)$$

$$E_4=\int\frac{Q^2}{u_0^2}\frac{u}{u_0}d\left(\frac{y}{b}\right)+E_1+E_2+E_3+E_5+E_6\approx\text{CONSTANT}=50$$

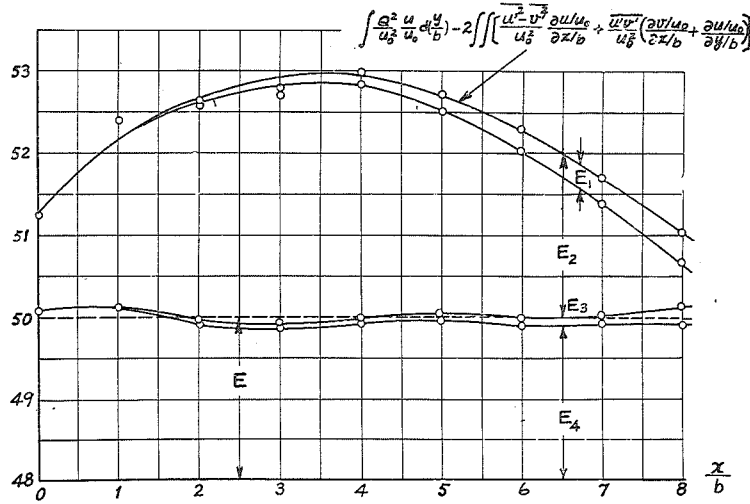

TABLE 10 Results of the Energy Balance of the Mean Flow

x/b	0	1	2	3	4	5	6	7	8
$E_2=\int \frac{P}{\rho u_0^2/2}\left(\frac{u}{u_0}\right)d\left(\frac{y}{b}\right)$	−1.1832	−2.2764	−2.6986	−2.8600	−2.9744	−2.6712	−2.2966	−1.6880	−1.0230
$\int \frac{Q^2}{u_0^2}\frac{u}{u_0}d\left(\frac{y}{b}\right)$	51.2461	52.3774	52.5783	52.6932	52.8123	52.4956	52.0074	51.3708	50.6615
$E_1=-2\int\left[\frac{u}{u_0}\frac{\overline{u'^2}}{u_0^2}+\frac{v}{u_0}\frac{\overline{u'v'}}{u_0^2}\right]d\left(\frac{y}{b}\right)$	0	−0.0150	−0.0348	−0.0563	−0.0632	−0.0821	−0.0830	−0.0828	−0.1000
$E_3=-2\int\int\left[\frac{\overline{u'^2}-\overline{v'^2}}{u_0^2}\frac{\partial u/u_0}{\partial x/b}+\frac{\overline{u'v'}}{u_0^2}\left(\frac{\partial v/u_0}{\partial x/b}+\frac{\partial u/u_0}{\partial y/b}\right)\right]\frac{dydx}{b^2}$	0	0.0065	0.0354	0.0835	0.1416	0.2036	0.2650	0.3227	0.3759
$E_5=\frac{2}{R}\int\int\left[4\left(\frac{\partial u/u_0}{\partial x/b}\right)^2+\left(\frac{\partial v/u_0}{\partial x/b}+\frac{\partial u/u_0}{\partial y/b}\right)\right]\frac{dydx}{b^2}$	0	$\times10^{-4}$ 2.2728	$\times10^{-4}$ 3.7125	$\times10^{-4}$ 4.7325	$\times10^{-4}$ 5.5689	$\times10^{-4}$ 6.3064	$\times10^{-4}$ 6.9441	$\times10^{-4}$ 7.4781	$\times10^{-4}$ 7.9151
$E_6=-\frac{2}{R}\int\left[2\frac{u}{u_0}\frac{\partial u/u_0}{\partial x/b}+\frac{v}{u_0}\left(\frac{\partial v/u_0}{\partial x/b}+\frac{\partial u/u_0}{\partial y/b}\right)\right]\frac{dy}{b}$	$\times10^{-4}$ −0.6250	$\times10^{-4}$ −0.2245	$\times10^{-4}$ −0.1182	$\times10^{-4}$ −0.0512	$\times10^{-4}$ 0.0229	$\times10^{-4}$ 0.0839	$\times10^{-4}$ 0.1181	$\times10^{-4}$ 0.1310	$\times10^{-4}$ 0.1164
Total (E_4)	50.0629	50.0925	49.8803	49.8604	49.9163	49.9460	49.8929	49.9228	49.9145

in the manner already explained. The value of E_4 must be equal to E which is fifty in this case. As will be seen in Table 10, their values for several vertical sections agree with only a slight difference which can be excused as the experimental errors.

Conclusions

The foregoing experimental study of flow past a normal plate in contact with a boundary, which was realized in an air tunnel by placing a tail plate at the midsection of the test plate on the downstream side, permits the following conclusions to be drawn:

1. The stable eddy behind a plate in contact with a boundary is some 3.6 times as long as the mean eddy pattern in the pendulating wake behind a plate that is far from a boundary. Elimination of the pendulation also results in a considerable decrease of the maximum velocity in the wake, with a corresponding alleviation of the pronounced pressure drop that otherwise occurs. As a result, the drag coefficient is reduced from 0.9 to 0.7 with respect to the half width of the plate.

2. Although the drag of a body is usually calculated from measurements of the momentum change between sections of uniform flow far upstream and far downstream from the body, measurements of velocity, pressure, and turbulence properly performed at sections of non-uniform flow near the body can also be used satisfactorily for this purpose.

3. The Pitot cylinder should not be used without correction in regions of pronounced velocity gradient, since its indications of both the direction and the magnitude of the velocity will then not be reliable.

4. In making air-tunnel studies of this sort, constriction effects should not be overlooked, especially in the region downstream from the body. It appears that a distribution of doublets along the tunnel permits a fairly good estimate to be made of the shape of tunnel boundaries that will simulate the conditions of unconfined flow.

5. Distributions of momentum and energies of the mean flow behind a normal slate in contact with a boundary on half plane, that cause the main difference from the flow over a plate far away from boundary, were shown in detail.

APPENDIX

Pressure Distribution around a Cylinder in Parallel Shear Flow

The measurement of velocity in the present experimental study was performed with Pitot cylinders. As stated before, a certain discrepancy was noticed, in the estimation of the direction of flow, between the results obtained with the 30.6° cylinder and those with the 180° cylinder. It is hence worth-while to clarify the characteristics of flow around a cylinder in the region of a steep velocity gradient.

This kind of study was first done by v. Sanden [10], and recently Tsien [11] has reported on a theoretical analysis of the same kind of problem. They attempted to investigate the performance of bodies near the surface of the ground. Sanden's study handled a numerical calculation for a wedge-shaped body, and Tsien was primarily interested in finding the aerodynamic forces in a shear flow, for which exact expressions for the pressure distribution in the neighborhood of the body were not required and hence were not given. If one attempts, however, to find the pressure on the surface of a cylinder or in the vicinity of a cylinder, he can not neglect any term in the solution. When a two-dimensional parallel shear flow is assumed, the exact solution of this problem is not difficult to obtain.

The velocity is assumed to have a constant gradient, as shown in Fig. 43. Then the velocity of the undisturbed flow at y may be expressed as

Fig. 43

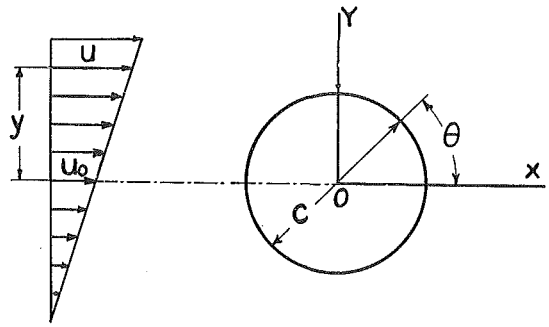

$$u = u_0\left(1 + K\frac{y}{c}\right) \tag{77}$$

The stream function of this undisturbed flow is

$$\begin{aligned}\psi_0 &= \int u\,dy \\ &= u_0\left(y + \frac{Ky^2}{2c}\right) + \text{constant}\end{aligned}$$

If it is understood that $\psi_0 = 0$ at $y = 0$, the constant in this equation must be zero. Therefore,

$$\psi_0 = u_0\left(y + K\frac{y^2}{2c}\right) \tag{78}$$

If ψ_1 expresses the stream function of the disturbed flow due to the existence of a cylinder in the field, the total stream function is

$$\psi = \psi_0 + \psi_1 \tag{79}$$

If a non-viscous fluid is assumed, the vorticity is constant everywhere in the field. Accordingly,

$$\frac{\partial v}{\partial x} - \frac{\partial u}{\partial y} = \text{constant}$$

Using the boundary conditions far away from the cylinder, one obtains

$$\frac{\partial v}{\partial x} = 0\,, \quad \frac{\partial u}{\partial y} = u_0\frac{K}{c}$$

Consequently,

$$\frac{\partial v}{\partial x} - \frac{\partial u}{\partial y} = u_0\frac{K}{c} \tag{80}$$

Velocity components at any point in the field are

$$u = \frac{\partial \psi}{\partial y}\,, \quad v = -\frac{\partial \psi}{\partial x} \tag{81}$$

Substitution of Eq. (81) into Eq. (80) gives

$$\frac{\partial^2}{\partial x^2}(\psi_0 + \psi_1) + \frac{\partial^2}{\partial y^2}(\psi_0 + \psi_1) = u_0\frac{K}{c}$$

or

$$\frac{\partial^2 \psi_1}{\partial x^2} + \frac{\partial^2 \psi_1}{\partial y^2} = 0 \tag{82}$$

This equation must be solved to find the stream function of the disturbed flow. In cylindrical coordinates, the equation becomes

$$\frac{\partial^2\psi_1}{\partial r^2}+\frac{1}{r^2}\frac{\partial\psi_1}{\partial r}+\frac{1}{r^2}\frac{\partial^2\psi_1}{\partial\theta^2}=0 \tag{83}$$

If $R(r)$ and $\Theta(\theta)$ are the functions of only r and θ, respectively, and if it is assumed for the solution of Eq. (83) that $\psi_1=R(r)\Theta(\theta)$, then

$$\begin{aligned}\frac{\partial\psi_1}{\partial r}&=\Theta\frac{dR}{dr}\ ,\quad \frac{\partial^2\psi_1}{\partial r^2}=\Theta\frac{d^2R}{dr^2}\\ \frac{\partial\psi_1}{\partial\theta}&=R\frac{d\Theta}{d\theta}\ ,\quad \frac{\partial^2\psi}{\partial\theta^2}=R\frac{d^2\Theta}{d\theta^2}\end{aligned} \tag{84}$$

Substituting Eq. (84) into Eq. (83), one obtoins

$$r^2\left\{\frac{1}{R}\left(\frac{d^2R}{dr^2}+\frac{1}{r}\frac{dR}{dr}\right)\right\}+\frac{1}{\Theta}\frac{d^2\Theta}{d\theta^2}=0$$

Since R and Θ are functions of r and θ, respectively, each of the two terms in this equation must be a constant and their sum must be zero. Consequently, if m is an arbitrary constant, then

$$\frac{1}{\Theta}\frac{d^2\Theta}{d\theta^2}=-m^2 \tag{85}$$

and

$$r^2\left\{\frac{1}{R}\left(\frac{d^2R}{dr^2}+\frac{1}{r}\frac{dR}{dr}\right)\right\}=m^2 \tag{86}$$

The general solution of Eq. (85) is

$$\Theta=A\cos m\theta+B\sin m\theta \tag{87}$$

Upon rewriting, Eq. (86) becomes

$$\frac{d^2R}{dr^2}+\frac{1}{r}\frac{dR}{dr}-\frac{R}{r^2}m^2=0 \tag{88}$$

If $R=r^\lambda$ is assumed, then $\frac{dR}{dr}=\lambda r^{\lambda-1}$ and $\frac{d^2R}{dr^2}=\lambda(\lambda-1)r^{\lambda-2}$. And so, Eq. (88) gives

$$\lambda(\lambda-1)r^{\lambda-2}+\lambda r^{\lambda-2}-m^2r^{\lambda-2}=0$$

or

$$\lambda=\pm m$$

Accordingly, the general solution of Eq. (88) is

$$R = Cr^m + Dr^{-m} \tag{89}$$

Using Eqs. (87) and (89), one can obtain the general solution of the Laplace equation given by Eq. (82)—namely:

$$\phi_1 = \sum_0^\infty (C_m r^m + D_m r^{-m})(A_m \cos m\theta + B_m \sin m\theta) \tag{90}$$

The coefficients in this equation must still be determined. On the surface of the cylinder, it is necessary that the radial component of the undisturbed velocity which can be introduced by ϕ_0 and the radial velocity which comes from ϕ_1 be equal in magnitude and opposite in direction, so that the radial velocity on the surface of the cylinder is zero. The horizontal component of the undisturbed flow on the surface of the cylinder can be obtained by substituting $y=(c/2)\sin\theta$ nto Eq. (77). That is

$$u = u_0\left(1+\frac{K}{2}\sin\theta\right)$$

Hence the radial component is

$$u_r = u_0\left(1+\frac{K}{2}\sin\theta\right)\cos\theta$$

On the other hand, the radial component which comes from ϕ_1 is

$$u_r = \left(\frac{1}{r}\frac{\partial\phi_1}{\partial\theta}\right)_{r=\frac{c}{2}}$$

Consequently,

$$\left(\frac{1}{r}\frac{\partial\phi_1}{\partial\theta}\right)_{r=\frac{c}{2}} = -u_0\left(\cos\theta+\frac{K}{4}\sin 2\theta\right) \tag{91}$$

From Eq. (90),

$$\frac{1}{r}\frac{\partial\phi_1}{\partial\theta} = \sum_m m(C_m r^{m-1} + D_m r^{-m-1})(-A_m \sin m\theta + B_m \cos m\theta)$$

Whence

$$\left(\frac{1}{r}\frac{\partial\phi_1}{\partial\theta}\right)_{r=\frac{c}{2}} = \sum_m \left\{C_m\left(\frac{c}{2}\right)^{m-1} + D_m\left(\frac{c}{2}\right)^{-m-1}\right\} \times \left\{-A_m \sin m\theta + B_m \cos m\theta\right\} m$$

Accordingly,

$$-u_0\left(\cos\theta+\frac{K}{4}\sin 2\theta\right)$$
$$=\sum_m\left\{-A_mC_m\left(\frac{c}{2}\right)^{m-1}\sin m\theta-A_mD_m\left(\frac{c}{2}\right)^{-m-1}\sin m\theta\right.$$
$$\left.+B_mC_m\left(\frac{c}{2}\right)^{m-1}\cos m\theta+B_mD_m\left(\frac{c}{2}\right)^{-m-1}\cos m\theta\right\}m$$

When $m=1$, comparing the coefficients of $\cos\theta$ and $\sin\theta$, one obtains

$$-u_0=B_1C_1+B_1D_1\left(\frac{c}{2}\right)^{-2},\quad A_1C_1-A_1D_1\left(\frac{c}{2}\right)^{-2}=0$$

For $m=2$, comparing the coefficients of $\sin 2\theta$ and $\cos 2\theta$, one obtains

$$-u_0\frac{K}{4}=2\left\{-A_2C_2\left(\frac{c}{2}\right)-A_2D_2\left(\frac{c}{2}\right)^{-3}\right\},\quad B_2C_2\left(\frac{c}{2}\right)+B_2D_2\left(\frac{c}{2}\right)^{-3}=0$$

The other terms for $m=0, 3, 4, 5, \cdots$, are all zero. At a point far away from the cylinder, there is no disturbance from the cylinder. This means that when $r=\infty$ and $\theta=\pi$, $\partial\psi_1/r\partial\theta$ is zero. For $m=1$, one obtains $B_1C_1=0$ in this case. In the same way, when $r=\infty$ and $\theta=\pi/4$, $\partial\psi_1/r\partial\theta$ must be zero again; and for $m=2$, one obtains $A_2C_2=0$. Now, six relations were obtained for the determination of the coefficients. Using these relations, one can find $C_1=0$, $A_1=0$, $C_2=0$, $B_2=0$, $B_1D_1=-u_0(c/2)^2$, and $A_2D_2=Ku_0(c/2)^3/8$. The substitutions of these values of the coefficients into Eq. (90) gives

$$\psi_1=-u_0\left(\frac{c}{2}\right)^2\frac{\sin\theta}{r}+\frac{u_0K}{8r^2}\left(\frac{c}{2}\right)^3\cos 2\theta \tag{92}$$

Accordingly, the stream function for the total flow is

$$\psi=\psi_0+\psi_1=u_0\left[\left(r-\frac{c^2}{4r}\right)\sin\theta+\frac{K}{2}\left(\frac{r^2}{c}\sin^2\theta+\frac{c^3}{32r^2}\cos 2\theta\right)\right] \tag{93}$$

This result is identical with the equation given by Tsien. Euler's equations of motion are

$$-\frac{1}{\rho}\frac{\partial p}{\partial x}=u\frac{\partial u}{\partial x}+v\frac{\partial u}{\partial y},\quad -\frac{1}{\rho}\frac{\partial p}{\partial y}=u\frac{\partial v}{\partial x}+v\frac{\partial v}{\partial y}$$

Substitution into these equations of the expressions for velocity given in Eq. (81) yields

$$\frac{1}{\rho}\frac{\partial^2 p}{\partial x^2}=-\frac{\partial^2\psi}{\partial x\,\partial y}\frac{\partial^2\psi}{\partial x\,\partial y}-\frac{\partial\psi}{\partial y}\frac{\partial}{\partial x}\left(\frac{\partial^2\psi}{\partial x\,\partial y}\right)+\frac{\partial^2\psi}{\partial x^2}\frac{\partial^2\psi}{\partial y^2}+\frac{\partial\psi}{\partial x}\frac{\partial}{\partial x}\left(\frac{\partial^2\psi}{\partial y^2}\right)$$

and

$$\frac{1}{\rho}\frac{\partial^2 p}{\partial y^2}=\frac{\partial^2\psi}{\partial y^2}\frac{\partial^2\psi}{\partial x^2}+\frac{\partial\psi}{\partial y}\frac{\partial}{\partial y}\left(\frac{\partial^2\psi}{\partial x^2}\right)-\frac{\partial^2\psi}{\partial x\partial y}\frac{\partial^2\psi}{\partial x\partial y}-\frac{\partial\psi}{\partial x}\frac{\partial}{\partial y}\left(\frac{\partial^2\psi}{\partial x\partial y}\right)$$

The sum of these two equations gives

$$\frac{1}{\rho}\nabla^2 p=2\left\{\frac{\partial^2\psi}{\partial x^2}\frac{\partial^2\psi}{\partial y^2}-\left(\frac{\partial^2\psi}{\partial x\partial y}\right)^2\right\}$$

in which

$$\psi=\psi_0+\psi_1\,,\quad \frac{\partial^2\psi}{\partial x\partial y}=0\,,\quad \psi_0=u_0\left(y+K\frac{y^2}{2c}\right),$$

$$\frac{\partial\psi_0}{\partial y}=u_0\left(1+\frac{K}{c}y\right),\quad \frac{\partial\psi_0}{\partial x}=0\,,\quad \frac{\partial^2\psi_0}{\partial x^2}=0\,,\quad \frac{\partial^2\psi}{\partial y^2}=u_0\frac{K}{c}$$

Accordingly,

$$\frac{1}{\rho}\nabla^2 p=2\left\{\frac{\partial^2\psi_1}{\partial x^2}\frac{\partial^2\psi_1}{\partial y^2}-\left(\frac{\partial^2\psi_1}{\partial x\partial y}\right)^2+\frac{Ku_0}{c}\frac{\partial^2\psi_1}{\partial x^2}\right\} \tag{94}$$

This is the Laplace equation for the pressure, which must be solved to obtain the pressure distribution in the field. Tsien's paper gives a solution, but it is not clearly applicable to the determination of the pressure in the vicinity of the cylinder.

Upon rewriting Eq. (90), one obtains

$$\psi_1=\sum_m\left\{A_m D_m(x^2+y^2)^{-\frac{m}{2}}\cos\left(m\tan^{-1}\frac{y}{x}\right)+B_m D_m(x^2+y^2)^{-\frac{m}{2}}\sin\left(m\tan^{-1}\frac{y}{x}\right)\right\}$$

in which the relations $A_m C_m=0$ and $B_m C_m=0$ are employed. It may seem awkward that the general expressions of coefficients are used in this equation, but these expressions are convenient for further computation. Since

$$\frac{\partial}{\partial x}\left(\tan^{-1}\frac{y}{x}\right)=\frac{-y}{x^2+y^2}$$

then

$$\frac{\partial\psi_1}{\partial x}=\sum_m\left[A_m D_m\left\{-mx(x^2+y^2)^{-\frac{m+2}{2}}\cos\left(m\tan^{-1}\frac{y}{x}\right)+m(x^2+y^2)^{-\frac{m+2}{2}}y\sin\left(m\tan^{-1}\frac{y}{x}\right)\right\}\right]$$

$$+B_mD_m\Big\{-mx(x^2+y^2)^{-\frac{m+2}{2}}\sin\Big(m\tan^{-1}\frac{y}{x}\Big) -m(x^2+y^2)^{-\frac{m+2}{2}}y\cos\Big(m\tan^{-1}\frac{y}{x}\Big)\Big\}\Big]$$

$$=\sum_m\Big[A_mD_m\Big\{-mr^{-(m+2)}r\cos\theta\cos m\theta+r^{-(m+2)}mr\sin\theta\sin m\theta\Big\} +B_mD_m\Big\{-mr^{-(m+2)}r\cos\theta\sin m\theta-r^{-(m+2)}mr\sin\theta\cos m\theta\Big\}\Big]$$

$$=\sum_m\frac{-m}{r^{m+1}}\Big\{A_mD_m(\cos\theta\cos m\theta-\sin\theta\sin m\theta) +B_mD_m(\cos\theta\sin m\theta+\sin\theta\cos m\theta)\Big\}$$

$$=\sum_m\frac{-m}{r^{m+1}}\Big\{A_mD_m\cos(m\theta+\theta)+B_mD_m\sin(m\theta+\theta)\Big\} \tag{95}$$

In the same way, one can obtain

$$\frac{\partial\psi_1}{\partial y}=\sum_m\frac{-m}{r^{m+1}}\Big\{A_mD_m\sin(m\theta+\theta)-B_mD_m\cos(m\theta+\theta)\Big\} \tag{96}$$

$$\frac{\partial^2\psi_1}{\partial x\partial y}=\sum_m\frac{m(m+1)}{r^{m+2}}\Big\{A_mD_m\sin(m\theta+2\theta)-B_mD_m\cos(m\theta+2\theta)\Big\} \tag{97}$$

$$\frac{\partial^2\psi_1}{\partial x^2}=\sum_m\frac{m(m+1)}{r^{m+2}}\Big\{A_mD_m\cos(m\theta+2\theta)+B_mD_m\sin(m\theta+2\theta)\Big\} \tag{98}$$

$$\frac{\partial^2\psi_1}{\partial y^2}=\sum_m\frac{m(m+1)}{r^{m+2}}\Big\{-A_mD_m\cos(m\theta+2\theta)-B_mD_m\sin(m\theta+2\theta)\Big\} \tag{99}$$

Accordingly,

$$\frac{\partial^2\psi_1}{\partial x^2}\frac{\partial^2\psi_1}{\partial y^2}=-\Big[\frac{6}{r^4}A_2D_2\cos4\theta+\frac{2}{r^3}B_1D_1\sin3\theta\Big]^2 \tag{100}$$

and

$$\Big(\frac{\partial^2\psi_1}{\partial x\partial y}\Big)^2=\Big[\frac{6}{r^4}A_2D_2\sin4\theta-\frac{2}{r^3}B_1D_1\cos3\theta\Big]^2 \tag{101}$$

Substitution of Eqs. (100), (101), and (98) into Eq. (94) gives, after multiplication by r^2,

$$\frac{1}{\rho}\Big(r^2\frac{\partial^2p}{\partial r^2}+r\frac{\partial p}{\partial r}+\frac{\partial^2p}{\partial\theta^2}\Big) =2\Big[\frac{-36}{r^6}(A_2D_2)^2-\frac{4}{r^4}(B_1D_1)^2+\frac{24}{r^5}A_2D_2\cdot B_1D_1\sin\theta +\frac{u_0K}{c}\sum_m\frac{m(m+1)}{r^m}\Big\{A_mD_m\cos(m\theta+2\theta)+B_mD_m\sin(m\theta+2\theta)\Big\}\Big] \tag{102}$$

This equation is non-homogeneous, and for such equations it is usually difficult to obtain the general solution. Nevertheless, the general solution of this equation is the sum of two special solutions, one of which can be obtained by equating the right-hand side to be zero, and the other of which must be obtained without equating the right-hand side to zero. The first special solution is easily obtainable in the manner already employed to find Eq. (90). An inspection of Eq. (102), for assuming a proper form of the second special solution, will give the following clues:

1. when the special solution is assumed properly, as will be seen in the left-hand side of Eq. (102), even if the terms are operated by $\partial^2/\partial r^2$ and $\partial/\partial r$, r^2 and r are multiplied, respectively, after operation. The operation of $\partial^2/\partial\theta^2$ does not change the powers of r. Consequently, the form of the special solution must have the same powers of r as the right-hand side of Eq. (102).

2. The operation of $\partial^2/\partial\theta^2$ does not change the forms inside the sine and cosine, but the coefficients in front of the sine and cosine change. Therefore, it is reasonable to assume the following form as the special solution of Eq. (102), when the right-hand side remains:

$$\frac{p}{\rho} = 2\left[-\left\{ \frac{a_1}{r^6} + \frac{a_2}{r^4} - \frac{a_3}{r^5}\sin\theta \right\} + \frac{u_0 K}{c} \sum_q \frac{b_q}{r^q} \left\{ A_q D_q \cos(q\theta + 2\theta) + B_q D_q \sin(q\theta + 2\theta) \right\} + \text{constant} \right] \tag{103}$$

If it is understood that the reference pressure is the pressure at a point far away from the cylinder, the constant which appears at the last of this equation is zero. From Eq. (103), one obtains

$$\frac{r^2}{\rho}\frac{\partial^2 p}{\partial r^2} = 2\left[-\left\{ \frac{42a_1}{r^6} + \frac{20a_2}{r^4} - \frac{30a_4}{r^5}\sin\theta \right\} + \frac{u_0 K}{c} \sum_q \frac{q(q+1)b_q}{r^q} \left\{ A_q D_q \cos(q\theta + 2\theta) + B_q D_q \sin(q\theta + 2\theta) \right\} \right]$$

$$\frac{r}{\rho}\frac{\partial p}{\partial r} = 2\left[-\left\{ \frac{-6a_1}{r^6} + \frac{-4a_2}{r^4} - \frac{-5a_3}{r^5}\sin\theta \right\} - \frac{u_0 K}{c} \sum_q \frac{-qb_q}{r^q} \left\{ A_q D_q \cos(q\theta + 2\theta) + B_q D_q \sin(q\theta + 2\theta) \right\} \right]$$

$$\frac{1}{\rho}\frac{\partial^2 p}{\partial\theta^2}=2\Bigg[-\left\{\frac{a_3}{r^5}\sin\theta\right\}+\frac{u_0K}{c}\sum_q\frac{-(q+2)^2b_q}{r^q}\left\{A_qD_q\cos(q\theta+2\theta)+B_qD_q\sin(q\theta+2\theta)\right\}\Bigg]$$

The sum of these three equations gives

$$\frac{r^2}{\rho}\frac{\partial^2 p}{\partial r^2}+\frac{r}{\rho}\frac{\partial p}{\partial r}+\frac{1}{\rho}\frac{\partial^2 p}{\partial\theta^2}=2\Bigg[-\left\{\frac{36a_1}{r^6}+\frac{16a_2}{r^4}-\frac{24a_3}{r^5}\sin\theta\right\}+\frac{u_0K}{c}\sum_q\frac{-b_q}{r^q}(4q+4)\left\{A_qD_q\cos(q\theta+2\theta)+B_qD_q\sin(q\theta+2\theta)\right\}\Bigg] \tag{104}$$

By comparing Eqs. (102) and (104), one can obtain

$$a_1=(A_2D_2)^2\,,\qquad a_2=\frac{1}{4}(B_1D_1)^2\,,\qquad a_3=A_2D_2\cdot B_1D_1$$

$$m=q\,,\qquad b_q=-\frac{m}{4}$$

Accordingly, one special solution of Eq. (102) is

$$\frac{p}{\rho}=2\Bigg[-\left\{\frac{1}{r^6}(A_2D_2)^2+\frac{1}{4r^4}(B_1D_1)^2-\frac{\sin\theta}{r^5}A_2D_2\cdot B_1D_1\right\}-\frac{Ku_0}{c}\sum_m\frac{m}{4r^m}\left\{A_mD_m\cos(m\theta+2\theta)+B_mD_m\sin(m\theta+2\theta)\right\}\Bigg] \tag{105}$$

The other special solution, which can be obtained by equating the right-hand side of Eq. (102) to zero, is at once

$$\frac{p}{\rho}=\sum_m(\zeta_m r^m+\vartheta_m r^{-m})(\alpha_m\cos m\theta+\beta_m\sin m\theta) \tag{106}$$

Consequently, the general solution of Eq. (102) is the sum of Eq. (105) and (106):

$$\frac{p}{\rho}=2\Bigg[-\left\{\frac{1}{r^6}(A_2D_2)^2+\frac{1}{4r^4}(B_1D_1)^2-\frac{\sin\theta}{r^5}A_2D_2\cdot B_1D_1\right\}-\frac{Ku_0}{c}\sum_m\frac{m}{4r^m}\left\{A_mD_m\cos(m\theta+2\theta)+B_mD_m\sin(m\theta+2\theta)\right\}\Bigg]+\sum_m(\zeta_m r^m+\vartheta_m r^{-m})(\alpha_m\cos m\theta+\beta_m\sin m\theta) \tag{107}$$

Next, ζ_m, ϑ_m, α_m and β_m must be evaluated. Euler's equation of motion for steady flow is

$$-\frac{1}{\rho}\frac{\partial p}{\partial x}=u\frac{\partial u}{\partial x}+v\frac{\partial u}{\partial y} \tag{108}$$

As x is a function of r and θ,

$$\frac{1}{\rho}\frac{\partial p}{\partial x}=\frac{1}{\rho}\frac{\partial p}{\partial r}\frac{\partial r}{\partial x}+\frac{1}{\rho}\frac{\partial p}{\partial \theta}\frac{\partial \theta}{\partial x} \tag{109}$$

and

$$\frac{\partial r}{\partial x}=\cos\theta\,,\qquad \frac{\partial \theta}{\partial x}=-\frac{\sin\theta}{r} \tag{110}$$

Performing the operations $\partial/\partial r$ and $\partial/\partial\theta$ upon Eq. (107), one obtains:

$$\begin{aligned}\frac{1}{\rho}\frac{\partial p}{\partial r}=2\Bigg[&-\left\{\frac{-6}{r^7}(A_2D_2)^2+\frac{-4}{4r^5}(B_1D_1)^2-\frac{-5\sin\theta}{r^6}A_2D_2\cdot B_1D_1\right\}\\&+\frac{Ku_0}{c}\sum_m\frac{m^2}{4r^{m+1}}\left\{A_mD_m\cos(m\theta+2\theta)+B_mD_m\sin(m\theta+2\theta)\right\}\Bigg]\\&+\sum_m m(\zeta_m r^{m-1}-\vartheta_m r^{-m-1})(\alpha_m\cos m\theta+\beta_m\sin m\theta)\end{aligned} \tag{111}$$

$$\begin{aligned}\frac{1}{\rho}\frac{\partial p}{\partial \theta}=2\Bigg[&\frac{\cos\theta}{r^5}A_2D_2\cdot B_1D_1\\&-\frac{Ku_0}{c}\sum_m\frac{m(m+2)}{4r^m}\left\{-A_mD_m\sin(m\theta+2\theta)+B_mD_m\cos(m\theta+2\theta)\right\}\Bigg]\\&+\sum_m m(\zeta_m r^m+\vartheta_m r^{-m})(-\alpha_m\sin m\theta+\beta_m\cos m\theta)\end{aligned} \tag{112}$$

Since it is assumed that $p=0$ at $r=\infty$, ζ_m must be zero in Eqs. (111) and (112). By substituting Eqs. (110), (111), and (112) into Eq. (109) one can obtain

$$\begin{aligned}\frac{1}{\rho}\frac{\partial p}{\partial x}=&2\left\{\frac{6}{r^7}(A_2D_2)^2+\frac{1}{r^5}(B_1D_1)^2\right\}\cos\theta-\frac{6}{r^6}(\sin 2\theta)\,A_2D_2\cdot B_1D_1\\&+\frac{Ku_0}{c}\sum_m\frac{m^2}{2r^{m+1}}\left\{A_mD_m\cos(m\theta+3\theta)+B_mD_m\sin(m\theta+3\theta)\right\}\\&-\frac{Ku_0}{c}\sum_m\frac{m}{2r^{m+1}}\Big\{A_mD_m\cos(m\theta+\theta)+B_mD_m\sin(m\theta+\theta)\\&\qquad-A_mD_m\cos(m\theta+3\theta)-B_mD_m\sin(m\theta+3\theta)\Big\}\\&-\sum_m\vartheta_m\frac{m}{r^{m+1}}\left\{\alpha_m\cos m\theta+\beta_m\sin m\theta\right\}\cos\theta\\&-\sum_m\vartheta_m\frac{m}{r^{m+1}}\left\{-\alpha_m\sin m\theta+\beta_m\cos m\theta\right\}\sin\theta\end{aligned} \tag{113}$$

On the other hand, use of Eqs. (78), (81), (95), (96) and (99) results in

$$u = \frac{\partial\psi}{\partial y} = \frac{\partial}{\partial y}(\psi_0+\psi_1)$$
$$= u_0\left(1+K\frac{y}{c}\right)+\sum_m \frac{-m}{r^{m+1}}\left\{A_mD_m\sin(m\theta+\theta)-B_mD_m\cos(m\theta+\theta)\right\}$$
$$v = -\frac{\partial}{\partial x}(\psi_0+\psi_1)$$
$$= \sum_m \frac{m}{r^{m+1}}\left\{A_mD_m\cos(m\theta+\theta)+B_mD_m\sin(m\theta+\theta)\right\}$$
$$\frac{\partial u}{\partial x} = \frac{\partial^2\psi_1}{\partial x\partial y}$$
$$= \sum_m \frac{m(m+1)}{r^{m+2}}\left\{A_mD_m\sin(m\theta+2\theta)-B_mD_m\cos(m\theta+2\theta)\right\}$$
$$\frac{\partial u}{\partial y} = \frac{\partial^2\psi_0}{\partial y^2}+\frac{\partial^2\psi_1}{\partial y^2}$$
$$= \frac{u_0K}{c}-\sum_m \frac{m(m+1)}{r^{m+2}}\left\{A_mD_m\cos(m\theta+2\theta)+B_mD_m\sin(m\theta+2\theta)\right\}$$

Accordingly

$$u\frac{\partial u}{\partial x}+v\frac{\partial u}{\partial y}$$
$$= u_0\sum_m \frac{m(m+1)}{r^{m+2}}\left\{A_mD_m\sin(m\theta+2\theta)-B_mD_m\cos(m\theta+2\theta)\right\}$$
$$+\frac{u_0K}{c}\sum_m \frac{m}{r^{m+2}}\Big[\left\{(m+1)A_mD_m\sin(m\theta+2\theta)-(m+1)B_mD_m\cos(m\theta+2\theta)\right\}\sin\theta$$
$$+A_mD_m\cos(m\theta+\theta)+B_mD_m\sin(m\theta+\theta)\Big]$$
$$-\frac{12}{r^7}(A_2D_2)^2\cos\theta+\frac{6}{r^6}A_2D_2\cdot B_1D_1\sin 2\theta-\frac{2}{r^5}(B_1D_1)^2\cos\theta \qquad (114)$$

Substituting Eqs. (113) and (114) into Eq. (108) and simplifying then yields

$$\sum_m \frac{m\vartheta_m}{r^{m+1}}\left\{\alpha_m\cos(m\theta+\theta)+\beta_m\sin(m\theta+\theta)\right\}$$
$$= u_0\sum_m \frac{m(m+1)}{r^{m+2}}\left\{A_mD_m\sin(m\theta+2\theta)-B_mD_m\cos(m\theta+2\theta)\right\}$$
$$+\frac{u_0K}{c}\sum_m \frac{m(m+2)}{2r^{m+1}}\left\{A_mD_m\cos(m\theta+\theta)+B_mD_m\sin(m\theta+\theta)\right\}$$

Noticing that only A_2D_2 and B_1D_1 are the terms which remain in the right-hand side of this equation, it can be expanded as follows:

$$\frac{1}{r^2}\left\{\vartheta_1\alpha_1\cos 2\theta+\vartheta_1\beta_1\sin 2\theta\right\}+\frac{2}{r^3}\left\{\vartheta_2\alpha_2\cos 3\theta+\vartheta_2\beta_2\sin 3\theta\right\}$$
$$+\frac{3}{r^4}\left\{\vartheta_3\alpha_3\cos 4\theta+\vartheta_3\beta_3\sin 4\theta\right\}+\underbrace{\cdots\cdots}_{\text{zeros}}$$
$$=\frac{1}{r^2}\left\{\frac{3u_0K}{2c}A_1D_1\cos 2\theta+\frac{3u_0K}{2c}B_1D_1\sin 2\theta\right\}$$
$$+\frac{1}{r^3}\left\{2u_0A_1D_1\sin 3\theta-2u_0B_1D_1\cos 3\theta\right.$$
$$\left.+\frac{8u_0K}{2c}A_2D_2\cos 3\theta+\frac{8u_0K}{2c}B_2D_2\sin 3\theta\right\}$$
$$+\frac{1}{r^4}\left\{6u_0A_2D_2\sin 4\theta-6u_0B_2D_2\cos 4\theta\right.$$
$$\left.+\frac{15u_0K}{2c}A_3D_3\cos 4\theta+\frac{15u_0K}{2c}B_3D_3\sin 4\theta\right\}+\underbrace{\cdots\cdots}_{\text{zeros}}$$

By comparing the coefficients in both sides of this equation, it is found that

$$\vartheta_1\alpha_1=0\,,\quad \vartheta_1\beta_1=-\frac{3u_0K}{2c}\left(\frac{c}{2}\right)^2,\quad \vartheta_2\alpha_2=u_0^2\left(\frac{c}{2}\right)^2+\frac{u_0^2K^2}{4c}\left(\frac{c}{2}\right)^3,$$
$$\vartheta_2\beta_2=0\,,\quad \vartheta_3\alpha_3=0\,,\quad \vartheta_3\beta_3=\frac{Ku_0^2}{4}\left(\frac{c}{2}\right)^3 \qquad (115)$$

These are all the terms which have values, the others all being zero. Consequently, the solution of Eq. (102) can be obtained by substitution of Eq. (115), and the values of A_2D_2 and B_1D_1 into Eq. (107):

$$\frac{p}{\rho}=-\frac{2}{r^6}\left\{\frac{K}{8}u_0\left(\frac{c}{2}\right)^3\right\}^2-\frac{1}{2r^4}\left\{u_0\left(\frac{c}{2}\right)^2\right\}^2+\frac{2\sin\theta}{r^5}\left\{-\frac{Ku_0^2}{8}\left(\frac{c}{2}\right)^5\right\}$$
$$-\frac{Ku_0}{2c}\left\{\frac{2}{r^2}\frac{K}{8}u_0\left(\frac{c}{2}\right)^3\cos 4\theta-\frac{1}{r}u_0\left(\frac{c}{2}\right)^2\sin 3\theta\right\}-\frac{1}{r}\frac{3u_0^2K}{2c}\left(\frac{c}{2}\right)^2\sin\theta$$
$$+\frac{1}{r^2}\left\{u_0\left(\frac{c}{2}\right)^2\cos 2\theta+\frac{u_0^2K^2}{4c}\left(\frac{c}{2}\right)^3\cos 2\theta\right\}+\frac{1}{r^3}\frac{Ku_0^2}{4}\left(\frac{c}{2}\right)^3\sin 3\theta$$

This equation can be rewritten in dimensionless form:

$$\frac{p}{\frac{1}{2}\rho u_0^2}=-\frac{K^2}{16r^6}\left(\frac{c}{2}\right)^6-\frac{1}{r^4}\left(\frac{c}{2}\right)^4-\frac{K}{2r^5}\left(\frac{c}{2}\right)^5\sin\theta$$

$$-\frac{K^2}{4cr^2}\left(\frac{c}{2}\right)^3\cos 4\theta+\frac{K}{cr}\left(\frac{c}{2}\right)^2\sin 3\theta$$
$$-\frac{3K}{cr}\left(\frac{c}{2}\right)^2\sin\theta+\frac{2}{r^2}\left(\frac{c}{2}\right)^2\cos 2\theta$$
$$+\frac{K^2}{2cr^2}\left(\frac{c}{2}\right)^3\cos 2\theta+\frac{K}{2r^3}\left(\frac{c}{2}\right)^3\sin 3\theta \qquad (116)$$

This is the general expression for the pressure in the field of the shear flow around a cylinder.

Since $r=c/2$ on the surface of the cylinder, Eq. (116) becomes

$$\frac{p}{\frac{1}{2}\rho u_0^2}=\left(1+\frac{K^2}{16}\right)+K\sin\theta+\left(\frac{K^2}{2}-4\right)\sin^2\theta-4K\sin^3\theta-K^2\sin^4\theta \qquad (117)$$

The results of Eqs. (116) and (117) were obtained by solving the equation generally. One can also obtain these results without going into the detail of computation when the Bernoulli equation is applied.

When the stream line which passes an arbitrary point (r, θ) in the field is identical with the stream line which passes $(-\infty, y)$, the following relation can be obtained from Eqs. (78) and (93):

$$y+\frac{Ky^2}{2c}=\left(r-\frac{c^2}{4r}\right)\sin\theta+\frac{K}{2}\left(\frac{r^2}{c}\sin\theta+\frac{c^3}{32r^2}\cos 2\theta\right)$$

The velocity at $(-\infty, y)$ is given by Eq. (77). Consequently, when the pressure at $(-\infty, y)$ is taken as reference, the total head along this stream line must be

$$g\rho H=\frac{1}{2}\rho u_0^2\left(1+K\frac{y}{c}\right)^2$$
$$=\frac{1}{2}\rho u_0^2\left[1+\frac{2K}{c}\left\{\left(r-\frac{c^2}{4r}\right)\sin\theta+\frac{K}{2}\left(\frac{r^2}{c}\sin^2\theta+\frac{c^3}{32r^2}\cos 2\theta\right)\right\}\right] \qquad (118)$$

Since the stream function is already shown in Eq. (93), the velocity components at an arbitrary point (r, θ) can be found easily, and the velocity at that point can be calculated. The velocity components are

$$u_r=-\frac{1}{r}\frac{\partial\psi}{\partial\theta}=-u_0\left[\left(1-\frac{c^2}{4r^2}\right)\cos\theta+K\left(\frac{r}{c}\sin\theta\cos\theta-\frac{c^3}{32r^3}\sin 2\theta\right)\right]$$
$$u_\theta=\frac{\partial\psi}{\partial r}=u_0\left[\left(1+\frac{c^2}{4r^2}\right)\sin\theta+K\left(\frac{r}{c}\sin^2\theta-\frac{c^3}{32r^3}\cos 2\theta\right)\right]$$

Accordingly, the square of the velocity at an arbitrary point (r, θ) is

$$\begin{aligned} q^2 &= u_r^2 + u_\theta^2 \\ &= u_0^2\left[1 - \frac{c^2}{2r^2}\cos 2\theta + \frac{c^4}{16r^4} + \frac{r^2K^2}{c^2}\sin^2\theta - \frac{c^2K^2}{16r^2}(3\sin^2\theta\cos^2\theta - \sin^4\theta)\right. \\ &\quad \left. + \frac{c^6}{32^2r^6} + \frac{2Kr}{c}\sin\theta - \frac{Kc^3}{16r^3}\sin 3\theta - \frac{Kc}{2r}\sin\theta\cos 2\theta + \frac{Kc^5}{64r^5}\sin\theta\right] \end{aligned} \tag{119}$$

Since the pressure can be found by

$$\frac{\Delta p}{\frac{1}{2}\rho u_0^2} = \frac{1}{\frac{1}{2}\rho u_0^2}\left(g\rho H - \frac{1}{2}\rho q^2\right)$$

the substitution of Eqs. (118) and (119) into this equation gives the same result as Eq. (116), but it is necessary to employ a special device to obtain the simple forms of coefficients as are given in Eq. (116).

In the same way, the result of Eq. (117) can be obtained easily. The stream function which constructs the surface of the cylinder will be given by putting $r=c/2$ and $\theta=\pi$ in Eq. (93), for convenience, since the surface of the cylinder is the same stream line without regard to the value of θ. Namely,

$$\psi_{r=\frac{c}{2}} = \frac{1}{16}Kcu_0 \tag{120}$$

The stream line far upstream from the cylinder which is destined to pass the surface of the cylinder must be given by equating Eq. (120) and Eq. (78). Consequently,

$$u_0\left(y + \frac{K}{2c}y^2\right) = \frac{1}{16}Kcu_0 \tag{121}$$

This relation gives the value of y which determines the location of the stream line at the point upstream which passes tne surface of the cylinder. Eq. (121) gives

$$y = -\frac{c}{K} \pm \sqrt{\frac{c^2}{K^2} + \frac{c^2}{8}} \tag{122}$$

Substitution of Eq. (122) into Eq. (78) gives

$$u = \pm u_0\sqrt{1 + \frac{K^2}{8}} \tag{123}$$

Since the pressure at $r=\infty$ is understood to be zero, the total head

along the stream line which passes the surface of the cylinder is

$$g\rho H = \frac{1}{2}\rho q^2 + p$$

On the other hand, the velocity on the surface of the cylinder can be obtained by introducing $r=c/2$ into $\partial\psi/\partial r$, since the velocity is tangential on the surface. Eq. (93) gives

$$\frac{\partial\psi}{\partial r} = u_0\left[\left(1+\frac{c^2}{4r^2}\right)\sin\theta+\frac{K}{2}\left(2\frac{r}{c}\sin^2\theta-\frac{c^3}{16r^3}\cos 2\theta\right)\right]$$

Consequently, the velocity on the surface of the cylinder is

$$q = u_0\left[2\sin\theta+K\sin^2\theta-\frac{K}{4}\right] \tag{124}$$

Since $g\rho H = \frac{1}{2}\rho u_0^2\left(1+\frac{K^2}{8}\right)$, the pressure distribution on the surface of the cylinder is

$$\frac{p}{\frac{1}{2}\rho u_0^2} = \left(1+\frac{K^2}{8}\right)-\left(2\sin\theta+K\sin^2\theta-\frac{K}{4}\right)^2$$

which gives the same result as Eq. (117). In other words, the results of Eqs. (116) and (117) were verified.

Obviously, when $K=0$ (in other words when the cylinder is located in a uniform flow) in Eq. (117), the pressure distribution on the surface of the cylinder is $p/(\rho u_0^2/2)=1-4\sin^2\theta$, which is a familiar equation in hydrodynamics. The point of the maximum pressure can be obtained by differentiating Eq. (117) with regard to θ and equating the derivative to zero:

$$K+(K^2-8)\sin\theta-12K\sin^2\theta-4K^2\sin^3\theta = 0 \tag{125}$$

On the other hand, the stagnation point can be obtained from the condition $(\partial\psi/\partial r)_{r=c/2}=0$. Using Eq. (93), one obtains

$$K\sin^2\theta+2\sin\theta-\frac{K}{4} = 0 \tag{126}$$

which gives

$$\sin\theta = \frac{1}{K}\left(-1\pm\sqrt{1+\frac{K^2}{4}}\right) \tag{127}$$

Since the absolute value of this quantity is always smaller than unity,

there are always stagnation points on the surface of the cylinder. As the condition given by Eq. (126) satisfies Eq. (125), the point of the maximum pressure on the surface of a cylinder and the stagnation point are identical.

The results of the numerical computations of Eq. (117) in the range of $90° \leqq \theta \leqq 270°$ are shown in Fig. 44. The effect of a velocity gradient on the pressure distribution of a cylinder will be clearly seen. In order to clarify the probable error in the estimations of velocity by means of a cylinder, a part of Fig. 44 was plotted to a larger scale as shown in Fig. 45. The movement of the stagnation points will be evident from this figure. The points of the maximum pressure were obtained with Eq. (126).

When the angle between the two holes in a cylinder is known, one can easily estimate the probable errors in the measurement of the direction of flow, with the aid of Fig. 45. Fig. 46 (a) shows the movement of the stagnation point and the probable error in determining the direction of flow with the 30.6° cylinder which was used in the present experimental study. As will be seen, the error in the direction of flow is always negative, and this tendency coincides with the results which were already detected by the measurements with 180° and 30.6° cylinders, as described above. Figure 46 (b) shows the probable error in the magnitude of velocity as measured with the 30.6° cylinder. Since there are two holes in the cylinder, it has two possible angular positions for the measurement of the velocity magnitude. Curves I and III correspond to these two cases, and Curve II shows the probable error when the two readings of the two angular positions are averaged for the estimation of the magnitude of the velocity.

As a calibration of a Pitot cylinder is required even for the measurement of uniform flow, the results obtained in Fig. 46 are not applicable to the determination of corrections. This study is intended instead to explain the performance of a cylinder in shear flow, and to provide a guide for the selection of the dimension of a Pitot cylinder.

FIG. 44

PRESSURE DISTRIBUTION ON THE SURFACE OF A CYLINDER IN SHEAR FLOW

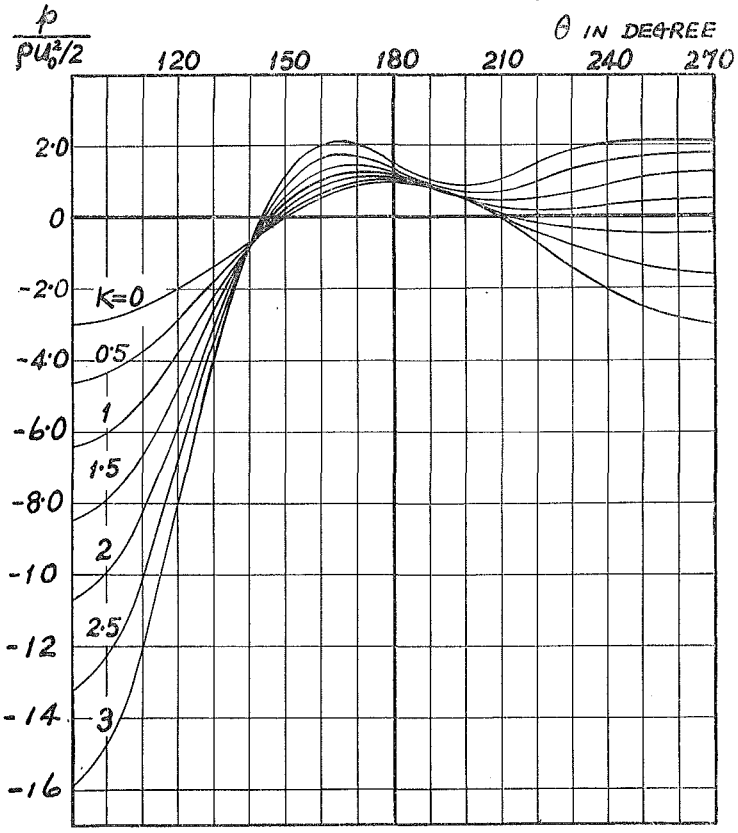

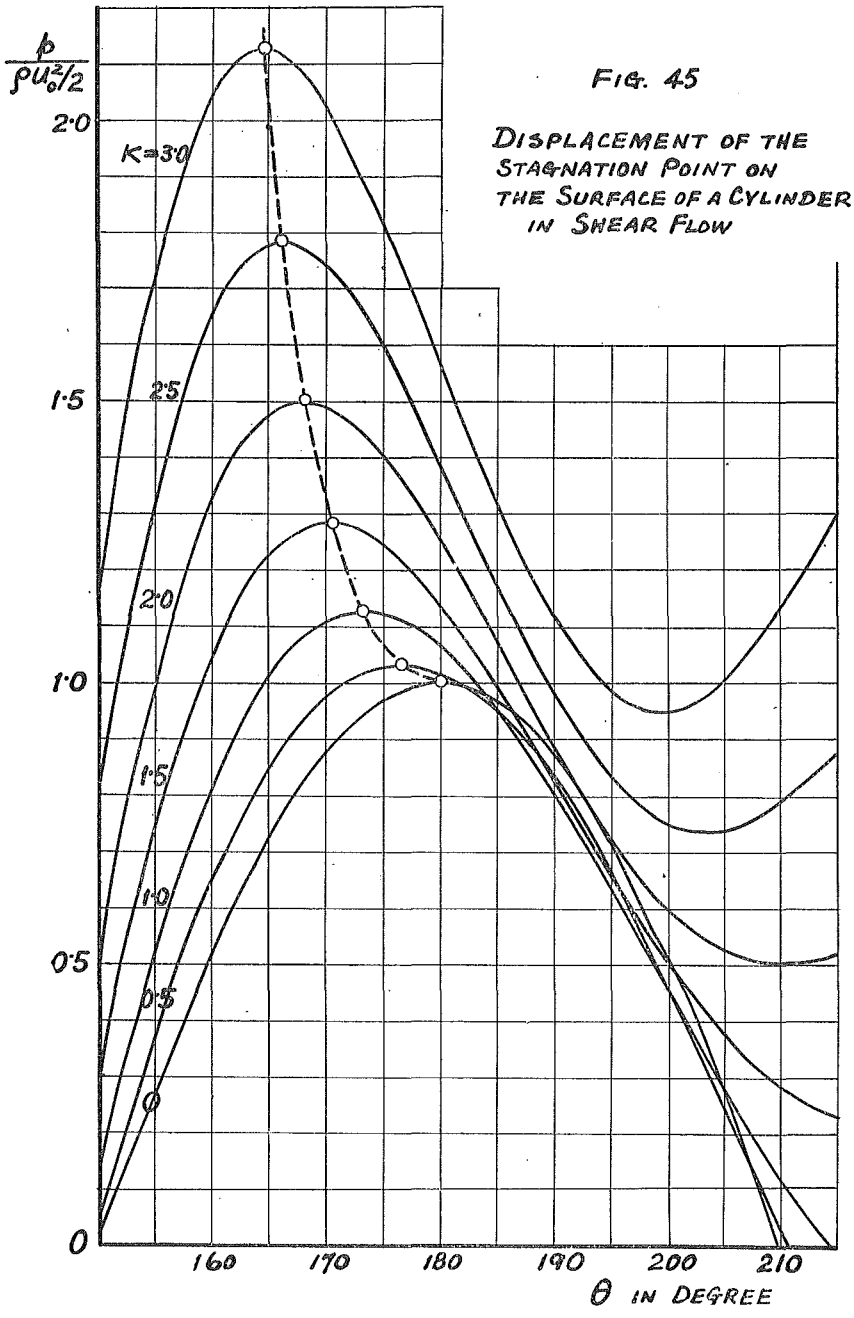

FIG. 45

DISPLACEMENT OF THE STAGNATION POINT ON THE SURFACE OF A CYLINDER IN SHEAR FLOW

Fig. 46(a)

Movement of the point of Maximum pressure on the surface of a cylinder and the probable error in the estimstion of the direction of flow with the 30.6° cylinder

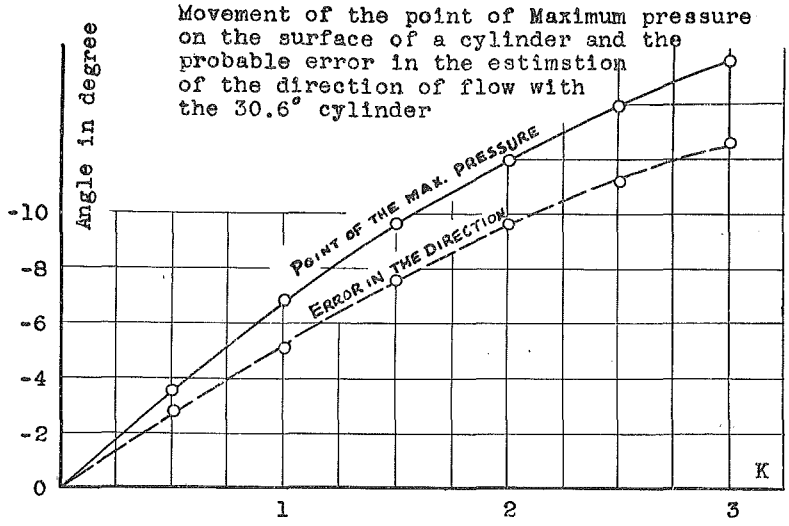

Fig. 46(b)

Probable error in the estimation of the magnitude of velocity with the 30.6° Pitot-cylinder

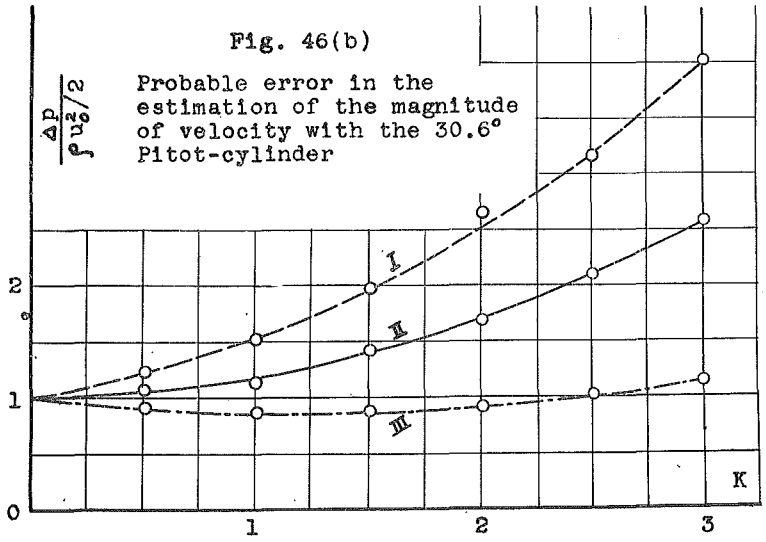

Acknowledgment

Most of the present experimental study was performed at the Iowa Institute of Hydraulic Research, State University of Iowa, U. S. A., and was partially supported by the Office of Naval Research under Contract N8onr-500 with the Iowa Institute of Hydraulic Research. The author wishes to extend from Japan his appreciation and to express his indebtedness to Dr. Hunter Rouse, who gave the opportunity to work under his direction. The author is also grateful to Dr. Louis Landweber who helped in the part of hydrodynamic analysis. The author wishes to express his indebtedness to the Faculty of Engineering, Hokkaido University and to the "Fulbright Scholarship Committee" for their kindly making possible his study in the U. S. A. This paper was prepared for print after the kind encouragement of Dr. Kikutaro Otsubo. A part of the reproduction of drawings was done by Mr. Hiroshi Yamaguchi in the Laboratory of Hydraulic machinery.

Bibliography

1. Fage, A., and Johansen, F. C., "The structure of vortex sheet," *Philosophical Magazine and Journal of Science,* Vol. 5, 7th series, Jan.-June 1928, pp. 417–441.
2. Fage, A., and Johansen, F. C., "On the flow of air behind an inclined flat plate of infinite span, "*Proc. of Royal Society,* A. 116, Sep.-Nov. 1927, pp. 170–197.
3. Hanin, M. "Generation of vortices behind a flat plate," *Cornell Univ. report submitted to the Office of Air Research,* Contract No. AF 33 (038)-21406, July 1953.
4. Fomichev, M. S., "Structure of a flow behind a flat plate in a viscous fluid," *Izv. Akad. Nauk SSSR Otd. Tekh. Nauk* No. 8, 1157–1165, Aug. 1953.
5. A. S. M. E. Applied Mechanics Reviews, Vol. 7, No.11, Nov. 1954, p. 495.
6. Roshiko, A. "On the wake and drag of bluff bodies," *Printing for 22nd Annual Meeting of the Inst. of the Aeronautical Science,* Jan. 25–29, 1954.
7. Hubbard, P. G., "Constant-temperature hot-wire anemometry with application to measurement in water," Ph. D. Dissertation, State University of Iowa, June 1954.
8. Operating Manual for the IIHR MK 3A hot-wire anemometer, Iowa Institute of Hydraulic Research, Sept. 1953.
9. Landweber, L., "The axial symmetric potential flow about enclosed bodies of revolution," Navy Dept., David Taylor Model Basin, Report No. 761, 1951.
10. v. Sanden, H., "Über den Auftrieb im naturlichen winde," *Zeitschrift für Mathematik und Physik,* 61, 225, 1912.

11. Tsien, Hsue-shen, "Symmetrical Joukowsky airfoils in shear flow," *Quarterly of Applied Mathematics,* Vol. 1, July 1943, p, 130.
12. Riabouchinsky, D., "On some cases of two-dimensional fluid motions," *Proc. of the London Mathematical Society,* Ser. 2, Vol. 25, 1926, pp. 185–194.
13. Prandtl, L., "Bericht über Untersuchungen zur ausgebildeten Turbulenz," *Zeitschrift für Angewandte Mathematik und Mechanik,* Bd. 5, 1925, s. 136.
14. Tollmien, W. "Berechnung turbulenter Ausbreitungsvorgänge," Z. A. M. M., Bd. 6, 1926, s. 468.
15. Kuo, Yung-Huai, "On the force and moment acting on a body in shear flow," *Quarterly of Applied Mathematics,* 1–2, Apr.-Jan., 1943–45, p. 273.
16. Siao, T. T., "Characteristics of Turbulence in an air-flow model of the hydraulic jump," Ph. D. Dissertation, State Univ. of Iowa, June 1954.
17. Borden, A., "Wall corrections for flow about two- and three-dimensional symmetrical bodies in rectangular channel of infinite and finite length," Navy Dept., David Taylor Model Basin Report No. 864, Dec. 1954.
18. Lamb, H., *Hydrodynamics,* 6th Ed., 1945, Dover Publications.
19. Hsu, H. C., "Characteristics of mean flow and turbulence at an abrupt two-dimensional expansion," Ph. D. Dissertation, State Univ. of Iowa, Feb. 1950.
20. Arie, M., "A contribution on the characteristics of a cylindrical Pitot-tube," *Trans. of the Japan Soeicty of Mechanical Engineers,* Vol. 22, No. 117, 1956, p. 365.